





This is to certify that the

dissertation entitled

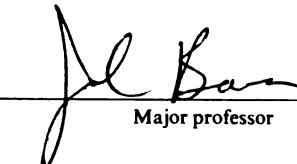
*Low Temperature Electronic Transport  
Properties of Alkali Alloys and Thin Potassium Wires*

presented by

*Jing Zhao*

has been accepted towards fulfillment  
of the requirements for

Ph.D. degree in Physics



Major professor

Date August 2, 1988



L



RETURNING MATERIALS:  
Place in book drop to  
remove this checkout from  
your record. FINES will  
be charged if book is  
returned after the date  
stamped below.

APR 28 1997

LOW TEMPERATURE ELECTRONIC TRANSPORT  
PROPERTIES OF ALKALI ALLOYS AND THIN POTASSIUM WIRES

By

Jing Zhao

A DISSERTATION

Submitted to

Michigan State University

in partial fulfillment of the requirements

for the degree of

DOCTOR OF PHILOSOPHY

Department of Physics and Astronomy

1988



ABSTRACT

LOW TEMPERATURE ELECTRONIC TRANSPORT

PROPERTIES OF ALKALI ALLOYS AND THIN POTASSIUM WIRES

By

Jing Zhao

We have performed high-precision measurements of the electrical resistivity and the thermoelectric ratio of high concentration KRb alloys, and KNa and LiMg alloys, and of thin potassium wires, over the temperature range from 4.2K to 0.07K.

The alkali alloy study reveals that the resistivity anomaly found in previous measurements of KRb alloys is a general phenomenon, and thus likely to be fundamental. The dependences of the anomaly upon temperature, residual resistivity, and magnetic field have been studied. For all three alloy systems with  $\rho_0 < 10^{-7} \Omega\text{m}$ , the anomaly is found to be approximately linear in both temperature and residual resistivity. Localization, electron-electron interaction, and Kondo effects appear to be ruled out as explanations for this regime. The anomaly is found to approach the electron-electron interaction limit when  $\rho_0 > 10^{-7} \Omega\text{m}$ . We also found the unexpectedly large magnitude of electron-electron scattering in pure Li to be due directly to the band structure of Li rather than indirectly to anisotropic scattering. The thermoelectric ratio  $G$  data suggest that adding impurities to K quenches phonon drag and many-body effects dominate the sign as well as the magnitudes of the thermal diffusion component of  $G$ .

Previous measurements of the temperature dependent resistivities of thin potassium wires have been extended to samples of different lengths, different bulk purities, and different surface conditions. The new data all show size-effect anomalies. The anomalies appear to be affected by surface corrosion, and do not generally depend upon sample length. For a given size of the anomaly the temperature dependence is independent of all parameters studied. The data do not appear to be explained by current theories of : interference between electron-electron scattering and surface scattering; reduction in surface scattering due to electron-phonon scattering; localization effects combined with Charge-Density-Waves (CDW); or simple CDW behavior. The low temperature limits of  $G$  for almost all of the samples are consistent with values of  $G_0^s = -0.6 \pm 0.2 V^{-1}$  and  $G_0^i = 0 \pm 0.2 V^{-1}$ .  $G_0^s$  is the surface contribution, and  $G_0^i$  is the impurity contribution. The surface contribution is compatible with completely diffuse surface scattering.

## ACKNOWLEDGMENTS

I gratefully thank my advisor Professor Jack Bass, whose invaluable supports and criticisms guided me through every stage of this research. I would also like to thank Professors P.A. Schroeder and W.P. Pratt Jr. for their precious advice, discussions, and help during this research.

I wish to thank Professor Hide Sato for his helpful discussions and generous help in many stages of this study.

I am also deeply indebted to Dr. Zhao-Zhi Yu, mainly from whom I learned to operate the dilution refrigerator and to make alkali metal samples. I thank everyone else for their aid and interesting discussions: Yao-Jin Qian for his help in taking some data and for permission use some of his data, and Yi-Yun Huang for her help in using computers. Finally, the financial support of Michigan State University, the National Science Foundation, and the MSU Center for Fundamental Materials Research are acknowledged.

## TABLE OF CONTENTS

Chapter	Page
LIST OF TABLES	vii
LIST OF FIGURES	viii
I. INTRODUCTION	01
1.1 Alkali Metals	03
1.2 Simple Transport Properties	04
1.3 Previous Work	06
1.3.1 General Background About the Resistivities of Simple Metals	06
1.3.2 Previous High Precision Low Temperature Electrical Resistivity Measurements of Potassium	08
1.3.3 Previous Work on High Precision Low Temperature Electrical Resistivity Measurements of <u>K</u> Rb Alloys	12
1.3.4 Previous High Precision Low Temperature Electron Resistivity Measurements of Pure Li	14
1.3.5 Previous Work on High Precision Low Temperature Electrical Resistivity Measurements of <u>Li</u> Mg Alloys	15
1.3.6 Previous Work on High Precision Low Temperature Electrical Resistivity Measurements of <u>K</u> Na Alloys	15
1.3.7 Previous Work on the Thermoelectric Ratio $G$ of <u>K</u> Rb, <u>K</u> Na, and <u>Li</u> Mg Alloys	15

1.4	Present Thesis	18
1.4.1	Low Temperature Electrical Resistivity	18
1.4.2	Thermoelectric Ratio $G$	21
II.	THEORY	22
2.1	Inelastic Electron-Impurity Scattering	22
2.2	Temperature-Dependent Elastic Scattering Contribution to the Impurity Resistivity	26
2.3	Kondo Effect	27
2.4	Two-Level Systems	29
2.5	Weak Localization and Interaction	29
2.6	Electron-Electron Scattering	34
2.7	Thermoelectric Power	36
III.	EXPERIMENTAL TECHNIQUES	40
3.1	Measuring System	40
3.1.1	Reaching Low Temperatures	41
3.1.2	High Sensitivity	41
3.1.3	High Precision	41
3.2	Measuring Method	42
3.2.1	Resistivity	43
3.2.2	Temperature Derivative of Resistivity $d\rho/dT$	44
3.2.3	Thermoelectric Ratio $G$	45
3.3	Sample Preparation	45
3.3.1	Glove Box	45
3.3.2	Sample Can	46
3.3.3	Sample	46
3.3.4	Potential Leads of Sample	47

IV. RESISTIVITY ANOMALIES AND THERMOELECTRIC BEHAVIOR IN <u>K</u> Rb, <u>K</u> Na, AND <u>Li</u> Mg ALLOYS AT LOW TEMPERATURES	49
4.1 Electrical Resistivity	50
4.1.1 Residual Resistivity per Atomic % Impurity	51
4.1.2 $T^2$ Resistivity Component	54
4.1.3 High Temperature Term	62
4.1.4 Low Temperature Anomaly	68
4.1.4.a Temperature and $\rho_0$ Dependences of the Anomaly	68
4.1.4.b Comparison with Theoretical Models	77
4.1.4.c Conclusions Concerning the Low Temperature Resistivity Anomaly	85
4.2 Thermoelectric Ratio $G$	86
4.2.1 The Lorentz Ratio $L$	87
4.2.2 $G$ Data	88
4.2.3 The Electron Diffusion Component $G$	93
4.2.4 The Phonon Drag Components	96
4.2.5 Conclusions	99
V. ELECTRON-ELECTRON SCATTERING	100
REFERENCES (Chapters 1 - 5)	106
VI. ELECTRONIC TRANSPORT PROPERTIES OF THIN POTASSIUM WIRES BELOW 1 K	111
6.1 Derivative of Electrical Resistivity, $d\rho/dT$	111
6.1.2 Theoretical Background	113
6.1.3 Samples Characterization and Experimental Procedure	116
6.1.4 Experimental Data and Analysis	123

6.1.5 Summary of Behavior and Comparison with Theories	133
6.1.6 Conclusions and Suggestions for Further Work	135
REFERENCES (Chapter 6.1 - 6.1.6)	137
6.2 Thermoelectrical Ratio G	152
6.2.1 Introduction	152
6.2.2 Review of Previous Work and Background Information	152
6.2.3 Experimental Data	156
6.2.4 Summary and Conclusions	160
REFERENCES (Chapter 6.2 - 6.2.4)	
APPENDIX 1	169
APPENDIX 2	173

## LIST OF TABLES

Table		Page
(1):	Experimental and Theoretical Values of B for <u>K</u> Rb, <u>K</u> Na, and <u>Li</u> Mg Alloys	61
(2):	Experimental and Theoretical Values of $G_0$ for <u>K</u> Rb, <u>K</u> Na, and <u>Li</u> Mg Alloys	95
(3):	Experimental and Theoretical Values of A for <u>K</u> Rb, <u>K</u> Na, and <u>Li</u> Mg Alloys	100



## LIST OF FIGURES

Chapter		Page
3 (Figure 1.)	The Low Temperature Circuit: The components inside the Broken Line are inside the sample can.	48
4 (Figure 1.)	$\rho_0$ versus atomic percent impurity concentration $c$ for <u>K</u> Rb, <u>K</u> Na, and <u>Li</u> Mg alloys. The insert shows the detailed data for dilute alloys. The solid lines indicate the best experimental values from reference 59, and the broken line for <u>K</u> Rb alloys is fit to a formula $\rho_0 = 1.14 \times 10^{-7} (1 - c) \Omega m$ . The open squares are the data measured by Oomi et al.	53
4 (Figure 2.)	$d\rho/dT$ versus $T$ for pure Rb, Li, K, and Na. The RRR for each pure alkali metal approximately has the following value: 400 for Rb, 1000 for Li, 5800 for K, and 4700 for Na respectively.	56
4 (Figure 3.)	$(1/T)d\rho/dT$ versus $T$ for all <u>K</u> Rb alloy samples.	57
4 (Figure 4.)	$(1/T)d\rho/dT$ versus $T$ for all <u>K</u> Na alloy samples.	58
4 (Figure 5.)	$(1/T)d\rho/dT$ versus $T$ for all <u>Li</u> Mg alloy samples.	59
4 (Figure 6.)	$(1/T)d\rho/dT$ versus $T$ for all concentrated <u>Li</u> Mg alloy samples.	60
4 (Figure 7.)	The coefficients of the $T^2$ term $A + B\rho_0$ versus $\rho_0$ for <u>K</u> Rb, <u>K</u> Na, and <u>Li</u> Mg alloy samples. The data were obtained by averaging over the flat regions on figures 3, 4, and 5.	64

4 (Figure 8.)	The coefficients of the $T^2$ term $A + B\rho_0$ versus $\rho_0$ for all <u>KNa</u> alloy samples. Notice the different $\rho_0$ values for each Na concentration.	65
4 (Figure 9.)	X versus T for <u>KRb</u> and <u>KNa</u> alloys. The solid curves are fit to Eq. 4.10, and the broken lines are fit to Eq. 4.5.	66
4 (Figure 10.)	$(1/T)d\rho/dT$ versus $T^{-1}$ , $T^{-2}$ , and $T^{-3/2}$ for the 23.6% <u>KRb</u> alloy.	71
4 (Figure 11.)	X versus T for 23.6% <u>KRb</u> . The long dashed, dashed, and dotted curves are fit to Eqs. 4.7, 4.6, and 4.8 respectively. The solid curve is fit to Eq. 4.6 along with an additional $T^5$ term.	72
4 (Figure 12.)	$d\rho/dT$ versus for <u>KRb</u> and <u>KNa</u> alloys.	74
4 (Figure 13.)	$d\rho/dT$ versus T for <u>LiMg</u> alloys.	75
4 (Figure 14.)	Intercepts of the data in Figures 11. and 12. versus $\rho_0$ .	76
4 (Figure 15.)	$(1/T) d\rho/dT$ versus $T^{-1}$ and $T^{-3/2}$ for 1%, 10%, and 32% <u>LiMg</u> alloys.	78
4 (Figure 16.)	The coefficients of the corresponding $T^{-3/2}$ term in $(1/T)d\rho/dT$ versus $\rho_0$ for all alloy samples. The dashed line is a $\rho_0$ dependence. The solid and long dashed lines are $\rho_0^{5/2}$ dependences for Li and K based alloys, respectively, from electron-electron interaction theory.	80
4 (Figure 17.)	$(1/T)d\ln\rho/dT$ versus T for 9.7% <u>KRb</u> and 1% <u>LiMg</u> alloys for magnetic fields of $B = 0$ (open symbols) and $B = 0.2T$ (filled symbols).	83

4 (Figure 18.)	(1/T)d $\rho$ /dT versus T for <u>K</u> Rb alloys with the solid lines fit to the ineffectiveness of electron-phonon scattering model by Kaveeh and Wiser. The dashed lines indicate the behavior expected from the standard theory. This figure is taken from reference 45.	84
4 (Figure 19.)	(1/T)d $\rho$ /dT versus T for dilute <u>Li</u> Mg alloys with the solid lines fit to the ineffectiveness of electron-phonon scattering model.	89
4 (Figure 20.)	The Lorentz ratio L versus T for 32% <u>Li</u> Mg and 2.2% <u>K</u> Rb alloys, and pure K.	90
4 (Figure 21.)	G versus T for all <u>K</u> Rb alloys, and pure K and Rb.	91
4 (Figure 22.)	G versus T for all <u>K</u> Na alloys, and pure K.	92
4 (Figure 23.)	G versus T for all <u>Li</u> Mg alloys, and pure Li.	97
4 (Figure 24.)	$G_0$ versus $\rho_0^{-1}$ for all alloy samples.	98
4 (Figure 25.)	G versus $T^2$ for <u>K</u> Rb alloys.	104
4 (Figure 26.)	The values of $A + B\rho_0$ determined from Figure 7. against $\rho_0$ for <u>Li</u> Mg alloys (open triangles) and pure Li (full triangle). The broken curve represents the expected behavior for <u>Li</u> Mg with anisotropic scattering, using the parameters suggests by Sinvani et al. Data for <u>K</u> Rb alloys (full circles) and for pure K (open circle) are given in the same units in the inset. Note that both the <u>Li</u> Mg and <u>K</u> Rb data extrapolate linearly to their respective pure metal data points.	105
6 - d $\rho$ /dT	d $\rho$ /dT versus T for the K(7300) samples, which were	

(Figure 1.a) prepared and cooled in a He atmosphere. This figure is taken from Reference 1, but the data have renormalized as described in the text, a few plotting errors have been corrected, some of the nominal sample diameters have been revised as described in the text, and some additional samples from Reference 3 have been added. Two nearly identical samples were always prepared and measured together; for the samples in Figure 1., the data for both wires in a pair was always fairly close. For simplicity, we omit the pairs of the thicker samples; paired samples are indicated by brackets. Two pairs of samples were annealed at room temperature to thin them further after their initial measurements; the arrows indicate the changes which occurred due to these annealings. 139

6 -  $\frac{dp}{dT}$   $\rho(T)$  versus  $T$  for selected data from Figure 1.a.

(Figure 1.b) were integrated by hand. Note that the integrated data have qualitatively similar form to the data of Figure 1.a. 140

6 -  $\frac{dp}{dT}$   $\frac{dp}{dT}$  versus  $T$  for thin K(7300) wires cooled in an

(Figure 2.) Ar atmosphere or in partial vacuum. This figure is taken from Reference 2, but the data have been renormalized as described in the text. The straight line indicating bulk behavior is the same line as in Figure 1. The samples connected by brackets were prepared and measured together. 141

6 -  $\frac{dp}{dT}$  The  $T^2$  coefficient  $A + B\rho_1$  for "bulk" ( $d \geq 1$  mm)

- (Figure 3.) samples of K as a function of residual resistivity  $\rho_1$ . The filled symbols indicate the data used to determine "bulk" behavior for K(7300), K(4800), and K(1700) (for definitions see text) in Figures 1., 2., 5., and 6. respectively. The K(7300) wires had  $d = 1.5$  mm, the K(4800) and K(1700) wires had  $d = 1.0$  mm. The straight line is a best fit to all of the data. Its slope of  $2.5 \times 10^{-5} \text{K}^{-2}$  is somewhat larger than those for Rb ( $1.3 \times 10^{-5} \text{K}^{-2}$ ) and Na ( $0.8 \times 10^{-5} \text{K}^{-2}$ ) impurities in K 142
- 6 -  $d\rho/dT$   $\rho$  versus  $1/d$  for K wires of different diameter and (Figure 4.) different bulk purity. The solid lines have a slope taken from Reference 16. The letter "s" indicates samples with shiny surfaces 143
- 6 -  $d\rho/dT$   $d\rho/dT$  versus  $T$  for the K(1700) samples. Pairs of (Figure 5.) samples prepared together are designated by identical symbols, with the open symbol designating the sample prepared first. Note that in each pair the anomaly is always larger for the sample prepared first, and the anomaly is independent of sample length. After their initial cooling, some of the samples were given room temperature anneals and then cooled and measured again. The progression of behavior after such anneals is indicated by the arrows. 144
- 6 -  $d\rho/dT$   $d\rho/dT$  versus  $T$  for the K(4800) samples. Pairs of (Figure 6.) samples prepared together are designated by identi-

cal symbols, with the open symbol designating the sample prepared first. Note that in each pair the anomaly is always larger for the sample prepared first, and the anomaly is independent of sample length, except for the sample pair denoted by diamonds. This pair was the only one that showed a length dependence approximately proportional to  $L^2$ . After their initial cooling, some of the samples were given room temperature anneals and then cooled and measured again. The progression of behavior after such anneals is indicated by the arrows 145

6 -  $dp/dT$   
(Figure 7.)

Intercomparison of data sets with four different size anomalies involving wires having different thicknesses, different bulk RRRs, and/or cooled in different gases. The curves through the low temperature data are fits up to 1.2K to an equation of the form  $\rho(T) = (A + B\rho_i)T^2 - CT^{7/3}$  where  $(A + B\rho_i)$  is determined by the behavior of thick K wires 146

6 -  $dp/dT$   
(Figure 8.)

$\Delta$  versus  $1/d$  for the data of Figures 1., 2., 5., and 6.  $\Delta$  is the deviation at 1.0K of the anomalous values of  $dp/dT$  in Figures 1., 2., 5. and 6. from the bulk behavior shown in each figure. The letter "s" indicates samples with shiny surfaces. 147

6 -  $dp/dT$   
(Figure 9.)

$\Delta$  versus  $(RRR/d)$  for the data of Figures 1., 2., 5., and 6. The scale for  $\Delta$  versus  $l/d$  is given at the top of the graph. The letter "s" indicates samples with shiny surfaces. 148

6 - $dp/dT$ (Figure 10.)	$\Delta$ versus $\rho_0 - \rho_1$ for the data of Figures 1., 2., 5. and 6. The letter "s" indicates samples with shiny surfaces.	149
6 - $dp/dT$ (Figure 11.a)	Figure 8. with arrows indicating changes in $\Delta$ which occur upon corrosion.	150
6 - $dp/dT$ (Figure 11.b)	Figure 8 with arrows indicating changes in $\Delta$ which occur upon corrosion.	151
6 - $G$ (Figure 1.)	$G$ versus $T$ for He cooled K(7300)	162
6 - $G$ (Figure 2.)	$G$ versus $T$ for Ar and Vac cooled K. For the vacuum cooled samples, about 10 $\mu$ Hg of residual He gas was left in the sample can at room temperature to ensure that the samples would cool properly. This gas affected the $G$ data above 1K, which is thus not as reliable as the remainder of the data in this paper.	163
6 - $G$ (Figure 3.)	$G$ versus $T$ for He cooled K(4800)	164
6 - $G$ (Figure 4.)	$G$ versus $T$ for He cooled K(1700)	165
6 - $G$ (Figure 5.)	$G_0$ versus $1/\rho_0$ for the data of Figures 1. - 4.	166
6 - $G$ (Figure 6.)	Test of $G(T) = G_0 + DT^2$ below 1K for selected data from Figure 4.	167
6 - $G$ (Figure 7.)	The $T^2$ coefficient $D$ from Figure 6., versus $\rho_0^{-1}$ , for the data of Figures 1. - 4.	168
APPENDIX 1:		
Figure A.1	$K^2 / (2k_f)^2$ versus $\alpha$ and $Y$	172

APPENDIX 2:

Figure A.2	$(1/T)dp/dT$ versus $T^{-3/2}$ for all 32% <u>Li</u> Mg alloys	175
Figure 1.3	G versus T for all 32% <u>Li</u> Mg alloys	176



## Chapter 1

### INTRODUCTION

Electrical transport measurements are an important tool for investigating electrons and phonons in metals. Historically such measurements have played an essential role in our understanding of metals. A special class of metals, called simple metals, have distinguished themselves because of their nearly free-electron like Fermi surfaces, for which the theoretical situation is enormously simplified. Among these "simple" metals, the alkali metals are believed to have the simplest electronic structure. Transport measurements on these metals have proved to be the best testing ground for theories concerning scattering of electrons by phonons in a metal.<sup>1</sup> The most recent revival of interest in electrical transport of simple metals started about a decade ago with the advent of high-precision low temperature electrical resistivity measurement techniques which made feasible investigations of some not well explored electron scattering processes, such as electron-electron scattering and inelastic electron-impurity scattering. Over the past decade coupled advances in theories and in experiments on simple metals have greatly enhanced our quantitative understanding of some fundamental electronic transport properties of metals.<sup>2,3,4,5</sup> However, anomalous behavior of the resistivity below 1K, and of a variety of other properties of alkali metals, have been discovered,<sup>6</sup> which are inconsistent with free-electron behavior in a defect free sample. These anomalies have raised the question as to whether a "simple" metal is really simple. The underlying motivation for this dissertation is to try to answer this question through exploring

ultra low temperature resistivity anomalies. If the alkali metals do behave as expected for free-electron metals, we wish to understand anomalies which they display, and these simplest metals should provide a best testing ground to quantitatively elucidate important phenomena like localization<sup>7</sup> and interaction<sup>7</sup> effects which have substantial current interest. On the other hand, if the hypothesis of an intrinsic Charge Density Wave ground state<sup>6</sup> applies to the alkali metals, we hope through this work to find evidence for the CDW.

This dissertation is a report of experimental studies of low temperature transport properties of some alkali metals and their alloys, mainly studies of the effects of adding various impurities to the alkali metals K and Li and of reducing the geometric sizes of K samples. In these studies we have performed a series of ultra-high precision (two parts in  $10^8$ ) and ultra-small signal ( $10^{-15}$  V) electrical resistivity measurements on alkali metals and their alloys at temperature from 4.2K to 80mK, using a SQUID and a high precision current comparator with the aid of a computer averaging technique. Also, thermoelectric ratios of all samples were measured which provided information additional to the electrical resistivity measurements. At temperatures below about 1K, the electrical resistivity and the thermoelectric ratio contain all the information about the macroscopic transport properties of our samples.

The main topics to be presented are: resistivity anomalies and thermoelectric behavior in KRb, KNa, and LiMg alloys below 1K (ch. 4); electron-electron scattering in Li (ch.5); and electronic transport properties of thin potassium wires below 1K (ch.6). Ch.6 is composed of two papers which will appear in Physics Review B.

### 1.1 Alkali Metals

In the past few years the alkali metals have attracted renewed theoretical and experimental interest from two contrasting points of view:

1) The monovalent metals Lithium, Sodium, Potassium, Rubidium and Cesium are generally considered to have the simplest electronic structures of all metals, with nearly spherical Fermi surfaces lying entirely inside the first Brillouin zone, and with no unfilled d or f shells to complicate calculations. Indeed, de Haas-Van Alphen measurements of their Fermi surfaces show the free electron picture to be valid to a remarkable degree,<sup>8</sup> with maximum deviations from sphericity ranging from 0.14% in K to 3.5-5.5% in Li where the Fermi surface comes closest to the Brillouin zone boundaries. Many properties of the alkali metals behave exactly as expected from free-electron-theory.<sup>9</sup> Furthermore, they all have a bcc structure at room temperature, and no superconducting phenomena have been seen in the alkali metals at any temperature yet reached. The alkali metals should serve as ideal testing grounds for theories of very low temperature transport properties, since for free-electron metals the Fermi surface integrals involved in calculating transport properties become tractable.

2) On the other hand, a variety of properties<sup>6</sup> of these metals show anomalous behavior that is inconsistent with free-electron Fermi surfaces. These anomalies have been attributed<sup>6</sup> to the presence of a Charge-Density-Wave (CDW) ground state due to a Fermi-surface instability of simple metals--a theory proposed by Overhauser in 1968.<sup>6</sup> The interest in this possibility has recently been restimulated by the report of CDW satellites in potassium by Giebultowicz et al.<sup>10</sup> from neutron diffraction experiments. However, an alternative interpretation of most of these anomalies involving possible martensitic embryos has also just been proposed.<sup>11</sup>

Among the alkali metals, Potassium is usually most favorable to study, since unlike Lithium and Sodium, which undergo martensitic phase transformations at about 75K and 35K respectively, Potassium does not undergo such a phase transformation. Moreover, the Debye temperature  $\theta$  of both Rubidium and Cesium is unusually low (55K and 40K, respectively) so that for these metals, electron-phonon scattering cannot be neglected until very low temperatures. The presence of electron-phonon scattering complicates investigations of less well understood scattering.(e.g. electron-electron scattering, and electron-dislocation scattering) Besides, Potassium has been claimed to be the best material to exhibit the existence of a CDW.<sup>6</sup>

## 1.2 Simple Transport Properties

The linearized macroscopic transport equations which relate fluxes and forces are:

$$\vec{J} = \vec{\sigma} \vec{E} - \vec{\epsilon} \vec{\nabla}T \quad (1a)$$

$$\vec{q} = T \vec{\epsilon} \vec{E} - \vec{K} \vec{\nabla}T \quad (1b)$$

or, for experimental convenience,

$$\vec{E} = \vec{\rho} \vec{J} + \vec{S} \vec{\nabla}T \quad (2a)$$

$$\vec{q} = T \vec{S} \vec{J} - \vec{\lambda} \vec{\nabla}T \quad (2b)$$

Here, the Onsager Relations have been used to reduce the number of independent coefficients in Eqs.1 and 2 to three.  $\vec{J}$  is the electrical current density,  $\vec{q}$  the heat flow current density,  $\vec{E}$  the electric field, and  $\vec{\nabla}T$  the temperature gradient. For the tensor coefficients:  $\vec{\sigma}$  is known as the electrical conductivity and  $\vec{\rho}$ , its inverse, as the electrical resistivity;

$\vec{\epsilon}$  as the thermoelectric tensor;  $\vec{K}$  the thermal conductivity; and  $\vec{S} = \frac{\vec{J}}{\rho \vec{E}}$  the thermopower.  $\vec{\lambda}$  is related to  $\vec{K}$  by

$$\vec{\lambda} = \vec{K} - T \vec{\epsilon} \rho \vec{\epsilon} \quad (3)$$

At low temperatures, the second term is very small for metals. Due to the cubic symmetry of simple metals, and in the absence of a magnetic field, all the tensors reduce to scalars, which greatly simplifies the situation. Experimentally one can measure each of these coefficients directly by controlling the situation in such a way that either  $\vec{\nabla}T$ ,  $\vec{J}$  or  $\vec{E}$  is made zero.

The thermoelectric ratio,  $G$  defined by

$$G = \frac{J}{q} \text{ at } E = 0, \quad (4)$$

is equal to

$$G = \frac{S}{LT}, \quad (5)$$

where  $L = K\rho/T$ . When elastic electron scattering is dominant,  $L$  becomes a constant:  $L_0 = \pi^2/3(k/e)^2$ --the ideal Lorentz number.  $G$  is favorable to our study because no  $\Delta T$  measurements are required to measure it.  $L_0 = K\rho/T$  further reduces the independent transport coefficients to two. This means, as long as  $L=L_0$ , measuring  $\rho$  and  $G$  of a sample will complete the measurement of all macroscopic transport coefficients of the sample.

In the following we primarily study electron scattering mechanisms by measuring the DC electrical resistivity, for which electrons are completely responsible, and the thermoelectric ratio, which gives additional information complementary to resistivity.

### 1.3 Previous Work

#### 1.3.1 General Background about the Resistivities of Simple metals

The resistivities of simple metals are expected to have the following contributions:<sup>12</sup>

$$\rho = \rho_0 + \rho_{e-e}(T) + \rho_{e-i}(T) + \rho_{e-p}(T) \quad (6)$$

Here  $\rho_0$  is the temperature independent residual resistivity caused by elastic scattering of electrons from impurities or lattice defects. At low temperatures, it's magnitude is much larger than the rest of the terms in Eq.6. The temperature dependent resistivity is composed of an electron-electron component  $\rho_{e-e}$ , an inelastic electron-impurity component  $\rho_{e-i}$ , and an electron-phonon component  $\rho_{e-p}$ .

The existence of the second term  $\rho_{e-e}$ , arising from electron-electron scattering and varying as  $T^2$ , was first predicted half a century ago by Landau and Pomeranchuk<sup>13</sup>. It's coefficient was predicted to be insensitive to small amounts of impurities or defects.<sup>12</sup> Since this term is very small, generally more than four orders of magnitude smaller than the residual resistivity  $\rho_0$ , it was not observed until about 1976 when an experimental breakthrough occurred in the measurement of low temperature electric resistivity. Use of a current comparator, and the application of a SQUID null detector--an extremely sensitive superconducting galvanometer, permitted the attainment of sub-ppm resolution.

The third term in Eq.6 is the contribution to the resistivity from inelastic impurity scattering of electrons; it is the effect of electron scattering by the thermal motion of impurities. It was first proposed by

Koshino in 1960<sup>15</sup> and recalculated by Taylor in 1964<sup>16</sup>, and accurately calculated for KRb alloys by Kus and Taylor in 1980.<sup>31</sup> It was predicted to have the form  $\rho_{e-1}(T) = B\rho_0 T^2$  and to have a very small magnitude in a high purity sample.

The last term, the electron-phonon scattering term, almost completely dominates the temperature variation from high temperatures down to a few K. About a decade ago it was shown<sup>1</sup> that the electrical resistivity of potassium and sodium from the melting point down to a few K could be understood quantitatively, since calculations agreed with experiment to within a few percent with no adjustable parameters. At low temperatures the Debye theory for Normal (N) electron-phonon scattering (ie: scattering not involving a reciprocal lattice vector) predicts  $\rho_{e-p} \propto T^5$ , which is called the Bloch law. For potassium  $\rho_{e-p}$  was found experimentally<sup>17</sup> to have the form

$$\rho_{e-p} = C T^n e^{-\theta^*/T}, \quad (7)$$

where  $\theta^*$  is a characteristic constant and  $n$  is approximately equal to one. This result can be well explained<sup>18</sup> by a combination of electron-phonon Umklapp (U) scattering processes (involving a reciprocal lattice vector) in alkali metals, along with the presence of phonon drag which reduces the Normal electron-phonon scattering part of  $\rho_{e-p}$ .<sup>17</sup> The phonon drag effect is due to the fact that the phonon system is unable to equilibrate itself at low temperatures. Empirically,  $\rho_{e-p}$  was found to be completely ignorable below about 1 K and 10 K for pure K and Li respectively.

Thus for sufficiently low temperatures, from standard theory one would expect the electrical resistivities of the alkali metals to have the form:

$$\rho = \rho_0 + AT^2 + B\rho_0 T^2 \quad (8)$$

where, in the standard picture, the coefficient A is insensitive to very small amounts of impurities, dislocations, etc., and the inelastic impurity scattering term will be small in a high purity sample. Four different experimental groups in the world have made high precision resistivity measurements of alkali metals. They are: the Nijmegen group in the Netherlands; the Israel group; the Alberta group in Canada; and our group at Michigan State University. Before describing our studies, we briefly review the historical developments of both experimental and theoretical investigations of ultra-low temperature resistivities and thermoelectric properties of K, Li, and KRb and LiMg alloys.

### 1.3.2 Previous High Precision Low Temperature Electrical Resistivity Measurements of Potassium

The first experimental search for evidence of electron-electron scattering in the resistivity of alkali metals was made by H. van Kempen et al.<sup>19</sup> in 1976. The samples were prepared by forcing molten high-purity potassium (purity 99.97%) under helium pressure into 1 m long polyethylene tubes with an inner diameter  $d=0.9\text{mm}$ . From 4.2K down to 1.1K the data could be fit to the formula

$$\rho = \rho_0 + A T^s + B T^n e^{-\theta^*/T}, \quad (9)$$

with best fit values:  $\theta^* = 19.9 \pm 0.2\text{K}$ ; n between 0.7 and 1.1; and s between 1 and 2. These results confirmed the importance of U-electron-phonon scattering in K at low temperatures. van Kempen et al. suggested that the  $AT^s$  form, which became dominant below about 1.5K, might represent the first observation of electron-electron scattering in the resistivity of the alkali



metals. However, the constant of proportionality  $A$  was very sample dependent, contrary to theoretical expectations.  $A$  depended strongly on the history of the sample; both  $A$  and  $\rho_0$  were found to decrease upon annealing at room temperature.

In 1978, J.A. Rowlands et al.<sup>17</sup> measured the temperature-dependent electrical resistivity of bare, high-purity potassium samples with diameter  $d=0.79\text{mm}$  and length  $L=1.8\text{m}$ , loosely wrapped into a helical groove in a 3 cm diameter teflon cylinder under a helium atmosphere. They claimed to observe a strong phonon drag effect, since between 4 and 2K the  $\rho(T)$  data for their well-annealed samples fell below the theoretical prediction of the Bloch limit. They reported that a best fit of their data from 0.5K to 1.3K was  $\rho(T) = B T^{3/2}$  with  $B \propto \rho_0$ , although  $\rho(T) \propto T^2$  could not be ruled out due to experimental uncertainties. They postulated that the  $\rho(T)$  might arise from the electron-electron interaction modified by a size effect and possibly also dislocation scattering. Alternatively, Bishop and Overhauser<sup>20</sup> proposed a new mechanism--scattering of electrons by phasons, the collective excitations associated with phase modulation of a CDW--to explain the  $T^{3/2}$  dependence.

The large unexpected variation of the  $AT^2$  term found in the above studies led to both theoretical study by Kaveh and Wiser<sup>21</sup> and further experimental study by B. Levy et al.<sup>22</sup> Kaveh and Wiser proposed a theory of electron-electron scattering in the presence of anisotropic scatterers such as dislocations. They postulated that electron-dislocation scattering in pure alkali metals is highly anisotropic, so that the resulting relaxation time will be anisotropic over the Fermi surface. A detailed discussion of this model will be given in Ch.2, since it led to our new studies of dilute LiMg alloys. In order to test Kaveh and Wiser's theory, Levy et al.

measured samples of diameter  $d=1\text{mm}$  inside polyethylene tubes. They reported that a statistical analysis of the data gave  $\rho = \rho_0 + AT^n$ , with  $n=2.0\pm0.1$  from 1.4 down to 1.1K. In order to study the sample dependence of the electron-electron contribution to the resistivity of K, they increased the sample  $\rho_0$  by heating and cold working their samples. They reported that  $A \propto (\rho_d/\rho_0)^2$ , where  $\rho_d$  is the contribution to  $\rho_0$  arising from electron-dislocation scattering. This result is consistent with the theory of Kaveh and Wiser mentioned above.

We note briefly, since it is not crucial to this thesis, that a recent more precise experimental study by Yu et al.<sup>23</sup>, in our laboratory, which obtained data down to 100mK, showed that K samples prepared in polyethylene (to simulate the conditions used by van Kempen et al. and by Levy et al.) displayed a Kondo like effect below about 1K. The characteristics of this effect were a resistivity minimum and a thermoelectric anomaly, both of which were eliminated by application of a magnetic field. No such effect was found when K samples were prepared inside Teflon tubing or in contact with Kel-F. Therefore, the data of van Kempen et al. Levy et al. most likely contained such a Kondo-like effect, although they could not tell this because their data did not extend below 1K.

In 1982 C.W.Lee et al.<sup>24</sup> in our lab reported 0.1 ppm precision measurements extending down to 70 mK on bare, free-hanging, high-purity potassium samples with diameters ranging from 0.9 to 3mm cooled in Ar gas. Their data varied closely as  $T^2$  from 1K down to about 0.35K, below which the variation was slower than  $T^2$ , in that the data showed an anomalous turn-up in  $(1/T)d\rho/dT$ . The coefficients A in the  $AT^2$  term in the resistivity were found to be practically the same for all high purity samples independent of annealing time at room temperature, and to have a mean value

of  $2.4 \pm 0.2 \text{ f}\Omega\text{m/K}^2$ , consistent with simple electron-electron scattering predictions.<sup>14</sup> No evidence of a size effect was found.

The Kaveh and Wiser theory of anisotropy of electron-dislocation scattering mentioned above, motivated a study of the effect of plastic deformation on the electrical resistivity of pure potassium down to 70mK by M.L. Haerle et al.<sup>25</sup> in 1983 at MSU. They reported that squashing a sample between two plates enhanced the anomalous turn-up at low temperatures found by Lee et al. They suggested an explanation based on a new temperature-dependent scattering process due to inelastic scattering of electrons by vibrating dislocations. The deformed samples showed complete recovery upon annealing at 165K. Further measurements were performed by S. Yin et al.<sup>26</sup> (MSU group) in 1987, who introduced dislocations into K samples by twisting, and cooled the samples down to 20mK. The data are consistent with the models of electron-dislocation scattering.

The contradiction between observations by Rowlands et al. of  $T^{3/2}$  resistivity behavior in  $d=0.8\text{mm}$  K wires cooled in He, and those by Lee et al. of very close to  $T^2$  behavior in  $d=0.9 \text{ mm}$  K wires cooled in Ar, provoked a size effect study by Yu et al. in 1984. They reported that when cooled in He, free hanging K wires thinner than  $d \approx 1 \text{ mm}$  showed anomalous deviations from the  $T^2$  variation expected for electron-electron scattering, and that wires thinner than the bulk mean-free-path for electron-impurity scattering ( $l \approx 0.2\text{mm}$  in their samples) displayed negative values of  $\rho/\text{dT}$ . When the bulk mean free path was reduced to  $0.04 \text{ mm}$  by adding Rb to K, a  $d=0.25 \text{ mm}$  wire of the dilute alloy showed little or no anomaly. The  $T^{3/2}$  resistivity variation of the data of Rowlands et al. with  $d=0.9\text{mm}$  measured from 0.5 to 1K was found to be consistent with the size effect data of Yu et al. for samples with  $d=0.8\text{mm}$  in the same temperature range. Yu et al. tentatively

attributed the anomalous behavior to a combination of electron-electron scattering plus the Gurzhi effect--a reduction in electron-surface scattering due to normal electron-electron scattering. Also it was noted that wires prepared and cooled in Ar gas, or prepared in He but cooled in vacuum, displayed anomalies having the same form as those prepared and cooled in He, but with magnitudes generally representative of thicker wires and with more variation between samples. This was rationalized as being due to the different atmospheres. These measurements stimulated proposals of three alternative models for the anomalous behavior: localization effects<sup>27</sup>; reduction in electron-surface scattering due to electron-phonon scattering<sup>28</sup>; and interference between electron-surface scattering and electron-electron scattering<sup>29</sup>. The authors of these models all challenged the applicability of the Gurzhi effect to the data of the measurements. These models, especially the localization model, led to our new experimental studies as we describe later.

### 1.3.3 Previous Work on High Precision Low Temperature Electrical Resistivity Measurements of KRb Alloys

In 1980 C.W. Lee et al.<sup>30</sup> reported resistivity measurements on bare, free-hanging KRb alloy samples with nominal concentrations of 0.05, 0.13, 0.32 and 2.24 At.% Rb from 180 mK to 4K. Below 1.3K the resistivities were found to have the expected form

$$\rho = \rho_0 + (A+B\rho_0)T^2 \quad (10)$$

where A was consistent with the A found in pure K, and  $B = (8.5 \pm 0.3) \times 10^{-6} / K^2$  was comparable to the theoretical values of  $13.7 \times 10^{-6} / K^2$  from P.L.Taylor<sup>16</sup> and  $12.5 \times 10^{-6} / K^2$  from Kus et al.<sup>31</sup>. Lee et al. claimed

these results as evidence of the contribution to the resistivity from inelastic electron-impurity scattering.

With improved accuracy of temperature measurement, and improved resistivity measurement precision by nearly an order of magnitude, further measurements of KRb alloys up to concentrations of 9.4 at.%KRb were carried out by M.L. Haerle et al.<sup>32</sup> in 1984. They reported data consistent with Eq.10 down to about 0.3K. However, below that temperature they observed divergences from the expected  $T^2$  behavior in the resistivities.(which could not be seen in Lee et al.'s measurements due to their larger uncertainties). These divergences were especially surprising because KRb should be the "simplest" alloy one can imagine. This is due to a combination of the simple electronic structure of K, the complete mutual solubility of K and Rb, and also their practically equal sizes. Haerle et al. characterized the data by using Eq.10 plus an additional term. The best form of this extra term was found to be  $-C\rho_0 T$ . It was also noted that the anomaly in the KRb alloys could not be due to the localization or electron-electron interaction effects because the measured anomalies are about two orders of magnitude larger than the predicted by both theories, and because the anomalies had a different  $\rho_0$  dependence from the predictions--the localization and interaction theories predicted that the extra term should be proportional to  $\rho_0^3$  and  $\rho_0^{5/2}$  respectively. Since no Kondo like anomalies were seen in the thermoelectric properties of the samples, it was noted that the Kondo effect was also unlikely to be the cause.

#### 1.3.4 Previous High Precision Low Temperature Electrical Resistivity Measurements of Pure Li

The electrical resistivity of Li down to Helium temperature was first measured by G. Krill in 1971<sup>33</sup>. The sample was high-purity Li with  $\rho_0 = 73 \text{ p}\Omega\text{m}$ . He reported that for the temperature range 10-40K the data for  $\rho$  varied as  $T^4$ , and for the temperature range 4.5-10K the data for  $\rho$  exhibited a  $T^2$  temperature dependence with a prefactor  $A = 33 \text{ f}\Omega\text{m/K}^2$ . A decade later, M. Sinvani et al.<sup>34</sup> extended measurements to 1.2K. Their sample was high-purity Li with  $\rho_0 = 121 \text{ p}\Omega\text{m}$ . Their data could be well fit to a  $T^2$  dependence with prefactor  $A = 30 \pm 1 \text{ f}\Omega\text{m/K}^2$ . This prefactor is more than an order of magnitude larger than that predicted for the electron-electron scattering contribution to the resistivity of Li by MacDonald et al.<sup>14</sup>, and Sinvani et al. attributed this anomalously large value of A to anisotropy of the electron relaxation time of pure Li, in accord with the theory of Kaveh and Wiser. Later on, we will discuss our new experimental studies designed to test the validity of Sinvani et al.'s attribution. Recently, Yu et al.<sup>23</sup>. (1984) measured free hanging, bare, high-purity Li samples down to 100mK. The data further confirmed the  $T^2$  dependence for  $\rho$  down to 1.2K, and the coefficient A was found to be consistent with the previous measurements. At temperatures below 1.2K, however, the resistivities were found to deviate from a  $T^2$  dependence; a turn up in  $(1/T)d\rho/dT$  was seen. Yu. et al. tentatively attributed this deviation to dislocation vibration effects similar to those seen in K as mentioned above.

### 1.3.5 Previous Work on High Precision Low Temperature Electrical Resistivity Measurements of LiMg Alloys

In 1985 G Oomi et al.<sup>35</sup> reported measurements of the resistivity of three LiMg alloys with magnesium concentrations of 1.0, 5.0 and 10at.% from 2 to 60K. Below 10K a term proportional to  $T^2$  and to the residual resistivity was identified and associated with inelastic impurity scattering of electrons. The data could be fit to Eq. 10 with  $A = (4.0 \pm 0.6) \times 10^{-14} \Omega \text{mK}^{-2}$  and  $B = (1.6 \pm 0.2) \times 10^{-6} \text{K}^{-2}$ . Within the uncertainties, the value of A was in agreement with that obtained for pure Li, as noted above, and the value of B was comparable to two theoretical predictions: one by P.L. Taylor<sup>16</sup>  $B = 3.4 \times 10^{-6} \text{K}^{-2}$ ; and one by Kus et al.<sup>31</sup>  $B = 3.1 \times 10^{-6} \text{K}^{-2}$ , when these were evaluated using  $\rho_0 = 1.0 \times 10^{-8} \Omega \text{m}$  for 1at.% LiMg. However, due to large uncertainties of the data, the detailed picture of how A changed upon adding Mg to Li was still not completely clear.

### 1.3.6 Previous Work on High Precision Low Temperature Electrical Resistivity Measurements of KNa Alloys

No measurements have been reported prior to ours.

### 1.3.7 Previous Work on the Thermoelectric Ratio G of K, KRb, KNa, Li and LiMg

More than twenty years ago, the Canadian group of D.K.C. MacDonald<sup>36</sup> measured the thermopower S of pure K, pure Li, dilute KRb and KNa alloys, and dilute LiMg alloys at temperatures from 3K down to 100mK. They approximated their thermopower data with the expression

$$S = AT + BT^3 + C \exp(-\theta^*/T), \quad (11)$$

where the first term is due to electron diffusion ( $S_{\text{diff}}$ ); the second term is due to Normal phonon drag ( $S_{\text{ph}}^{\text{N}}$ ); and the last term is due to Umklapp phonon drag ( $S_{\text{ph}}^{\text{U}}$ ). This form for  $S$  was based upon the predicted low temperature behavior for a simple, free electron metal with a spherical Fermi surface that does not contact the Brillouin Zone boundary. For K samples with RRRs ranging from 4000 to 10,000 and with diameters from 0.07 to 0.8mm, MacDonald et al. found the data could all be fit to Eq.11, but the data showed a large variability between samples and also in the same sample measured at different times. They concluded that there was no obvious dependence on the residual resistivity or on the diameter of the specimen. The thermopower of Li was found to be linear with  $T$  below 2 or 3K, which is what would be expected for the electron diffusion component alone. MacDonald and coworkers reported that the effects of alloying on the phonon drag component of dilute K and Li alloys were to decrease the magnitude of both normal and Umklapp phonon drag. The diffusion thermopowers of all the dilute alloys were found to obey the Gorter-Nordheim rule:<sup>36</sup>

$$S_{\text{diff}} = (\rho_p S_p + \rho_i S_i) / (\rho_p + \rho_i), \quad (12)$$

which distinguished two contributions to  $S_{\text{diff}}$  :  $S_p$  due to the host metal and  $S_i$  due to the impurity. However, the signs and the magnitudes of the impurity parts of  $S_{\text{diff}}$  for KRb, KNa, and LiMg alloys could not be understood by the simple model of the scattering by impurities of free electrons on a spherical Fermi surface.

In 1974, Nielsen and Taylor<sup>37</sup> investigated theoretically the many-body contributions to the electron diffusion thermopower. They found that some second-order corrections to the matrix elements for electron scattering involving intermediate virtual phonon states could make a large contribution to the diffusion thermopower while leaving the conductivities



essentially unaltered. Based on this model, they explained the signs and magnitudes of the diffusion thermopowers of KRb and KNa alloys.

In 1980, C.W. Lee<sup>38</sup> reported G measurements on pure K and KRb alloys from 4.2K down to 80mK. They fit their pure K data to the form

$$G = G_0 + B^* T^2 + (C^*/T) e^{-\theta^*/T} \quad (13)$$

This is approximately derived from Eq.11 as  $G = SL/T$  and  $L \approx L_0$  at low temperatures (for K,  $L=L_0$  only below 1K). In Eq.13,  $G_0$  is the diffusion term,  $B^* T^2$  the Normal phonon drag term, and the exponential is the Umklapp phonon drag term. For pure K, Lee et al. found  $G_0 = -0.03 \pm 0.03 V^{-1}$ ,  $B^* = -0.30 \pm 0.01 V^{-1} K^{-2}$ , and  $\theta^* = 23 \pm 2 K$ . These results were consistent with those of MacDonald et al. For KRb alloys, Lee et al. found the same three terms as above, with the normal and Umklapp phonon drag terms quenched more and more as the impurity concentration increased. The diffusion term  $G_0$  was found to approximately obey the Gorter-Nordheim rule with  $G_1 = +0.48 \pm 0.01 V^{-1}$ , the Rb impurity scattering part of the diffusion thermoelectric power.

In 1983, M. L. Haerle et al.<sup>25</sup> reported G measurements on deformed pure K samples from 4.2 to 0.08K. They claimed that Eq.13 could fit their data for  $T \geq 0.2 K$ , with  $\theta^* = 18 \pm 2 K$ ,  $G_0 < 0$ ,  $B^* < 0$ , and  $C^* > 0$ . Below 0.2K, they found G of the deformed samples to deviate from Eq.13. An additional term  $A^* T$ , contributed by dislocation scattering, was needed in Eq.13 to fit their data.

Recently, Yu et al.<sup>23</sup> measured G for thin K wires and KRb alloys up to 9.4at.%. The thin K data were reported fit to Eq.13 well. They found the magnitude of  $G_0$  became larger, and the magnitudes of  $B^*$  and  $C^*$  became smaller, as the sample diameter decreased. They also reported that G for

two 0.07at.% KRb samples were well fit by Eq.13 with  $G_0 = 0.35 \pm 0.05 V^{-1}$ ,  $B^* = -0.20 \pm 0.01 V^{-1} K^{-2}$ ,  $C^* = 2570 \pm 270 V^{-1} K$ , and  $\theta^* = 23$ . For 9.4%KRb they found the simple Eq.13 could no longer be fit to the G data. No explanation was provided.

#### 1.4 Present Thesis

##### 1.4.1 Low Temperature Electrical Resistivity

As noted about, it has been shown by Lee et al.<sup>30</sup> and Yu et al.<sup>23</sup> that the behaviors of pure, bulk, free-hanging K and Li samples are as expected from standard theory (representative primarily of standard electron-electron scattering) down to at least 0.3 and 1K for K and Li respectively. It also has been shown that adding small amounts of Rb to K produces the behavior expected for inelastic electron-impurity scattering.<sup>38</sup> However, at low enough temperatures, resistivity anomalies which deviate from conventional theories were discovered in pure K, in thin K wires, in Li, and in KRb alloys by previous investigators in our laboratory. The sources of most of these anomalies are not yet understood. This dissertation is a report of three additional experimental studies designed to further extend our understanding of the ultra-low temperature resistivity of alkali metals and their alloys. The three specific topics which we focused on are the following:

##### 1. Low temperature resistivities of different alkali alloys and concentrated alkali alloys

The resistivity anomaly found in KRb alloys below 0.5K by Haerle and Yu et al.<sup>32</sup> seems very interesting. The anomaly was found to be too big to be due to localization or interaction, and the G behavior did not support a

Kondo effect either. We pursued the sources of the anomaly in two directions:

(a) To see whether the anomalous behavior is not unique to KRb alloys, and thus likely to be fundamental, we measured KNa and LiMg alloys. KNa was measured because Na has a very different ion size from K. LiMg was measured because Mg has a different number of valence electrons from Li, and also because the alloys undergo a phase transition to a different crystal structure upon cooling. Li was chosen because it is the only alkali metal which has significant solubility for heterovalent solutes.<sup>39</sup> We also investigated the influence of a magnetic field on the anomaly to test for a Kondo effect.

(b) To see whether the anomaly approaches the behavior predicted by Localization and Interaction as the impurity content increases, (i.e. higher  $\rho_0$ ), we extended our study to more concentrated KRb and LiMg alloys (KNa alloys have a very limited solubility range). This extension is significant because these alloys consist of metals with much simpler electronic structures than any previously used to study localization and interaction effects, and because the dominant inelastic scattering mechanism in these alloys--inelastic electron-impurity scattering--differs from the inelastic electron-phonon scattering which dominated previous studies. The LiMg alloys are of special interest since their  $\rho_0$  can be made comparable to those studied in other systems that show localization and interaction effects.

## 2. Electron-electron scattering in Li: explaining the unexpectedly large A and testing Kaveh and Wiser's theory

As noted above, the unexpectedly large magnitude of A, the electron-electron scattering contribution to the resistivity in pure Li, was a

puzzle. As expected for electron-electron scattering, this  $A$  was found to be insensitive to small amounts of impurities or defects. However, it is about one order of magnitude larger than calculated for Li in the BCC structure with a free electron Fermi surface. In contrast, the experimental results are in good agreement with calculations in Al<sup>40</sup> and K.<sup>14</sup> Among the alkali metals, Li is most distorted from a spherical Fermi surface, and Li also undergoes a phase transformation at about 75K. The large value of  $A$  is surely related to this phase transformation. However, this can happen in two very different ways: (a) According to Kaveh and Wiser's anisotropic electron-dislocation theory, the large magnitude of  $A$  is caused by the highly anisotropic scattering of dislocations or defects introduced into Li during its transformation. This mechanism is very sensitive to addition of a small amount of impurities since electron-impurity scattering should be nearly isotropic. (b) The complex Fermi surface of Li caused by its phase transformation can produce a large value of  $A$  due to increased Umklapp electron-electron scattering. This mechanism will not be affected by adding small amounts of impurities to the sample. We thus made detailed measurements of dilute LiMg alloys to elucidate whether the unusually large value of  $A$  in pure Li is indirectly determined by anisotropic scattering according to Kaveh and Wiser's model, or directly determined by the change in the Fermi surface.

### 3. Experimental tests of proposed models of size effect in K

The discovery of a "size" effect anomaly in high-purity thin K wires by Yu et al.<sup>41</sup> stimulated substantial theoretical interest, as noted above. To clarify the physical mechanism behind this phenomenon, we conducted new experiments in the following specific directions: (a) To check for the sample length dependence predicted for  $dp/dT < 0$  by Farrell et al.<sup>27</sup>, we

measured samples having different lengths and with diameters less than 0.1mm. (b) Surface contamination has been shown to play a role in anomalies in  $K$  associated with torque anisotropy<sup>42</sup> and optical absorption.<sup>43</sup> To investigate the role of surface contamination, (involving visible whitening of the sample surface which was inevitable in the previous measurements), we measured samples with different surface conditions: some  $K$  samples were deliberately corroded by keeping them inside the sample can for a long time at room temperature; others were corroded by bringing them out to the air for a while; and in the later runs thin  $K$  wires were successfully kept shiny after the measurements. (c) To see effects of the penetration of surface corrosion into the body of the sample, samples were made by mixing pure  $K$  with corroded white material. (d) To investigate the influence of the electron mean free path on the "size" effect, we prepared our samples from two different bulk purity sources of potassium (both of which had RRRs different from that used by Yu et al.). Also, to check that greatly reducing the electron mean free path does indeed greatly reduce the "size" effect, we measured  $K(0.1\%Rb)$  samples with diameter 0.1mm, which was much larger than the electron mean free path of the sample.

#### 1.4.2 Thermoelectric Ratio $G$

Thermoelectric properties contain information about electron and phonon scattering in metals which is complementary to that obtained from electrical resistivity measurements. In this study we have performed thermoelectrical measurements on all of our samples in addition to resistivity measurements.

## Chapter 2

## THEORY

2.1 Inelastic Electron-Impurity Scattering

In the usual analysis of the electric conductivity of metals, the impurity atoms are regarded as static defects. This leads to a temperature-independent residual resistivity  $\rho_0$ . However, the impurity atoms actually oscillate. The electrons will then experience additional inelastic scattering from the impurity ions, and this leads to an effect called the Koshino-Taylor effect which was first proposed by Koshino<sup>15</sup> in 1960. He showed that an additional  $T^2$  dependent term should be expected at low temperatures due to incoherent scattering which takes into account the thermal motion of an impurity ion. P.L. Taylor (1962)<sup>16</sup> criticized Koshino's model on the grounds that, in an expansion of the lattice displacements, Koshino had omitted the second-order processes in electron-phonon-impurity interaction which give a contribution almost cancelling the first-order processes. In 1963 Koshino<sup>15</sup> calculated the effect to second order and showed that at high temperatures the effect is cancelled out, but at low temperatures the cancellation only reduces the effect by a factor of two from his previous estimation. In 1964 Taylor<sup>16</sup> recalculated this effect by considering first-order processes in inelastic scattering and zeroth- and second-order processes in elastic scattering and assuming dilute alloys with the impurity having an atomic mass close to that of the solvent. Using the Debye model for phonons, he derived an explicit result:

$$\rho = \rho_0 ( 1 - 2W_0 + 2W_1 T^2 ) \quad (2.1)$$

where  $2W_0 = 3\hbar^2 K^2 / 4Mk_{BD}$  and  $2W_1 = \pi^2 \hbar^2 K^2 / 2Mk_{BD}^3$ . Here  $k_{BD}$  is the Debye energy,  $M$  is the mass of a solvent ion assumed to be equal to that of the impurity, and  $K = \langle \vec{k} - \vec{k} \rangle$  is the average scattering vector.  $2W_0$  and  $2W_1$  are typically of order  $10^{-2}$  and  $10^{-5}$  respectively. The term  $\rho(T) = 2W_1 \rho_0 T^2$  is the  $\rho(T) = BT^2$  term in Eq. 8 arising from incoherent electron scattering. Thus

$$B = 2W_1 = \pi^2 \hbar^2 K^2 / 2Mk_{BD}^3 \quad (2.2)$$

The resistivity in Eq. 2.1 can also be separated into two terms, elastic and inelastic:

$$\rho = \rho_0(1 - 2W_0 - 2W_1 T^2) + 4\rho_0 W_1 T^2 = \rho_{e-l}^{el} + \rho_{e-l}^{inel}. \quad (2.3)$$

At low temperatures the Debye-Waller factor has the form  $e^{-2W} = \exp\{-2(W_0 + W_1 T^2 + \dots)\}$ , thus the first term in Eq. 2.3, due to elastic electron-impurity scattering, is just the expansion in powers of  $T^2$  of the low temperature Debye-Waller factor. From Eq. 2.3 we also see that the elastic electron-impurity scattering reduces the inelastic scattering effect by half, and reduces the residual resistivity  $\rho_0$  by  $2W_0$  at the zero of temperature, which is a quantum zero-point motion effect. Recently several authors<sup>38,35</sup> estimated the magnitude of  $B$  by taking  $K \approx 2k_F$ , which approximately corresponds to isotropic scattering. (Ap. 1) They found that the calculations gave magnitudes close to the experimental results for KRb and LiMg alloys.

In 1966 Kagan and Zhernov considered the more general case that electrons are not only scattered by the impurity ion itself, but also by a noticeable number of atoms that surround the impurity atom and whose oscillations are perturbed. In addition to the same incoherent terms obtained

by Taylor, they derived another term, due to coherent inelastic electron-impurity scattering, which they estimated might be of the same order as the incoherent term at temperatures near 1K. This term has the form

$$\Delta\rho \propto \rho_0 S T^5 / \theta_D^6 \quad (2.4)$$

where  $S = (M_1 - M_0)/M_0 + (Z_1 - Z_0)/Z_0$ .  $Z_0$  and  $Z_1$  are the charge of the host ion and the charge of the impurity ion,  $M_0$  and  $M_1$  are the mass of the host ion and the mass of the impurity ion. Thus, this term is positive for KRb and LiMg alloys but negative for KNa alloys.

Kus et al.<sup>31</sup> in 1979 made a more accurate calculation of  $\rho_{e-1}^{el}$  and  $\rho_{e-1}^{inel}$  (Eq.2.3) for KRb and LiMg alloys. The derivation was made without the Debye temperature approximation and contained the effect of the mass difference between host and impurity ions. By using the phonon dispersion curve and the RPA screened Ashcroft pseudopotential of K together with a Rb Ashcroft pseudopotential in which the potential radius was determined from the experimental residual resistivity results, they obtained  $B = 12.5 \times 10^{-6} K^{-2}$  for KRb alloys. For LiMg alloys the valence difference means that the RPA screening is not very reliable. However, the same procedure was used to estimate B for LiMg, and they obtained  $B = 3.1 \times 10^{-6} K^{-2}$ .

Very recently in association with the calculation of a new resistivity term caused by a phonon vertex correction, see below, Hu and Overhouser re-derived Taylor's formula. However, they criticised the use of  $K = 2k_F$  as an approximation. ( $2k_F$  is the maximum momentum transfer). By assuming a Gaussian pseudopotential for Rb in K (see Ap.1) with the scale factor  $\alpha=1$ , they argued that the Koshino-Taylor term is too small to account for the experimental results in KRb alloys. Their result is very sensitive to the choice of  $\alpha$  (Ap.1), and thus without justification of a specific value of  $\alpha$  their argument is weak.



Since the pseudopotential used in Kus's calculation of LiMg is not proper, we decided to try an alternative estimation by using a screened Coulomb potential which should be a reasonable approximation of the scattering potential for a heterovalent impurity such as Mg in Li.<sup>44</sup> With the only parameter in the screened Coulomb potential being determined from the experimental value of  $dp_0/dc$  (the change of the residual resistivity per atomic percent impurity in the alloy), we calculated K in Taylor's expression for LiMg alloys, and obtained (Ap.1)  $K = 0.77(2k_F)$ . The result of B gives a better agreement with experiment, as shown in table 2 in ch.4.

Very recently Kaveh and Wiser<sup>45</sup> suggested that the theory of inelastic electron impurity scattering should be modified based on the Pippard ineffectiveness condition--that long wavelength phonons are ineffective in scattering electrons for which the electron mean free path  $l$  is shorter than the phonon wavelength. They proposed that in deriving the second term in Eq.2.3 there should be a cutoff in  $q$  space in the integral over all phonon states  $q$  in the first Brillouin zone. They wrote the coefficient of the second term in Eq.2.3 as

$$D(T) = C \int_{q>q_{\min}}^3 \{ T^3 (e^{h\omega(q)/kT} - 1) \times (1 - e^{-h\omega(q)/kT}) \}^{-1}, \quad (2.5)$$

where  $C$  is a temperature-independent constant and  $\omega(q)$  is the frequency of the phonon of wave vector  $q$ . Assuming that the electron-phonon interaction is cut off at  $q_{\min} = \pi/l$ , Eq.2.5 modifies  $D$  to be a positive constant

$(4W_1)$  at high temperatures and to smoothly change to a negative constant  $(-4W_1)$  at zero temperature. The  $C$  in Eq.2.5 was determined from experimental data at high temperatures, and  $l$  was obtained from  $p_0$  measurements. Since

$\rho_0$  provides the value of the "transport" electron mean free path  $l_{tr}$ , they used the Born-approximation expression for  $\rho_0$  and an Ashcroft pseudopotential appropriate to homovalent impurities to estimate the ratio of  $l$  to  $l_{tr}$  as

$$l = 0.5l_{tr} \quad (2.6)$$

For heterovalent impurities, (Mg in Li), we use a screened Coulomb potential<sup>44</sup> which yields

$$l = 0.66l_{tr} \quad (2.7)$$

Kaveh and Wiser claimed this modification of the Koshino-Taylor term gave an excellent fit to the low temperature anomalous resistivities of KRb alloys up to 23.6%.

## 2.2 Temperature-Dependent Elastic Scattering Contribution to the Impurity Resistivity

Very recently S. Hu and A.W. Overhauser proposed a model<sup>46</sup> in which the many-body electron-phonon vertex correction, together with a partial failure of Migdal's theorem, leads to a new temperature-dependent term in the electrical resistivity caused by elastic impurity scattering.

$$\Delta\rho \propto \lambda \rho_0 (T/\theta_D)^2 \ln(\theta_D/T) \quad (2.8)$$

where  $\lambda$  is the electron-phonon coupling constant. As mentioned above, they argued that the magnitude of the Koshino-Taylor term should be smaller than the experimental results based on their evaluation of the average scattering vector  $K$  by a Gaussian potential with  $\alpha=1$ . With this Gaussian potential ( $\alpha=1$ ) they calculated the magnitude of the term in Eq.2.8, and obtained results comparable with the KRb alloy data. Thus, Hu and Overhauser proposed that the correction to the electron-impurity scattering

by the many-body effects of electron-phonon interaction should account for the  $T^2$  term in the alloy resistivities. However, since no justification of the important parameter  $\alpha$  was given, the magnitude of the term in Eq.2.8 seems not clear.

### 2.3 Kondo Effect

In 1964 Kondo<sup>47</sup> proposed a theory to explain the striking phenomena in which the resistivities of alloys made of a non-magnetic host metal with a magnetic impurity (concentrations of ppm are often enough to show the effect) fall as temperature rises at low temperatures. Kondo assumed that the impurity ions were isolated and formed localized moments which were paramagnetic, and that the nearby electron gas formed spatially extended spin correlations with relatively low energy. The interaction between a conduction electron and the ion was represented by an isotropic s-d exchange interaction of the form

$$H = -J \vec{S}_s \cdot \vec{S}_d$$

$J$  is the s-d exchange coupling constant, and  $\vec{S}_s$  and  $\vec{S}_d$  are the conduction electron spin and the impurity spin. This contribution to the electron scattering is distinctive in that, in contrast to scattering by an ordinary potential, the electron spin may be flipped in the process. Calculated in first order interaction this simply gives an additional temperature independent resistivity. However, Kondo found that the second-order scattering processes give a temperature dependent resistivity. In particular, if  $J$  is negative, the resistance due to this scattering falls as the temperature rises. An outline of his derivation is as follows. The matrix element of the transition from  $k\uparrow$  to  $k\uparrow$  (the other possibilities give same results) can be written as

$$|\langle k' + | -J\vec{S}_s \cdot \vec{S}_d | k + \rangle|^2 = \left(\frac{J}{2N}\right)^2 \langle S_{dz} \rangle^2 \left[1 - \frac{J}{2N} \sum_{k''} \frac{2f(k'') - 1}{\epsilon_k - \epsilon_{k''}}\right]^2 \quad (2.9)$$

where  $f(k'')$  is the Fermi function for the intermediate state  $k''$ . It is this  $f(k'')$  (originating from the Pauli principle) which produces the temperature dependent scattering. Evaluating the Fermi function near  $T=0$  the  $\sum_{k''}$  becomes

$$\int \frac{d\epsilon'' [2f(\epsilon'') - 1]}{\epsilon_k - \epsilon''} \approx -2 \ln \left| \frac{\delta\epsilon}{E_f} \right| \quad (2.10)$$

where we let the initial state energy differ from the Fermi energy by  $\delta\epsilon$  (which is the order of  $k_B T$ ). Thus the additional resistivity from this effect has the form<sup>48</sup>

$$\rho_K \approx c \rho_m \left[ 1 + \frac{J}{E_f} \ln \left( \frac{k_B T}{E_f} \right) \right], \quad (2.11)$$

where  $c$  is the impurity concentration and  $\rho_m$  is the first Born scattering term. The contribution to the resistivity of Eq.2.11 is called the Kondo effect. This effect is expected to have a strong magnetic field dependence, since the application of a magnetic field can be thought<sup>48</sup> of as equivalent to displacing the initial state from the Fermi energy by the Zeeman energy,  $\delta\epsilon = -\mu_0 H$ . We see from Eq.2.10 that this reduces the divergence just as does a change in temperature. Further increasing an external field to  $g\mu_B \approx kT_K$  will break up the spin correlated state of the conduction electrons near the ion, removing the local spin degrees of freedom necessary for Kondo scattering, and thus destroying the Kondo effect. Estimation of other higher-order terms in the scattering led to an energy dependent resistivity and this was expected to give a giant thermoelectric power.

## 2.4 Two-level Systems

In order to explain the logarithmic temperature dependent resistivity anomaly found in disordered metals which showed no magnetic field dependence, Cochrane et al.<sup>49</sup> proposed a "two level systems" model. (TLS) In analogy to the Kondo model, the TLS are internal degrees of freedom which result from atoms being free to tunnel between two alternative positions of local equilibrium. Such double wells are assumed to result from the disordered structure and to disappear on crystallization. In order to have a mechanism similar to the Kondo effect, Cochrane et al. further postulated that the electron--perhaps corresponding to d-like wave functions localized around the atom--could distinguish between the two positions of the tunneling atom, a degree of freedom analogous to the spin degree of freedom for the electrons in the Kondo model. A derivation similar to that of the Kondo effect gives the resistivity caused by TLS as

$$\Delta\rho \propto \ln[k_B^2(T^2 + T_K^2)/D^2], \quad (2.12)$$

where  $T_K$  is a temperature which is analogous to Kondo temperature, and  $D$  is the electron band width. More recently, it has come to be generally believed that the logarithmic behavior of the resistivities of disordered metals is dominated by quantum localization and interaction effects. The applicability of the TLS thus remains cloudy.

## 2.5 Weak Localization and Interaction

The periodicity of the crystal permits the classification of electronic wave functions as Bloch waves. However, the crystalline state is an ideal theoretical situation. Traditionally, the weak-disorder limit is described by the scattering of Bloch waves by impurities, and this leads to a Boltzmann transport equation for the quasiparticles. In the past few years there has been a growing realization that disordered materials cannot

be understood by forcing them into the mold of ordered systems. New concepts must be introduced which treat the disorder from the beginning. The new understanding is based on advances in two different areas of the problem.

The first is the problem of Anderson localization. The traditional view of the electronic wave function in a random potential had been that scattering causes the Bloch waves to lose phase coherence on the length scale of the mean free path  $l$ . Nevertheless, the wave function remains extended throughout the sample. In 1958, Anderson<sup>50</sup> pointed out that if the disorder is very strong, the wave function may become localized, in that the envelope of the wave function decays exponentially from some point in space. Thus the electrons are diffusively instead of freely propagating. For weak disorder, i.e., for  $(k_F l)^{-1} \ll 1$ , it is possible to calculate corrections to the Boltzmann transport theory for  $\sigma$  by using diagrammatic perturbation in the first principles calculation of a noninteracting electron gas which is weakly scattered by rigid random impurities. It turns out that to higher order in  $(k_F l)^{-1}$  there are significant scale-dependent corrections to conductivity arising from singular backscattering. Thus, the physics of the weak localization phenomenon can be interpreted as an echo of plane wave scattered by impurities.  $(k_F l)^{-1} \ll 1$  can also be called the quantum interference regime. There are two different lifetimes of the conduction electrons, the elastic lifetime  $\tau_0$  and the inelastic lifetime  $\tau_1$ .  $\tau_0$  is the lifetime of the electron in an eigenstate of momentum, whereas  $\tau_1$  is the lifetime in an eigenstate of energy. At low temperature the latter can exceed the former by several order of magnitude.

As a consequence, a conduction electron in state  $k$  can be scattered by impurities without losing its phase coherence. Since the electron has wave-like character, in reality one has to consider two partial waves of the electron which propagate on a closed loop in opposite directions. (This has been beautifully demonstrated in the experimental observation of Flux Quantization in Normal Rings.<sup>51</sup>) If one considers the two partial waves to interfere, this gives twice the probability to return to the origin as compared to classical diffusion (their amplitudes add instead of their intensities). This quantum peak in the diffusion profile can be considered as an echo. The tendency of the electron to return to its starting point is called weak localization because it is thought of as a precursor of localization. Therefore, there are corrections of quantum mechanical interference to the classical transport theory which assumes that the particle moves quasiclassically between the collisions. It can be shown theoretically, that the resulting conductivity is no longer a material constant but a length-dependent conductivity. Thouless<sup>52</sup> (1977) pointed out that inelastic scattering introduces random fluctuations in the time evolution of an electronic state. Such fluctuations destroy the coherent phase and, thus, limit the quantum interference necessary for localization; the scale-dependent localization effects are cut off beyond  $L_{th}$  (coherent length). This brings the temperature into play.

$$L_{th} = (D\tau_i)^2 \quad (2.13)$$

where  $D$  is the diffusion constant. Including only the singular back scattering process, and supposing  $\tau_i \propto T^{-p}$ , the correction to conductivity, arising from localization has the form<sup>7</sup>

$$\Delta\sigma_{lo}(T) = \frac{e^2}{\hbar} \frac{T^{p/2}}{2a} \quad (2.14)$$

where  $L_{th} = a T^{-p/2}$ . Thus, the correction to  $(1/T)d\rho/dT$ , which we are interested in, is

$$\frac{1}{T} \frac{d\rho_{lo}}{dT} = - \frac{\rho_0^2}{T} \frac{d\sigma_{lo}}{dT} \quad (2.15)$$

where we take  $\rho \approx \rho_0$  in the prefactor.

The second aspect of the disordered problem is the interaction among electrons in the presence of a random potential. The fact that electrons are diffusively instead of freely propagating leads to a profound modification of the traditional view based on the Fermi-liquid theory of metals. It was first predicted by Altshuler and Aronov<sup>53</sup> in 1979 that Coulomb interactions in a disordered electron gas lead to another resistivity anomaly. The physical idea is that since the electron motion is diffusive, the electrons spend a longer time in a given region in space relative to the plane-wave state, and their interaction is enhanced. The effective electron-electron interaction is retarded. A sudden change of the charge distribution in a disordered metal cannot be screened immediately, since the electrons can only propagate by diffusion they need time to screen the charge distribution. The conductivity can be calculated using the Kubo formula to lowest order in the interaction, which gives the following corrections to the conductivity of three dimensional systems:<sup>7</sup>

$$\Delta\sigma_{in} = \frac{e^2}{\hbar} \frac{1}{4\pi} \frac{1.3}{\sqrt{2}} \left( \frac{4}{3} - \frac{3}{2} \tilde{F} \right) \sqrt{kT/D} \quad (2.16)$$



where  $\tilde{F} = [32/3][1+3F/4 - (1 + F/2)^{3/2}]F$ ,  $F = (1/x)\ln(x+1)$ ,  $x = (2k_f/k_0)^2$ , and  $k_0$  is the Thomas-Fermi screening vector. This gives a correction to  $(1/T)d\rho/dT$  of the form

$$\frac{1}{T} \frac{d\rho}{dT} = - \frac{\rho_0^2}{T} \frac{d\sigma_{in}}{dT} \quad (2.17)$$

In the alloy systems we studied, the dominant electron inelastic scattering term is  $\rho_{e-i}^{inel} = 2B\rho_0 T^2$ , as indicated from Eq.2.2 and 2.3. Thus  $1/\tau_i = (ne^2/m)2B\rho_0 T^2$ , where  $n$  is electron density. In Eq.2.16  $D$  is related to the conductivity by the Einstein relation  $\sigma = D(e^2/\hbar)(dn/d\epsilon_f)$ . By using the free electron value of the Fermi wave vector  $k_f$ , we can calculate the magnitudes of the quantum correction terms of Eq.2.14 and 2.16. Assuming that alloying does not change the host Fermi wave vector,<sup>44</sup> we have for the K and Li based alloys

$$\Delta \frac{1}{T} \frac{d\rho}{dT} = -9.6 \times 10^7 \rho_0^3 T^{-1} - 3.7 \times 10^4 \rho_0^{5/2} T^{-3/2} \quad (\Omega m T^{-2}) \quad (2.19)$$

$$\Delta \frac{1}{T} \frac{d\rho}{dT} = -7.8 \times 10^7 \rho_0^3 T^{-1} - 5.7 \times 10^4 \rho_0^{5/2} T^{-3/2} \quad (\Omega m T^{-2}) \quad (2.20)$$

respectively. At temperatures below about 0.6K, for all of our alloys with  $\rho_0 < 17 \times 10^{-8} \Omega m$ , the second term in Eq.2.19 and 2.20, (arising from the interaction effect) has a magnitude about one order bigger than the first term (arising from the localization). Thus the interaction effect is predicted to be dominant below that temperature. Considering the change of electron density from the host in the high concentration LiMg alloys, Eq.2.20 can be represented as

$$\Delta \frac{1}{T} \frac{d\rho}{dT} = -4.2 \times 10^6 n_c^{2/3} \rho_0^3 T^{-1} - 2.6 \times 10^4 n_c^{1/6} \left( \frac{4}{3} - \frac{3}{2} \tilde{F} \right) \rho_0^{5/2} T^{-3/2}$$

$(\Omega m T^{-2})(2.21)$

where  $n_c \times 10^{27}$  is the electron density of the LiMg alloy with concentration  $c$ . Assuming  $n_c \times 10^{27} = (1-c)n_{Li} + cn_{Mg}$ , the correction to the magnitude of the interaction term in Eq.2.21 is estimated to be less than 5%. Thus, the correction is small, and we can use Eq.2.20 to compare with the experimental data.

## 2.6 Electron-Electron Scattering

An electron-electron resistivity term was predicted to vary with  $T^2$  a long time ago by Landau and Pomeranchuk.<sup>13</sup> (1936) In order to understand such a temperature dependence, and the more recent developments on the magnitude of  $\rho_{e-e}$ , it is necessary to take a closer look at the Boltzman transport mechanism for  $\rho_{e-e}$ .

The electron equilibrium state density in  $\vec{k}$  space is represent by the Fermi-Dirac function  $f^0(\vec{k})$ . Deviations from this equilibrium distribution, caused by an external electrical field, are considered to first order and characterized by a deviation function  $\phi$ :

$$f(\vec{k}) = f^0(\vec{k}) - \phi(\vec{k}) \frac{\delta f(\vec{k})}{\delta \epsilon(\vec{k})}$$

The linearised BTE then reads:

$$-e\vec{v}(\vec{k})\vec{E} \frac{\delta f(\vec{k})}{\delta \epsilon(\vec{k})} = P\phi(\vec{k})$$

where  $P$  is an operator representing scattering events. The resistivity follows from the variational principle as

$$\rho(T) = \frac{\langle \phi, P\phi \rangle}{\left| \int v_k \phi_k \frac{\delta f^0}{\delta \epsilon_k} d\vec{k} \right|^2} \quad (2.22)$$

Ziman<sup>12</sup> gives the complete expression of  $\langle \phi, P\phi \rangle$  for electron-electron scattering as

$$\begin{aligned} \langle \phi, P\phi \rangle = & \frac{1}{8k_B T} \iiint \{ \phi(\vec{k}_1) + \phi(\vec{k}_2) - \phi(\vec{k}_3) - \phi(\vec{k}_4) \}^2 \\ & \times P_{1,2}^{3,4} d\vec{k}_1 d\vec{k}_2 d\vec{k}_3 d\vec{k}_4 \end{aligned} \quad (2.23)$$

Here  $P_{1,2}^{3,4}$  is the transition probability of the two electrons being mutually scattered from states  $\vec{k}_1, \vec{k}_2$  to state  $\vec{k}_3, \vec{k}_4$ . This can be calculated once the scattering potential is known. In the relaxation time approximation it is easy to show from the BTE that  $\phi = \tau(\vec{k}) \vec{v}(\vec{k}) \cdot \vec{E}$ . This makes the factor from  $\phi(\vec{k})$  in Eq.2.23 looks like:

$$\{ \tau(\vec{k}_1) v(\vec{k}_1) + \tau(\vec{k}_2) v(\vec{k}_2) - \tau(\vec{k}_3) v(\vec{k}_3) - \tau(\vec{k}_4) v(\vec{k}_4) \}^2 \quad (2.24)$$

In the isotropic limit where  $\tau(\vec{k})$  is a constant, and in the simple metals which have a free-electron spherical Fermi surface so that  $v(\vec{k}) \propto \vec{k}$ , this factor becomes:

$$\{ \vec{k}_1 + \vec{k}_2 - \vec{k}_3 - \vec{k}_4 \}^2 \quad (2.25)$$

We see that Eq.2.25 vanishes for Normal scattering (momentum conservation), and thus from Eq.2.23 and 2.22  $\rho_{e-e} = 0$ . On the other hand, for Umklapp scattering, Eq.2.25 =  $g^2$  ( $g$  is a reciprocal lattice vector), and thus in an isotropic system only U-scattering gives a contribution  $\rho_{e-e}$  to the resistivity .

Assuming that the electron-electron interaction can be approximated by a screened Coulomb potential, Eq.2.22 can be calculated<sup>13</sup>, with the result  $\rho_{e-e} \propto g^2 (k_B T)^2$ .

Using different pseudopotentials, screening lengths, etc. other estimates of the magnitudes of this  $T^2$  term for simple metals have been published. Lawrence and Wilkins<sup>54</sup> developed a theory of the screened Coulomb interaction between electrons and calculated the screened Coulomb interaction contribution in K, Na, and Rb. MacDonald et al.<sup>14</sup> refined this theory, and found that in alkali metals the contribution of the screened Coulomb interaction was much smaller than calculated by Lawrence and Wilkins. MacDonald et al. proposed that the magnitude for U-electron-electron scattering in the alkali metals is dominated by a phonon-exchange contribution.

## 2.7 Thermoelectric Power

It is believed that there are two principal contributions to the thermoelectric power of a metal; a contribution from thermal diffusion of conduction electrons through the metal,  $S_d$ , and the phonon-drag thermoelectric power,  $S_p$ , arising from interaction between the electrons and the non-equilibrium phonon system of the lattice.  $S_p$  can be further considered as composed by two parts;  $S_p^N$ , arising from N-electron-phonon scattering processes, and  $S_p^U$  arising from U-electron-phonon scattering.

Generally,  $S_d$  can be written as<sup>37</sup>

$$S_d = \frac{\pi^2 k_B^2 T}{3e} \xi \quad (2.26)$$

where the dimensionless parameter  $\xi$  is given by the Mott rule

$$\xi = - \frac{\delta \ln \rho(\epsilon_f)}{\delta \ln \epsilon_f} \quad (2.27)$$

and for free-electron like metals it can be written as

$$\xi = \frac{3}{2} + \left( \frac{\delta \ln \rho(\tau_f)}{\delta \ln \epsilon_f} \right). \quad (2.27)$$

Applying Matthiessen's rule  $\rho = \rho_1 + \rho_2$  to Eq.2.26 and Eq.2.27, one gets the Gorter-Nordheim relation

$$S = (\rho_1 S_1 + \rho_2 S_2) / \rho \quad (2.28)$$

where the subscripts 1 and 2 represent the two different electron scattering processes.

The mechanism of the thermoelectric power due to phonon-drag can be understood as follows: For a pure unstrained sample at low temperatures, phonon-electron scattering is the dominant scattering process for the phonons. As a result of the phonon current generated by the temperature gradient, an electron within the metal will be "dragged" along by the phonon current as in viscous flow. Consequently, electrons tend to pile up at the cold end of the sample. This charge imbalance generates an internal electric field which exerts a retarding force on the streaming electrons, and ultimately a steady state is attained in which the total electric current vanishes. The resulting thermoelectric voltage divided by the temperature gradient at the two ends of the sample is  $S_p$ .

For the normal phonon-drag contribution, Klemens<sup>55</sup> and others gave the following theoretical expressions valid for free electrons and the Debye approximation.

$$S_p^N = 3 \frac{k}{e} \left( \frac{T}{\theta} \right)^3 \int_0^{\theta/T} \frac{x^4 e^{-x}}{(1 - e^{-x})^2} f(x) dx, \quad (2.29)$$

where:  $x = \hbar\omega/kT$  and  $\theta$  is the Debye temperature;  $f(x)$  is the fractional probability of a phonon being scattered by an electron rather than by anything else; i.e.

$$f = \frac{1/l_e}{1/l_i + 1/l_e}, \quad (2.30)$$

where  $l_i$  and  $l_e$  are phonon mean free paths for impurity and electron scattering, respectively.

The Umklapp scattering contribution  $S_p^U$  in alkali metals was predicted by Guenault and MacDonald<sup>36</sup> to be

$$(2.31)$$

The exponential temperature dependence is due to the fact that in a metal with a spherical Fermi surface which does not touch the Brillouin zone, a minimum phonon wave vector ( $q_{\min}$ ) is needed for a U-phonon-electron scattering to take place. In Eq. 2.31  $\theta^* \propto q_{\min}$ .

Thus at low temperatures, one expects the thermoelectric power  $S$  of alkali metals to have the general form

$$S = AT + BT^3 + C(T)\exp(-\theta^*/T). \quad (2.32)$$

A theory of  $S_d$  which considers the electron scattering as a many-body problem was developed by Nielsen and Taylor.<sup>14</sup> They considered a model in which free electrons were scattered by phonons or impurities, and calculated the second-order corrections to the scattering probabilities for these processes. They found the second-order electron-phonon interactions are strongly energy dependent near the Fermi level and, thus, contribute significantly to the thermopower.

For pure metals they proposed a correction to Eq. 2.27

$$\Delta\xi_1 = \frac{\epsilon_f NVm}{k_\theta^2 M} \psi_1\left(\frac{T}{\theta}\right) \quad (2.33)$$

where  $V$  is the  $q=2/3k_f$  component of the Fourier-transformed screened ionic pseudopotential,  $N$  is the number of ions,  $M$  and  $m$  are the mass of ion and electron respectively, and  $\psi_1$  is a temperature dependent function. At low temperatures  $\psi_1 \propto T^3 \ln T$ . Since such an effect is close to the  $T^3$  dependence of the simple phonon-drag theory of  $S_p^N$  (Eq.2.29), and yet involves no phonon flux, the  $\Delta\xi_1$  component is often referred to as "phony phonon drag". Due to the attraction of the ion potential,  $\Delta\xi_1$  is inherently negative.

For dilute alloys at low temperatures, Nielsen and Taylor obtained two second-order corrections to Eq.2.27

$$\Delta\xi_B = 6 \frac{\epsilon_f NUm}{k_\theta^2 M} \frac{n_0}{N} \quad (2.34)$$

$$\Delta\xi_C = \frac{\epsilon_f NVm}{k_\theta^2 M} \left(\frac{2N}{n_0}\right)^{1/3} \quad (2.35)$$

where  $U$  is the  $q=2/3k_f$  component of the Fourier-transformed impurity-scattering potential,  $n_0/N$  is the valence. While  $\Delta\xi_C$  is inherently negative, the sign of  $\Delta\xi_B$  will be the same as the net scattering potential of the impurity, and may be positive or negative.

## CHAPTER 3

### EXPERIMENTAL TECHNIQUES

Experimental techniques are very essential to this study. Typically, in the metal systems we studied the temperature dependent resistivity is much smaller than the residual resistivity; the ratio of  $\rho(T)/\rho_0$  is on the order of  $10^{-4}$  to  $10^{-6}$ . Thus, if one wants to measure the resistivity change as a function of temperatures with 1% accuracy, one has to resolve one part in  $10^{-6}$  to  $10^{-8}$ . Furthermore, the resistances of our samples are in the range of  $10^{-6}$  to  $10^{-4} \Omega$ . In order to avoid self magnetoresistance and heating, the current passing through the sample should be kept as small as possible. For a current of 100mA, to obtain the above high resolution, one has to be able to detect a signal as small as  $10^{-15}$  V. Recent developments in high-precision and small signal low temperature measurement techniques at MSU allow us to reach temperature below 100mK, with a voltage sensitivity about  $10^{-15}$  V (limited by Johnson noise), and a precision in resistance measurement approaching two parts in  $10^8$ . The system is unique. Moreover, the alkali metals are very reactive, so inert gas glove boxes and well sealed sample cans are crucial to preparing reliable samples.

In this chapter, the main equipment used in the experiments is briefly described; details were given in ref.38 and 55. Sample preparation and some improvements in equipment are also described.

### 3.1 Measuring System

#### 3.1.1 Reaching Low Temperatures

Continuously variable temperatures from 4.2K down to below 100mK were obtained with a locally built dilution refrigerator. The system could be cooled down to liquid nitrogen temperature ( $\sim 77.4$ K) in about 20 hours by



adding liquid nitrogen to the outer dewar of the refrigerator, and then cooled further to liquid helium temperature (4.2K) by transferring liquid helium to the inner dewar. The latter transfer took about 2 hours and about 25 liters of liquid He.

### 3.1.2. High Sensitivity

High voltage sensitivity ( $\leq 10^{-15}$  V) was obtained by using a SQUID null detector with several noise shielding facilities. It is essential to screen out radio-frequency noise, magnetic fields, and vibrations that can affect the operation of the SQUID. To eliminate power line interference, batteries were used as the power source of the resistance bridge system. Furthermore, the whole measuring system was enclosed in a commercial double-layered screened room. The outer galvanized steel layer of the screened room reduced low frequency electromagnetic fields and the inner copper layer reduced high frequency fields. Additionally, the refrigerator body was magnetically shielded with  $\mu$  metal wrapped outside the dewar and superconducting Nb metal wrapped inside the dewar. To eliminate vibration, the refrigerator was mounted on a commercial vibration isolation air floating system. All mechanical pumps were located outside the screened room, and the pumping lines were vibration isolated through specially designed flexible metal bellows. With these facilities we are able to operate the SQUID with sensitivity limited by the Johnson noise of the samples.

### 3.1.3. High Precision

High precision was achieved by using a resistance bridge consisting of a commercial direct-current comparator modified to be compatible with a SQUID by D. Edmunds et al.<sup>55</sup> The ratio of two currents (the master current  $I_m$  to the slave current  $I_s$ ) could be read with a set of eight decimal dials of the current comparator. A fraction of the last dial could be obtained

by using a computer averaging technique. This give a resolution of the current ratio approaching two parts in  $10^8$ .

### 3.2 Measuring Method

The main low temperature measuring circuit is shown in Fig. 1. This was a four terminal resistance bridge with a master and a slave current that could be passed through any two of three resistors,  $R_1$ ,  $R_2$  and  $R_s$ . The SQUID served as a null detector. A standard current reversal technique was used to eliminate the influence of thermal EMFs. When the bridge was balanced,  $I_m R_i = I_s R_j$  ( $i$  and  $j$  could be any two of 1, 2, and  $s$ ), the ratio  $C$  of the two resistors was obtained directly from the numbers on the 8-digital dials of the current comparator,  $C = I_s / I_m = R_i / R_j$ . The system could also be used to measure the voltage caused by a temperature gradient. In Fig.1:  $R_1$  and  $R_2$  were samples which are generally made as identical as possible to obtain optimal precision in determining  $C$ ;  $R_s$  is an InSn alloy resistor used as a standard resistor ( $R_s = 1.208 \mu\Omega$ ) which became superconducting at about 3.8K ;  $L_t$  were two superconducting inductances with  $L_1 \sim 20 \mu H$  and  $L_2 \sim 460 \mu H$ , respectively, which were used to keep the time constant of the circuit close to 1 second so that the SQUID could lock properly;  $U_1$ ,  $U_2$ ,  $L_1$ ,  $L_2$ ,  $G_1$ , and  $G_2$  were all Dale 4K (0.1%) resistor heaters used to generate temperature gradients  $\Delta T$  for a variety of measurements;  $GRT_1$  and  $GRT_2$  were two germanium resistance thermometers. The electrical leads were all superconducting leads ( $T_c > 4.2K$ ) and the thermal links are made of silver and copper.  $R_{L1}$  and  $R_{L2}$  were 0.1% AgAu alloys used for weak thermal links between the mixing chamber and the samples.  $U_1$ ,  $L_1$ , and  $R_{L1}$  or  $U_2$ ,  $L_2$ , and  $R_{L2}$  were arranged so that  $\Delta T \times T$  measurements could be checked in-situ to make sure that no systematic errors appeared, for details see Ref.38. The master current was normally preset: for  $G$  measurements  $I_m$  generally was set

to 2 or 5mA and for  $dp/dT$  measurements 20 or 50mA. The current dependences were checked; no current dependences were ever seen in this study.

### 3.2.1 Resistivity

$R(4.2K)$  could be obtained by comparing with  $R_s$  while the refrigerator was at Liquid He temperature.  $R_s$ , which was in series with the SQUID, was designed to superconduct when the dilution refrigerator was in operation so that  $R_s$  would not affect the sensitivity of other measurements. Shortly after each run, circulation was stopped, and the refrigerator temperature rose to near 1K where it remained for a while due to the liquidation of the mixture helium. By warming up  $R_s$  until it became normal,  $R(1K)$  could be measured by comparing it with  $R_s$ . RRR is defined by  $RRR=R(295)/R(1K)$ , where  $R(295)$  was measured at room temperature by a Keithley digital nanovoltmeter with an error  $< 1\%$ . Sample diameters( $\pm 2\%$ ) could be estimated from the diameters of the dies and lengths( $\pm 10\%$ ) were generally measured at room temperature so that  $\rho(1K)$  could be calculated from them. The change in  $\rho(1K)$  caused by the thermal contraction was estimated at less than  $0.1\%$ , which is smaller than other sources of uncertainty. For pure K and pure Li samples, the resistivities could also be obtained by  $\rho(1)=RRR\rho(295)$ , where  $\rho(295)$  for K and Li are  $71.9n\Omega m$  and  $93.2n\Omega m$ , respectively. In this study for pure samples the difference between  $\rho_0(0K)$  and  $\rho(1K)$  was less than  $0.1\%$ , and for alloy samples the difference between  $\rho_0(0K)$  and  $\rho(4.2K)$  was negligible. Hence, we take

$$\rho_0 = \rho(1K) \quad \text{for pure samples,}$$

$$\rho_0 = \rho(4.2K) \quad \text{for alloy samples.}$$

The total errors in determining  $\rho(4.2K)$  and  $\rho(1K)$  were about  $15\%$ , if the samples were not severely corroded during the cooling, otherwise, a special method had to be used to estimate  $\rho_0$ . (see Ch.6).

### 3.2.2 Temperature derivative of resistivity $d\rho/dT$ .

$d\rho/dT$  was obtained by the resistance bridge in the following way: If  $R_2$  was to be measured, then  $R_1$  was kept at a constant temperature  $T_1$  by regulating the mixing chamber temperature with a commercial temperature controller. When the system reached equilibrium,  $R_2$  stayed at a constant temperature  $T_2$  ( $T_2 \approx T_1$ ). Comparing  $R_1$  with  $R_2$  would give  $C(T_2) = R_2(T_2)/R_1(T_1)$ . The temperature of  $R_2$  was then warmed up to  $(T_2 + \Delta T)$  by using heater  $L_2$ . Comparing  $R_1$  with  $R_2$  again gave  $C(T_2 + \Delta T) = R_2(T_2 + \Delta T)/R_1(T_1)$ . Hence,

$$\frac{\Delta C}{C} = \frac{C(T_2 + \Delta T) - C(T_2)}{C(T_2)} = \frac{\Delta R_2}{R_2}$$

$\Delta T$  was typically 0.1K and the change of  $L/A$  in  $\Delta T$  was less than  $10^{-7}\%$ .<sup>23</sup> (where  $L$  is the length of the sample and  $A$  is the cross section of the sample). Hence

$$\frac{\Delta C}{\Delta T C} = \frac{\Delta R_2}{R_2 \Delta T} = \frac{\Delta \rho_2}{\rho_2 \Delta T} \doteq \frac{1}{\rho_2} \frac{d\rho_2}{dT}$$

Since in the temperature range considered in this study  $(\rho - \rho_0)/\rho_0 < 0.1\%$ .

We have

$$\frac{d\rho}{dT} = \frac{\rho_0 \Delta C}{\Delta T C}$$

Now we summarize the uncertainties in the  $d\rho/dT$  measurement. The thermometers  $GRT_1$  and  $GRT_2$  were carefully calibrated and tested. Between 0.1 and 2K, the accuracy of the  $\Delta T$  measurements was estimated to be  $2.6\%$ .<sup>25</sup> In the calculation of the quantity  $\rho_0 \Delta C / (C \Delta T)$ ,  $C$  had precision better than 0.1ppm, which was the distinguishable magnitude from temperature dependence

as mentioned earlier. The error in  $\rho_0$  would affect the quantity of interest  $dp/dT$  only by multiplying  $dp/dT$  by a constant close to 1. Except at the lowest temperatures, typically the uncertainty in  $\Delta C$  was less than a few percent. The uncertainty at the lowest temperatures could be as high as 25-100%. Hence, the main error in  $dp/dT$  at high temperatures came from measuring  $\Delta T$  and came from  $\Delta C$  at low temperatures.

### 3.2.3 Thermoelectric ratio G.

As defined Ch.1,

$$G = \frac{J}{q}, \text{ at } E=0, \text{ i.e. } G = \frac{I}{Q}, \text{ at } E=0.$$

G was measured by heating the end of the sample with  $G_1$  or  $G_2$  and sending the slave current  $I_s$  of the current comparator through the sample to cancel out the resulting thermally generated voltage, which was detected by the SQUID. Since  $I_s$  was always equal to  $CI_m$  and the heating power was equal to  $R_G I_G^2$ , ( $R_G$  was resistance of the G heater and  $I_G$  was the heating current),

$$G = CI_m / R_G I_G^2$$

The currents in G measurements were determined with an accuracy of less than 0.5%. Due to the thermal EMF noise and Johnson noise, the major source of uncertainty in G was in determination of C. At the lowest temperatures, the uncertainty in C could be 5% or more.

## 3.3 Sample Preparation

### 3.3.1 Glove box

Two commercial (Vacuum Atmospheres Company) glove boxes were used to prepare the highly reactive alkali samples. One was filled with He and maintained an Oxygen level less than 0.5 ppm indicated by an Oxygen analyzer. The He gas was purified by a Dri-train Mo 40-1 purifier. The other one was filled with Ar and purified with a locally built Ar purifier.

Fresh potassium inside these two glove boxes stayed shiny for at least 2 hours.

### 3.3.2 Sample can

Specially designed sample cans were used in this study. These were sealed with indium o-rings and equipped with superconducting leads and silver thermal link wires.<sup>38</sup> After samples were sealed in a can inside the glove boxes, the can was transferred to the dilution refrigerator where the measurements were made. For cans filled with He gas, molecular sieve was used to absorb the residual He gas in the cans at low temperatures. The samples studied in chapter 4 and 5 were all made and kept under Ar. The original Niomax superconducting wires of the sample cans were later replaced by copper clad superconducting wires with about 2 inches of copper cladding etched off in the middle of the wires to isolate them thermally. Since copper is much easier to solder, this switch solved the problem of stability of superconducting wire solder joints.

### 3.3.3 Sample

The samples were fabricated from 99.95% pure K, Rb and Na obtained from Callery Chemical Division of Mine Safety Inc., and 99.99% pure Li obtained from Atomergic Chemetals Corp. All the samples in this study were wires prepared by extrusion from stainless steel presses through stainless steel dies. The thin K wires were made from a special die with a 0.1mm stainless steel capillary. K, Rb and Na melt not far above room temperature. Inside the Ar filled glove box, the alloy constituents for the KRb and KNa alloys were weighed out, melted and mixed together inside a glass container on a hot plate. The liquid alloys were poured into the stainless presses. Because of the high melting point of Mg, an initial master Li(1%) Mg alloy was made inside a stainless steel crucible under Ar

atmosphere in an induction furnace, and then diluted to make less concentrated alloys by adding Li and melting on a hot plate inside the glove box. We later found that mixing Mg into molten Li in a stainless crucible on a hot plate inside the glove box also gave satisfactory alloys, and this procedure was used for 1%LiMg, 10%LiMg, 20%LiMg, and 30%LiMg alloys. The two 1%LiMg alloys prepared in different ways gave the same results on all the measurements. A 49%LiMg sample was made in the induction furnace. The high concentration 30% LiMg and 49 LiMg samples were annealed at 70% of their melting temperatures under vacuum for 2 days.

### 3.3.4 Potential leads of sample

Our measurements are four probe measurements. Most of the two potential leads were made of the same material as the samples, which are, generally, soft and sticky. For higher than 10% LiMg samples, potential leads made from the same alloys were directly soldered with a soldering iron inside the glove box, because the alloys were hard and unsticky. This method sometimes gave unexpected  $dp/dT$  results which might be due to the metals on the iron tip diffusing into the samples or some compounds formed during the relatively high temperature soldering of the high concentration LiMg samples. We later developed a cold welding technique which used potassium as the low temperature thermal and electrical connector. Potassium is insoluble in Li, Mg and Cu, and is sticky at room temperature which makes it easy to cold weld onto samples and copper connectors.

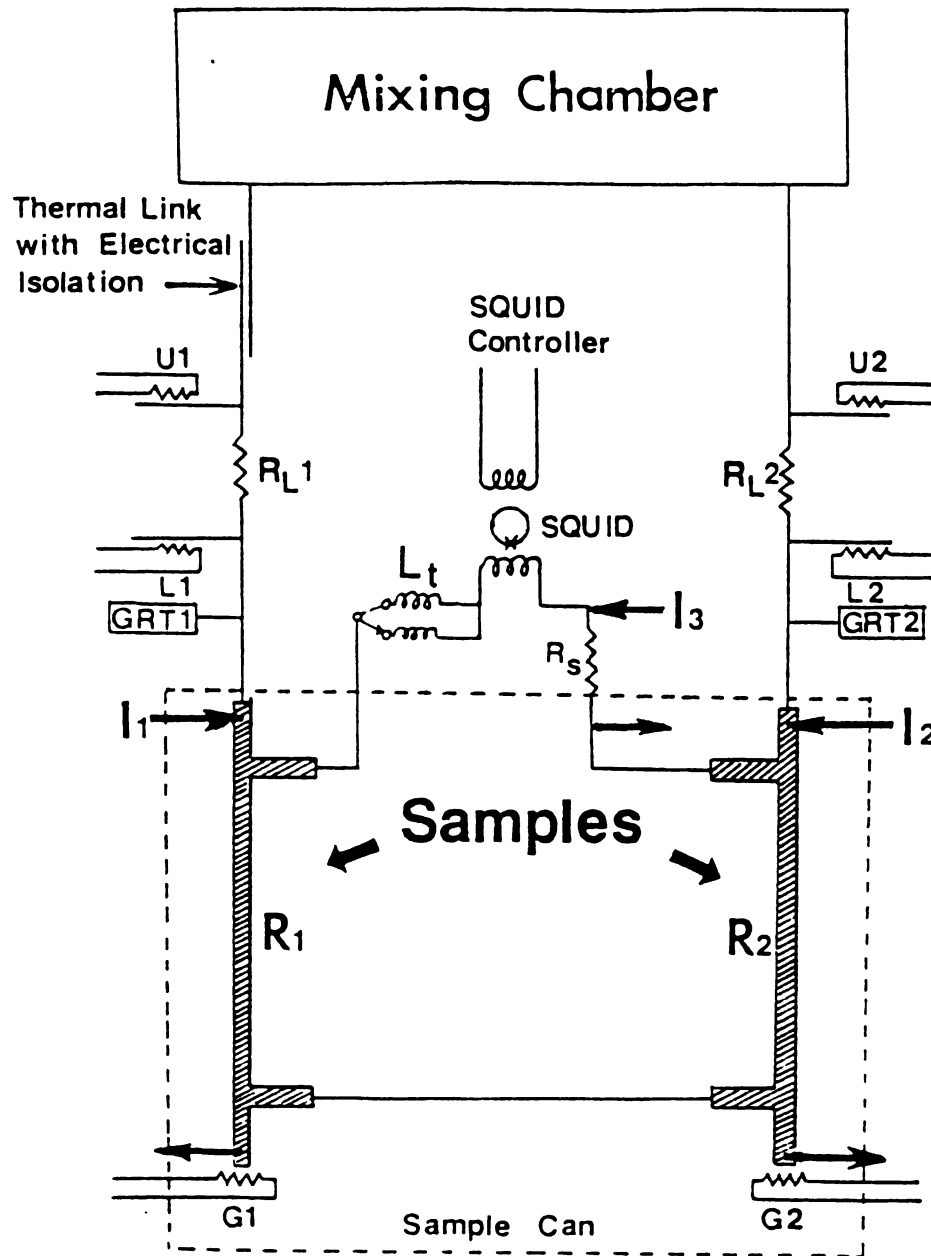


Fig.1 The low temperature circuit. The components inside the broken line are inside the sample can.



## Chapter 4

RESISTIVITY ANOMALIES AND THERMOELECTRIC  
BEHAVIOR IN KRb, KNa, AND LiMg ALLOYS BELOW 1K

In order to understand the low temperature resistivity anomaly found in KRb alloys,<sup>32</sup> we further studied the low temperature resistivities and thermoelectric ratios of high concentration KRb alloys, and KNa and LiMg alloys. The anomaly seems to be a very general effect, and thus important to elucidate. Very recently a number of workers<sup>56,57,58</sup> have shown that as the electron mean free path becomes short the quantum corrections of localization and interaction become important in analysing the resistivity of various disordered metals for which  $\rho_0 > 5 \times 10^{-7} \Omega\text{m}$ . Our KRb, KNa, and LiMg alloy samples have relatively simpler electronic structures than other systems studied, and this permits us to hope that the theoretical prediction based on a free-electron model will give quantitative comparison with the experimental data. Moreover, our samples cover the residual resistivity range of  $10^{-10} \Omega\text{m}$  to  $1.7 \times 10^{-7} \Omega\text{m}$ , which allows us to study how the quantum corrections become important as impurities are introduced into the crystalline metals. The study of bulk samples has an advantage in solving the relative importance and interplay of the interaction and the localization effects, since, in 2D samples both of the effects, though having large magnitudes, have very similar formulae.

#### 4.1 Electrical Resistivity

As noted before, at low temperatures where the contribution of electron-phonon scattering to the resistivity can be neglected, the resistivity  $\rho$  of dilute KRb and LiMg alloys could be understood in terms of Eq.4.1,

$$\rho = \rho_0 + AT^2 + B\rho_0 T^2. \quad (4.1)$$

except at the very lowest temperatures. The term  $AT^2$  is attributed to electron-electron scattering, and the term  $B\rho_0 T^2$  is attributed to inelastic electron-impurity scattering. At the lowest temperatures, both previous high-precision measurements of the electrical resistivities of KRb<sup>32</sup> and our new measurements of KRb, KNa, and LiMg alloys reveal anomalous departures from the expected  $T^2$  dependence at low temperatures, and these departures grow with increasing  $\rho_0$ .

We assume that the resistivities of these alloy systems can be described as

$$\rho = \rho_0 + f(\rho_0, T) + AT^2 + B\rho_0 T^2 + g(\rho_0, T) \quad (4.2)$$

where  $f$  is a low temperature anomalous contribution to  $\rho$  and  $g$  is a high temperature term which only becomes significant at  $T > 1.2K$ . The quantity we studied can be expressed as

$$\frac{1}{T} \frac{d\rho}{dT} = \frac{f'}{T} + 2A + 2B\rho_0 + \frac{g'}{T} \quad (4.3)$$

where  $f'$  is the derivative of the low temperature anomaly and  $g'$  is the derivative of the high temperature term. To examine if  $f$  and  $g$  are linear with  $\rho_0$ , we can normalize the data as

$$X = \frac{1}{\rho_0 T} \frac{d\rho}{dT} - \frac{2A}{\rho_0} = \frac{f'}{\rho_0 T} + 2B + \frac{g'}{\rho_0 T} \quad (4.4)$$

If both  $f$  and  $g$  are proportional to  $\rho_0$ , then  $X$  should be independent of the concentrations of the alloy samples. Thus a plot of  $X$  vs  $T$  for all samples should fall on a single curve. In Eq.4,  $2A/\rho_0$  is small for the concentrated alloys, so that we will make little error in  $X$  if we take  $A$  to have the value derived from the low concentration data. ( $A=2.4\text{f}\Omega\text{m}/\text{K}^2$  for K)

In this section we present our experimental results, together with several dilute KRb data measured by previous investigators<sup>23</sup>. The data are analysed in the following terms: (1) Residual Resistivity per Atomic % Impurity; (2)  $T^2$  resistivity component; (3) High temperature components ; and (4) The low temperature anomaly.

#### 4.1.1 Residual Resistivity per Atomic % Impurity

Fig. 1 shows the residual resistivities of our samples as functions of the nominal impurity concentrations  $c$ . As shown in the insert to Fig.1, all of our dilute alloy data fall well on the best values of  $d\rho_0/dc$ --straight lines--obtained by other people.<sup>59</sup> K and Rb are mutually soluble at all concentrations. In contrast, K and Na do not tend to alloy with each other, and the maximum solubility of Na in K is only about 1at.% even with fast cooling. Mg has a maximum solubility of 70at% in Li. Fig.1 also shows that our concentrated LiMg alloys (filled squares) are consistent, to within experimental uncertainties, with the measurements of Oomi et al<sup>35</sup> (open squares). These results give us confidence that the impurities in our samples were in solution. The  $\rho_0$  for all KRb alloys can be fit into the formula  $\rho_0 = Dc(1-c)$  with  $D = 1.14 \times 10^{-7} \Omega\text{m}$ , as the dotted line shown in Fig.1. This implies that the solutes occupy random lattice sites in KRb alloys. Some segregated KNa alloy samples with  $\rho_0$  much smaller than that

expected from their concentrations ( $c \geq 0.1$ ) were also made by keeping the samples at room temperature for an extended time.

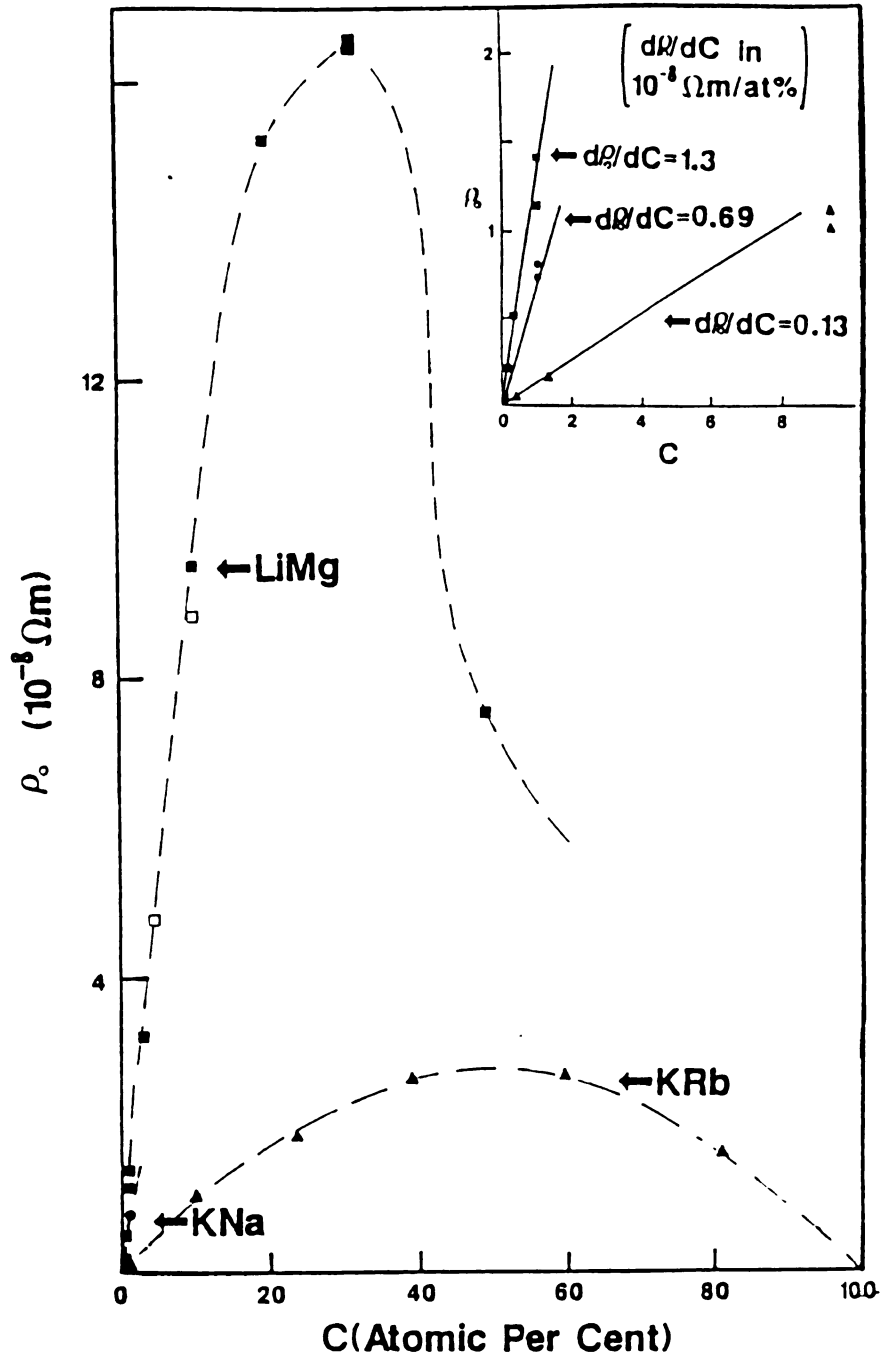


Figure.1:  $\rho_0$  versus atomic percent impurity concentration  $c$  for KRb, KNa, and LiMg alloys. The insert shows the detailed data for dilute alloys. The solid lines indicate the best experimental values from ref.59, and the broken line for KRb alloys is fit to a formula  $\rho_0 = 1.14 \times 10^{-7} c(1-c) \Omega m$ . The open squares are the data measured by Oomi et al.

#### 4.1.2 $T^2$ Resistivity Component

We now turn to the temperature dependent resistivity, choosing first a method of presentation which displays the  $T^2$  component as a horizontal line, and also displays the low temperature anomaly and high temperature behavior most clearly. We start with the data of pure alkali metals depicted in Fig.2. The turn up of the data at high temperatures is due to electron-phonon scattering processes. Notice that the turn up points of each metals are in the order of their Debye temperatures [ $\theta(\text{Li}) > \theta(\text{Na}) > \theta(\text{K}) > \theta(\text{Rb})$ ], which can be explained based on the Umklapp electron-phonon scattering and the presence of phonon drag in the alkali metals.<sup>71</sup> The turn up at the lowest temperatures are probably due to electron-dislocation scattering.<sup>60</sup> From Fig.2, we see in spite of a turn up at both low and at high temperatures the data for pure Li, Na, and K all show a region of flat behavior expected from simple electron-electron scattering theory. As impurities are added, we would expect that the inelastic electron-impurity scattering becomes dominant at low temperatures (Eq.4.1). Fig.3 .4, 5, 6 show plots of  $1/T (d\rho/dT)$  versus  $T$  for KRb, KNa, and LiMg alloy systems respectively. In the absence of an anomaly, each of these plots would be a horizontal straight line as given by Eq.4.1. This is generally true for very dilute (0.38%) KRb alloys as shown in Fig.4, for pure K up to 1 K (since electron-phonon scattering becomes important about 1K) as shown in Fig.4, and for pure Li up to high temperatures (since  $\theta_D(\text{Li})$  is higher) as shown in Fig.5. As the impurity concentrations are increased we see that an anomalous turn-down begins to develop at the lowest temperatures in all three alloy systems, and at temperatures above about 1.2K a turn up also develops for KRb and KNa alloys. Notice that both the  $T^2$  term and the

anomalies grow in size with increasing impurity content. Fig.6 shows concentrated LiMg data to illustrate how large the low temperature anomaly grows as  $\rho_0$  becomes large. An interesting feature of the LiMg data in Fig.5 is the smooth transition from an upward turning anomaly in pure Li to a downward turning anomaly in concentrated LiMg. This seems to be a detailed display of the competition between two different mechanisms.

Fig.7 shows the coefficients of the  $T^2$  terms in KRb, KNa, and LiMg as a function of the residual resistivity  $\rho_0$ . We see that the coefficients are consistent with straight lines for each alloy, as would be expected from Eq.4.1. The large uncertainties for the more concentrated alloys result from the fact that the  $T^2$  terms can no longer be well determined due to the large anomalies. Besides, the Koshino-Taylor theory, which predicted a  $T^2$  dependence, is appropriate only for low impurity concentration alloys; as the impurity concentration increases the coherent scattering of electrons by impurities and by the deformed phonon spectrum may not be negligible. The values of A found by extrapolating the data back to  $\rho_0=0$  agree well with values measured on the pure host metals. The detailed discussions of these values of A are the topic of ch.5.

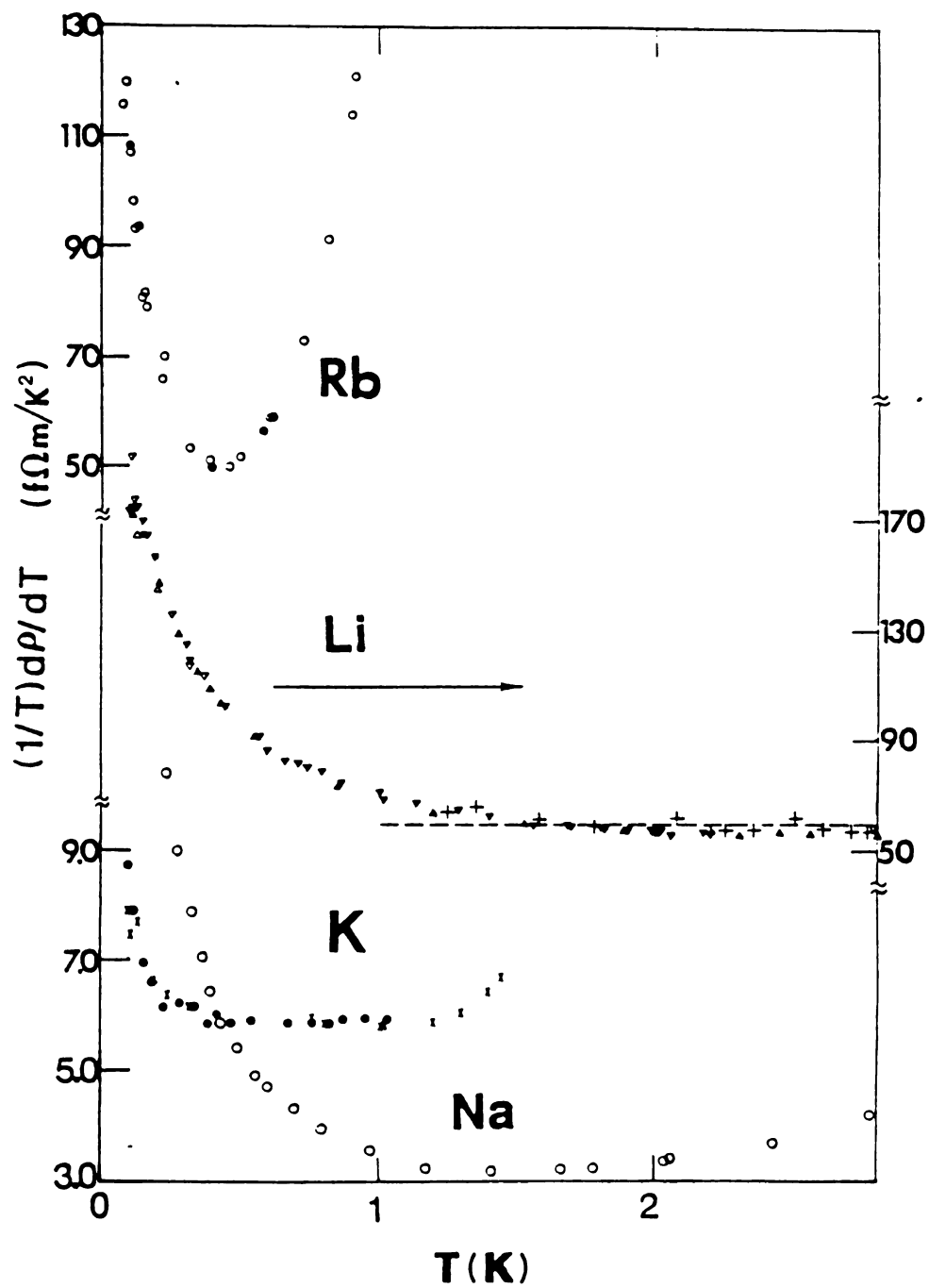


Figure.2:  $d\rho/dT$  versus  $T$  for pure Rb, Li, K, and Na. The RRR for each pure alkali metal approximately has the following value: 400 for Rb, 1000 for Li, 5800 for K, and 4700 for Na respectively.



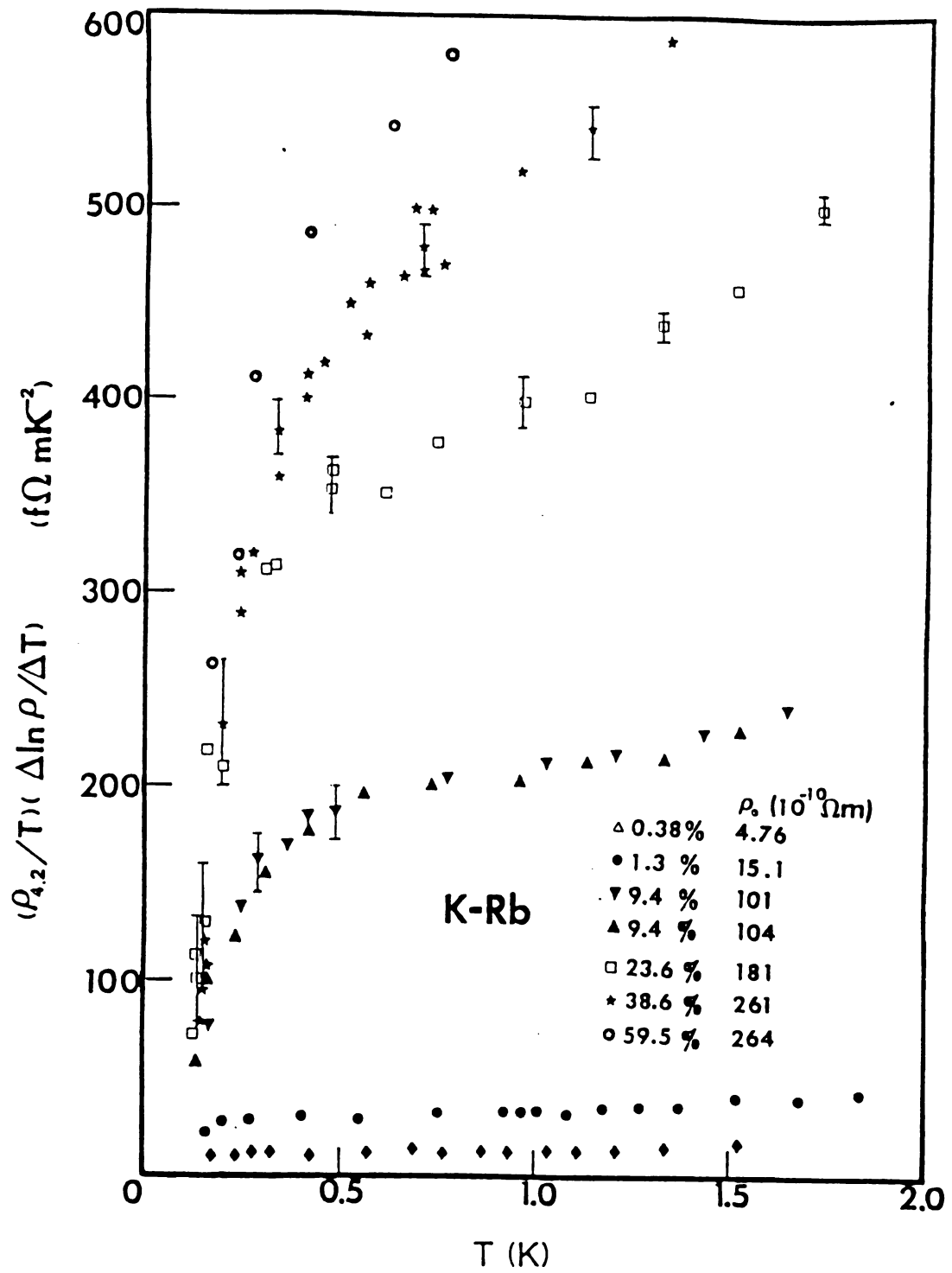


Figure.3:  $(1/T)d\rho/dT$  versus  $T$  for all KRb alloy samples.

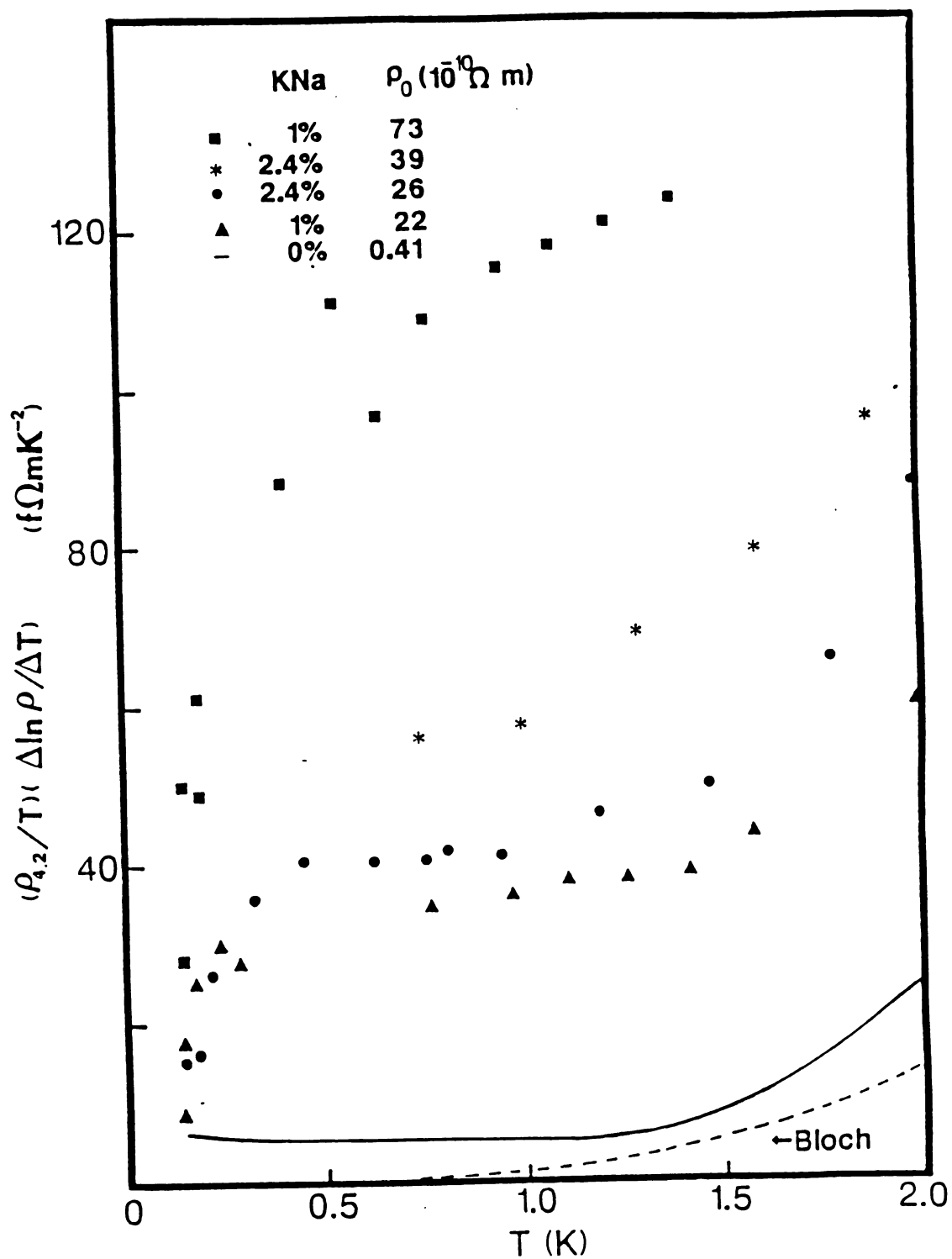


Figure.4:  $(1/T)dp/dT$  versus  $T$  for all KNa alloy samples.

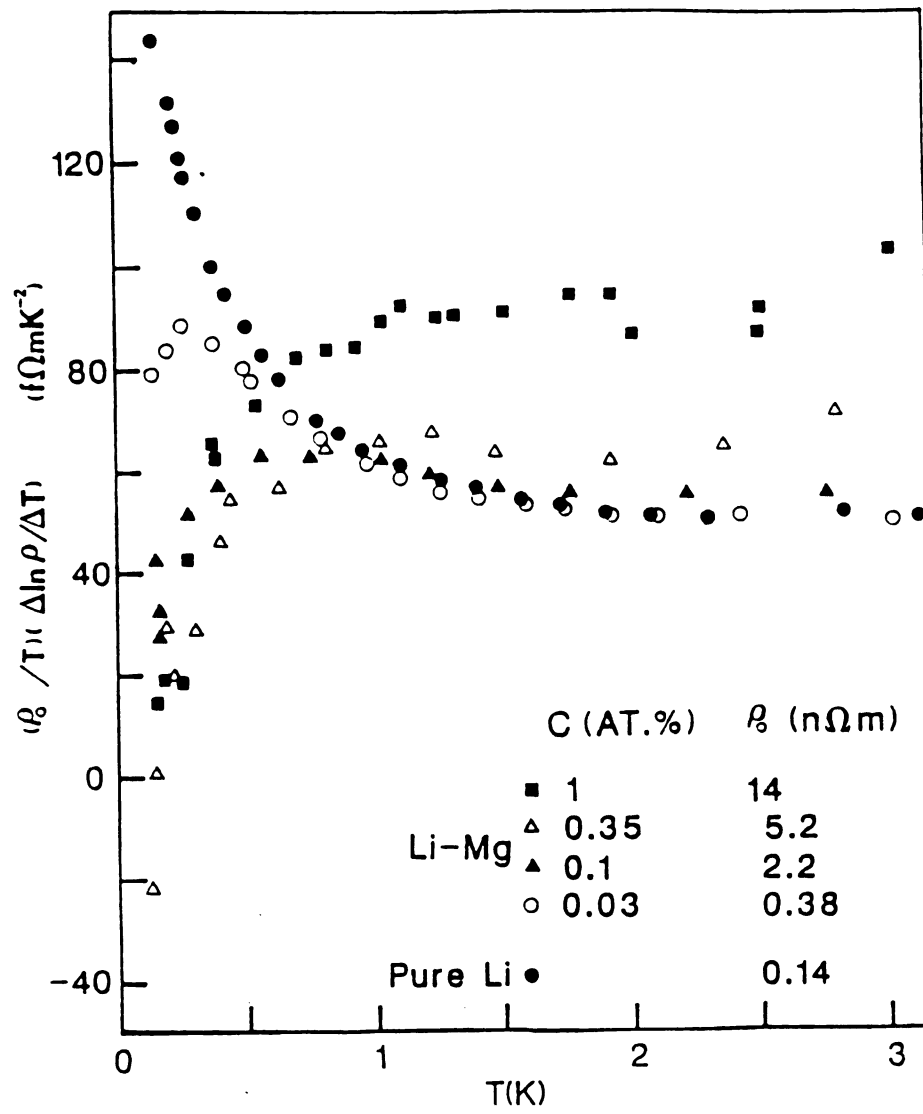


Figure.5:  $(1/T)d\rho/dT$  versus  $T$  for dilute LiMg alloy samples.

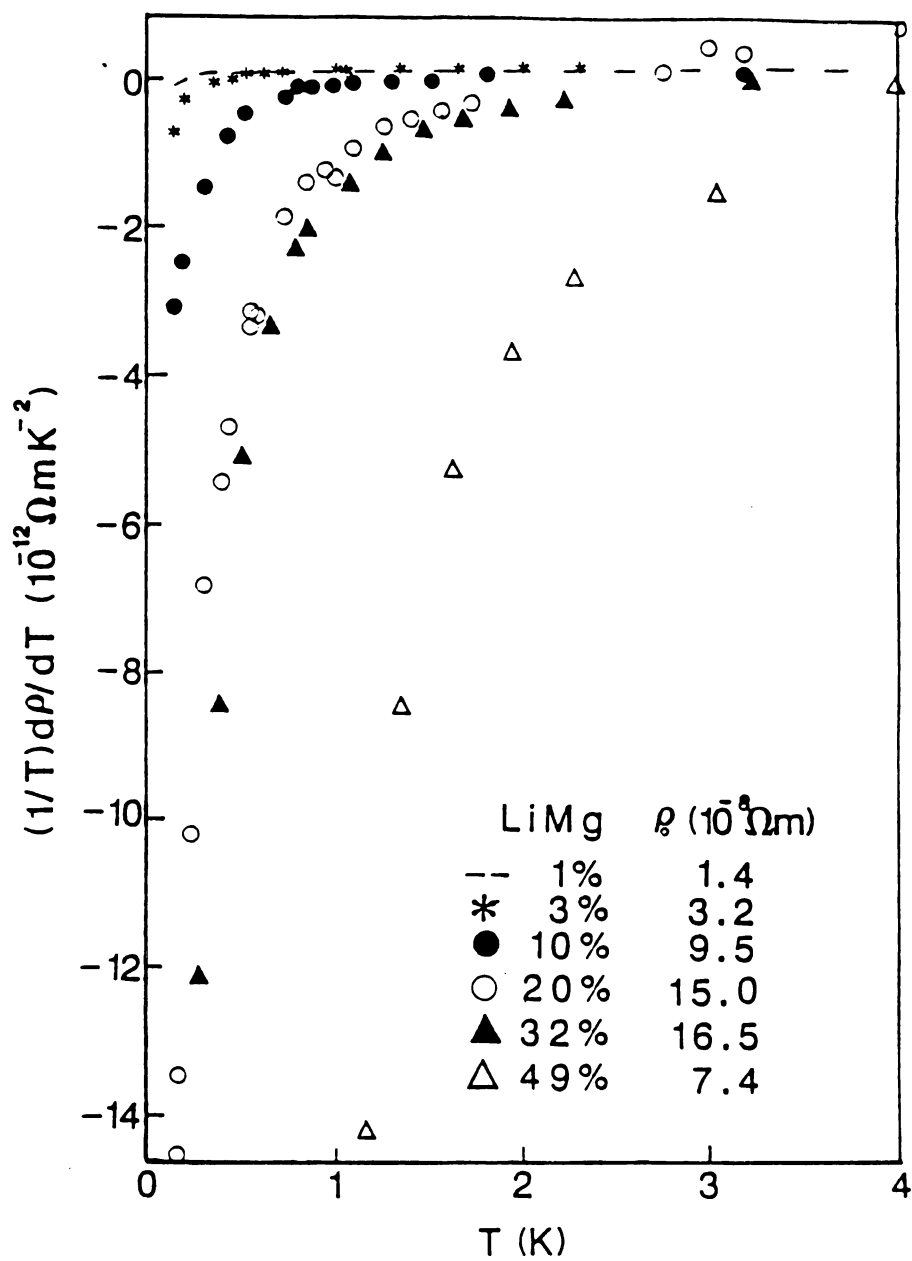


Figure.6:  $(1/T)d\rho/dT$  versus  $T$  for all concentrated LiMg alloy samples.

Table 1  $B(10^{-6}K^{-2})$ 

sample	B(a)	B(b)	B(c)	B(ex)
<u>K</u> Rb	12.5		3.6	12.3±0.5
<u>K</u> Na				7.5±0.5
<u>Li</u> Mg	3.1	2.2		1.5±0.1

a--Kus et al.

b--Screened Coulomb potential

c--Hu Gaussian

Table 1 lists the values of the slopes (i.e. B) of the alloys, and the values of theoretical calculations for comparison. B(a) was obtained by Kus et al, and is the best calculated value for K as discussed in chapter 2. The B(a) were calculated without the Debye temperature approximation and with a quite good pseudopotential for Rb in K. B(a) also took into account the mass difference between host and impurity ions. The screened Coulomb pseudopotential is considered<sup>44</sup> a reasonable approximation for heterovalent impurity scattering. B(b) is evaluated from Taylor's expression for such a potential for Mg in Li with the screening length determined from  $dp_0/dc$  data. Considering the approximations involved in the Koshino-Taylor theory, the agreement between the experiments and the theories is good.

As mentioned in Chapter 2, very recently S. Hu and A.W. Overhauser proposed a model<sup>46</sup> in which the many-body electron-phonon vertex correction, together with a partial failure of Migdal's theorem, leads to a new temperature-dependent term in the electrical resistivity caused by elastic impurity scattering. Based on a Gaussian potential for Rb in K they calculated the magnitude of  $B$  ( $B(c)$  in table 1) from Taylor's expression and the magnitude of the electron-phonon vertex correction term, and they argued that the magnitude of the Koshino-Taylor term should be smaller than the experimental results and thus the many body effects of the electron-phonon interaction should account for the  $T^2$  term in the KRb alloy resistivities. However, in their evaluations, they do not justify the determination of the parameter  $\alpha$ , which is essential to the magnitude of their calculations. Considering the agreement of experiment results with the better calculation results  $B(a)$  and  $B(b)$  in table 1, we think it is unlikely that the electron-phonon vertex correction is the dominant contribution to the  $T^2$  behavior in the resistivities of these three alloy systems.

Fig.8 shows a detailed  $(A + \rho_0 B)$  versus  $\rho_0$  plot for all the KNa data. The fact that all of the data fall on a single line, suggests that the magnitude of  $T^2$  term is not sensitive to segregation in KNa alloys.

#### 4.1.3 High Temperature Term

The Debye temperature of Li ( $\theta_D \approx 369K$ ) is so high that electron-phonon scattering is unimportant in our current temperature range. As shown in Figs.5 and 6, for the samples containing up to 10 at.% Mg ( $\theta_D \approx 300K$ ) no significant high temperature deviations are observed. (For the samples containing higher than 10% Mg, the data are dominated by the low temperature anomaly).

As discussed in Ch.1, for pure K ( $\theta_D \approx 90K$ ) electron-phonon scattering can be neglected below 1K, since phonon-drag greatly reduces the Bloch  $T^5$  component of the N-electron-phonon resistivity and the exponential U-electron-phonon component becomes very small below 1K. When Rb or Na is added into K, the resistivities at high temperatures begin to increase faster than that of pure K, as depicted in Figs.3 and 4. It seems that the data can be scaled by  $\rho_0$ , as illustrated in Fig.10. We see there that the values of X for KNa all fall on a single curve, to within the uncertainties, as also do the values of KRb alloys up to 23.6%. The 1.3% KRb data which were measured by M.L. Haerle in the early days have a large uncertainty, and the deviation from the curve for 38.6% KRb may be due to the decreasing of the Debye temperature by Rb as will be discussed below.

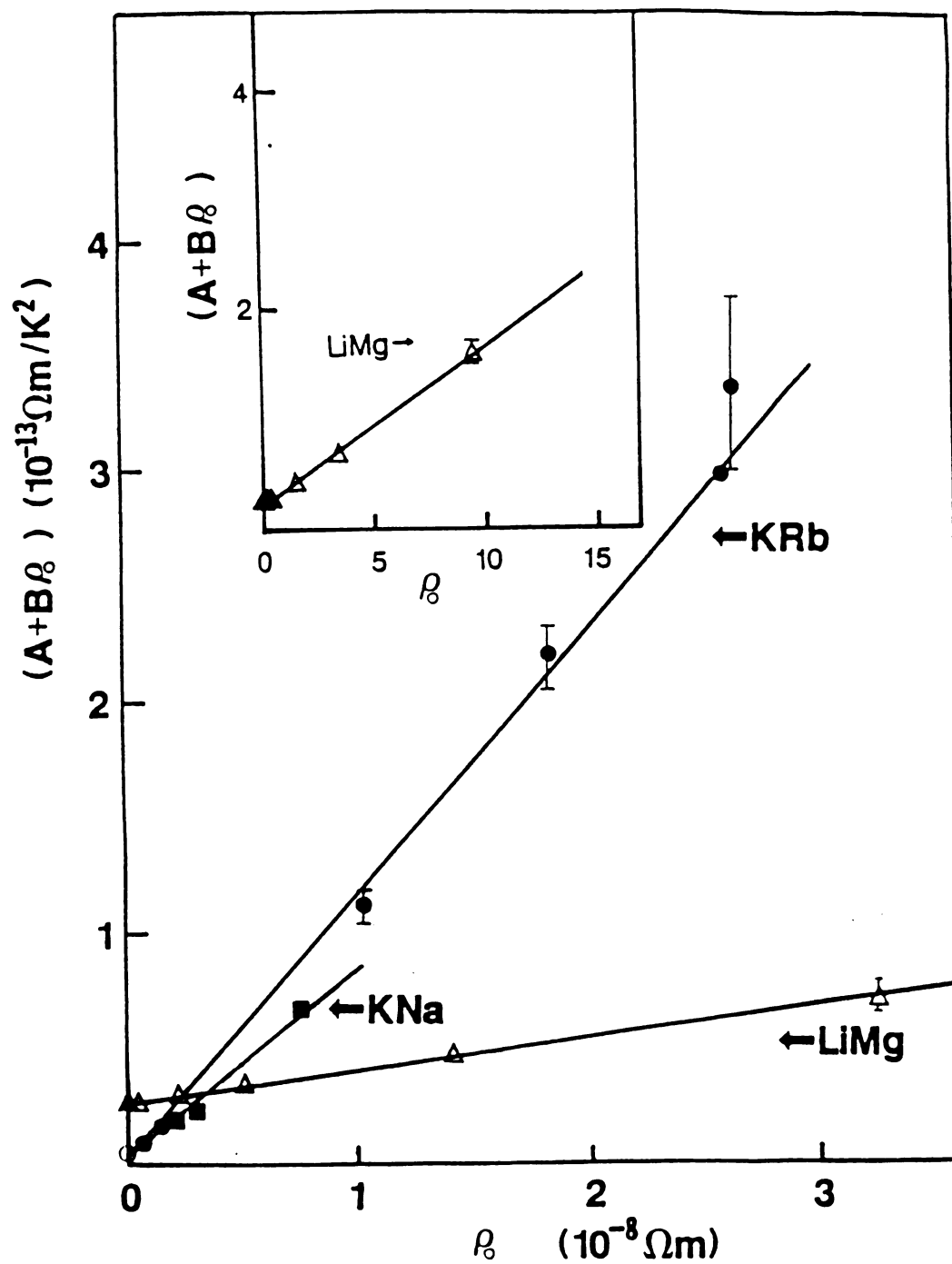


Figure.7: The coefficients of the  $T^2$  term  $A + B\rho_0$  versus  $\rho_0$  for KRb, KNa, and LiMg alloy samples. The data were obtained by averaging over the flat regions on figs.3,4,5.



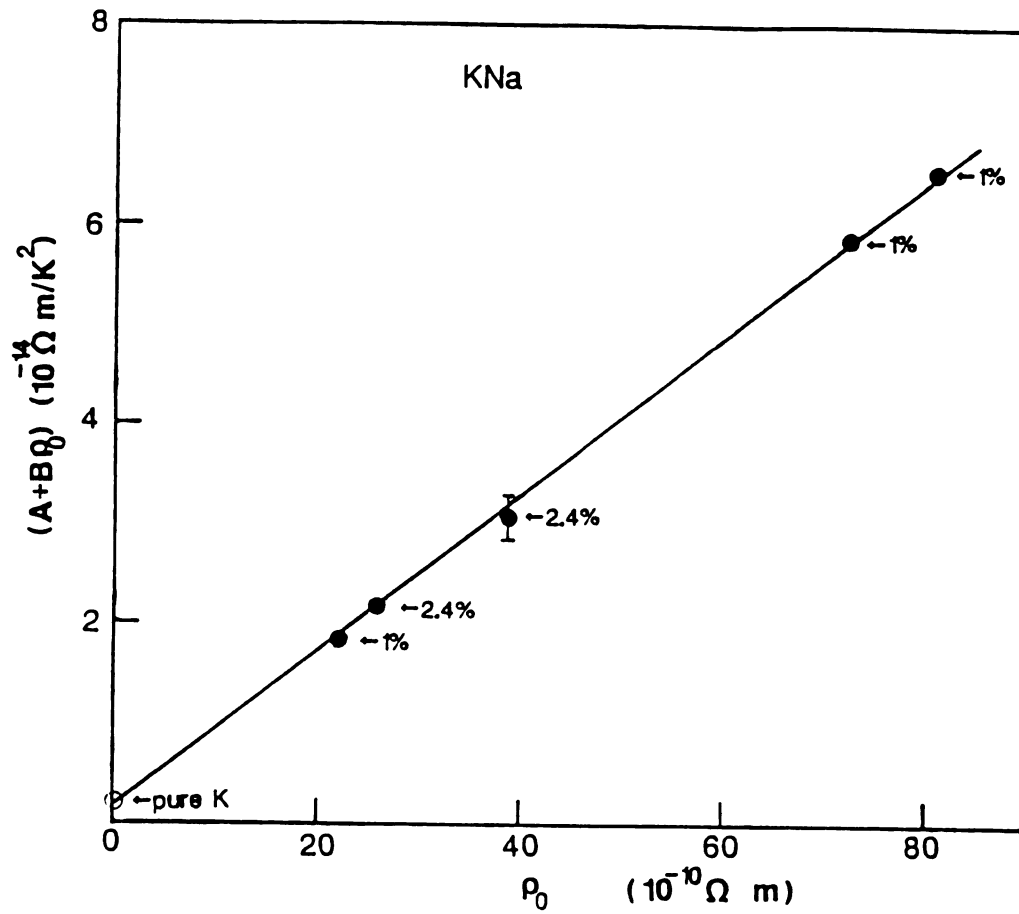


Figure.8: The coefficients of the  $T^2$  term  $A + B\rho_0$  versus  $\rho_0$  for all KNa alloy samples. Notice the different  $\rho_0$  values for each Na concentration.

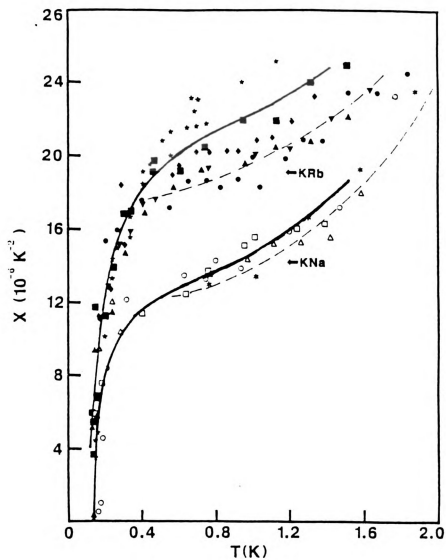


Figure.9:  $X$  versus  $T$  for  $\text{K-Rb}$  and  $\text{K-Na}$  alloys. The solid curves are fit to Eq.4.10, and the broken lines are fit to Eq.4.5.

The different horizontal positions of the two curves are just the difference between the two Bs as indicated in Eq.4.4. The fact that such normalization brings the data for each alloy onto a single curve means that  $f$  and  $g$  are both approximately proportional to  $\rho_0$  for not too high concentration alloys. Fits of  $X=2B+DT^3$  for the high temperatures are shown in Fig.9 as the solid lines, and this suggests that

$$g \propto \rho_0 T^n, \quad n \sim 5 \quad (4.5)$$

Due to the experimental uncertainties  $n$  only can be determined to within  $4 \leq n \leq 6$ .

As mentioned in Ch.2, there is a theoretical prediction for a term similar to Eq.4.5 by Y. Kagan and A.P. Zhernov<sup>61</sup>. In their calculation of coherent electron-impurity scattering, they obtained a term proportional to  $\rho_0 T^5$  due to scattering by the deformed phonon spectrum. However, the leading term,  $\propto \rho_0 T^5$ , was predicted to be positive for KRb but negative for KNa; this contradicts the experimental results.

Alternatively, quenching of phonon-drag might provide an explanation for a  $T^5$  term. The effects of impurities quenching phonon-drag can also be seen in the thermoelectric ratio data of the alloys, as we will present later. We noted above that phonon-drag effects<sup>3</sup> largely reduce the N-electron-phonon Bloch  $T^5$  term in pure K. As impurities are added to K, the  $T^5$  N-electron-phonon component might become visible if the impurities quench phonon-drag. In such a case, we would expect the magnitude of  $T^5$  component ( $T^3$  in  $1/Tdp/dT$ ) to grow as  $\rho_0$  increases. To compare the magnitude with such a theory, we plot the Ekin and Maxfield theoretical calculation of the Bloch  $T^5$  term of pure K in the limit of no phonon-drag as the dotted line in Fig.4. ( $\rho_{e-p}^N = 3.5 \times 10^{-16} T^5 \Omega \text{ m/T}^5$ ). We see that adding the Bloch  $T^5$  term (dotted line) to the pure K data (solid line)

could give comparable magnitudes to account for the increases of the dilute KNa and KRb data at high temperatures (see Fig.3). For more concentrated alloys we would then have to invoke decreasing of  $\theta_D$  due to alloying to further increase the magnitudes of electron-phonon scattering of both Normal and Umklapp scattering processes.  $\theta_{\text{alloy}} = c\theta_{\text{imp}} + (1-c)\theta_{\text{host}}$ , which will decrease upon adding Rb ( $\theta \approx 55\text{K}$ ) impurity to K. The magnitude of the Bloch  $T^5$  component (Normal part) is predicted to be proportional to  $1/\theta_D^6$ , and the magnitude of the Umklapp part of electron-phonon scattering should grow fast in alloys with very high Rb concentration, as illustrated in the extreme case of the data of relatively pure Rb in Fig.2 where the turn up at high temperature is believed to be dominated by U-electron-phonon scattering process. Therefore, as the Rb concentration further increases, we would expect the magnitudes of both the normal  $T^5$  term and the Umklapp component to increase in high concentration KRb alloys; the U-electron-phonon component dominates in the very high concentration KRb alloys; and the behavior finally approaches that of Rb. In fact a rough estimation shows that both the Normal  $T^5$  term and the Umklapp term are needed to account for the big magnitudes of the high concentration KRb alloys data. Hence the high temperature resistivity behavior shown in Fig.3 can be attributed to the decreases of the Debye temperatures of the alloys.

#### 4.1.4 Low Temperature Anomaly

##### 4.1.4.a Temperature and $\rho_0$ Dependences of the Anomaly

As illustrated in Figs. 3, 4, 5, and 6, a low temperature resistivity anomaly begins to develop as  $\rho_0$  increases in all three alloy systems. In particular, Fig.6 illustrates how in LiMg this anomaly---plotted in the form of  $(1/T)d\rho/dT$ ---crosses the zero line (indicating a resistivity

minimum) and turns down enormously as  $\rho_0$  is further increased. The LiMg alloy system was chosen because it gives such a high  $\rho_0$  and yet has a relatively simple electronic structure. As displayed in Fig.9 the low temperature resistivity anomaly  $f(\rho_0, T)$  for all KNa and KRb alloys is proportional to  $\rho_0$ . The large turn up at low temperatures in dilute LiMg alloy data complicates a similar analysis, and we will demonstrate below in Fig.13 the linear  $\rho_0$  dependence of dilute LiMg data by a different plot. To analyze in detail how the low temperature anomaly varies with  $T$ , we first consider the three temperature dependences expected for localization,<sup>7</sup> electron-electron interaction<sup>7</sup>, and the Kondo effect<sup>47</sup>.

$$f \propto -T \quad (\text{localization}) \quad (4.6)$$

$$f \propto -T^{1/2} \quad (\text{electron interaction}) \quad (4.7)$$

$$f \propto -\ln T \quad (\text{Kondo effect}) \quad (4.8)$$

for which  $(1/T)d\rho/dT$  should be proportional to  $T^{-1}$ ,  $T^{-3/2}$ , and  $T^{-2}$  respectively. When we plot  $(1/T)d\rho/dT$  as a function of these three powers of  $T$  for various samples, we find that for all the KRb and KNa samples and for dilute LiMg the graphs with the  $T^{-1}$  abscissa give slightly better fits than those with  $T^{-3/2}$ , and that the  $T^{-2}$  graphs give the worst fits. (Caution should be exercised in concluding that a specific form is appropriate.) Examples of such fits are shown in Fig.10 for a 23.6% KRb alloy. The dashed, long dashed, and dotted curves in Fig.11 illustrate how the three fits to the 23.6% KRb alloy data in Fig.10 look when converted into a plot of  $(1/T)d\rho/dT$  versus  $T$ . We note that all three curves fall below the data at sufficiently high temperatures. This is due to the onset of the extra term discussed in the previous section. The solid curves in Fig.11 and in Fig.9 illustrate how a resistivity term linear in  $T$  (the

long-dashed line) along with an additional  $T^5$  term fit the 23.6% KRb data. A similar fit for the KNa alloys is illustrated by the solid line in Fig.9.

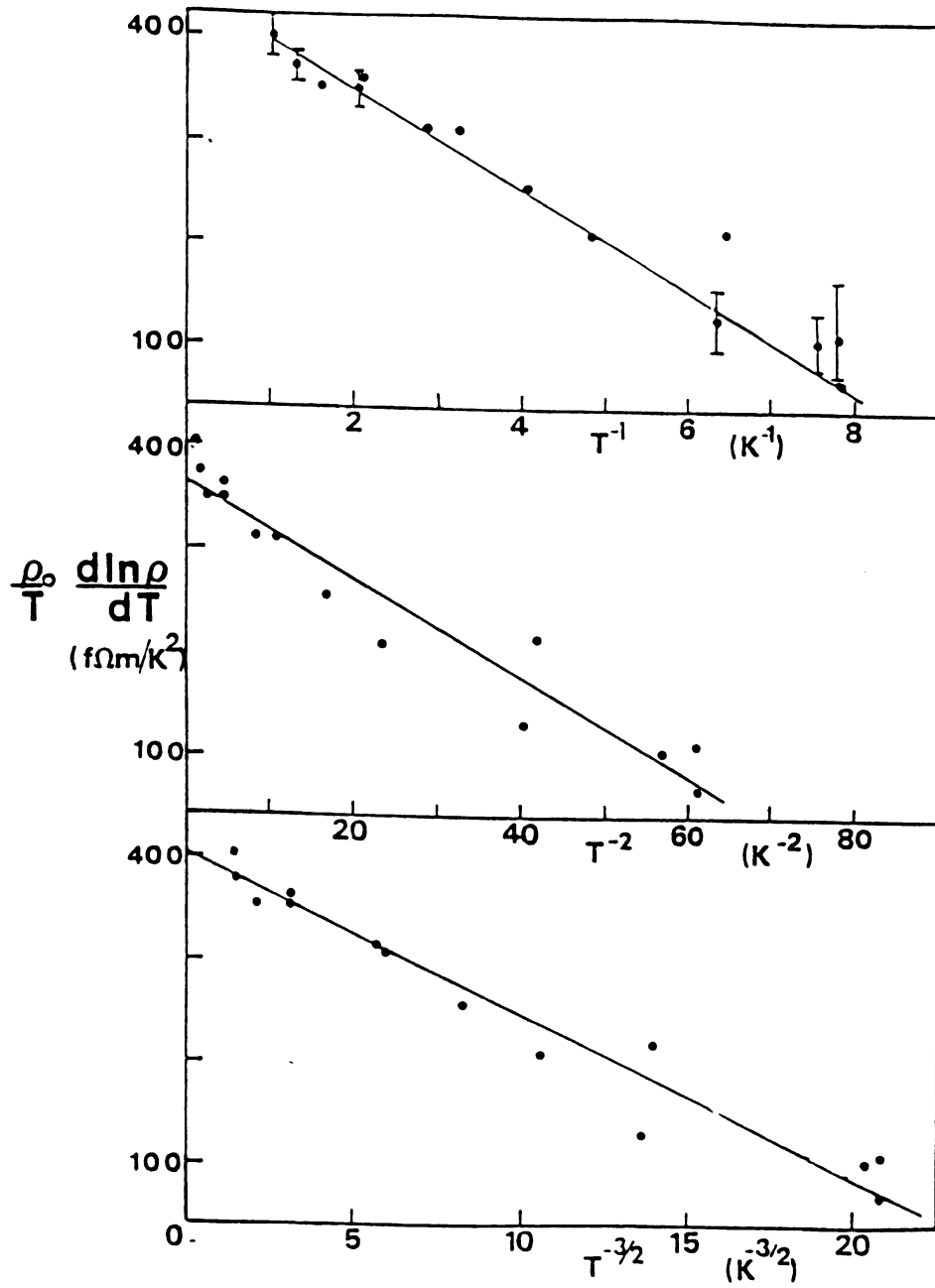


Figure.10:  $(1/T)d\rho/dT$  versus  $T^{-1}$ ,  $T^{-2}$ , and  $T^{-3/2}$  for the 23.6% KRb alloy.

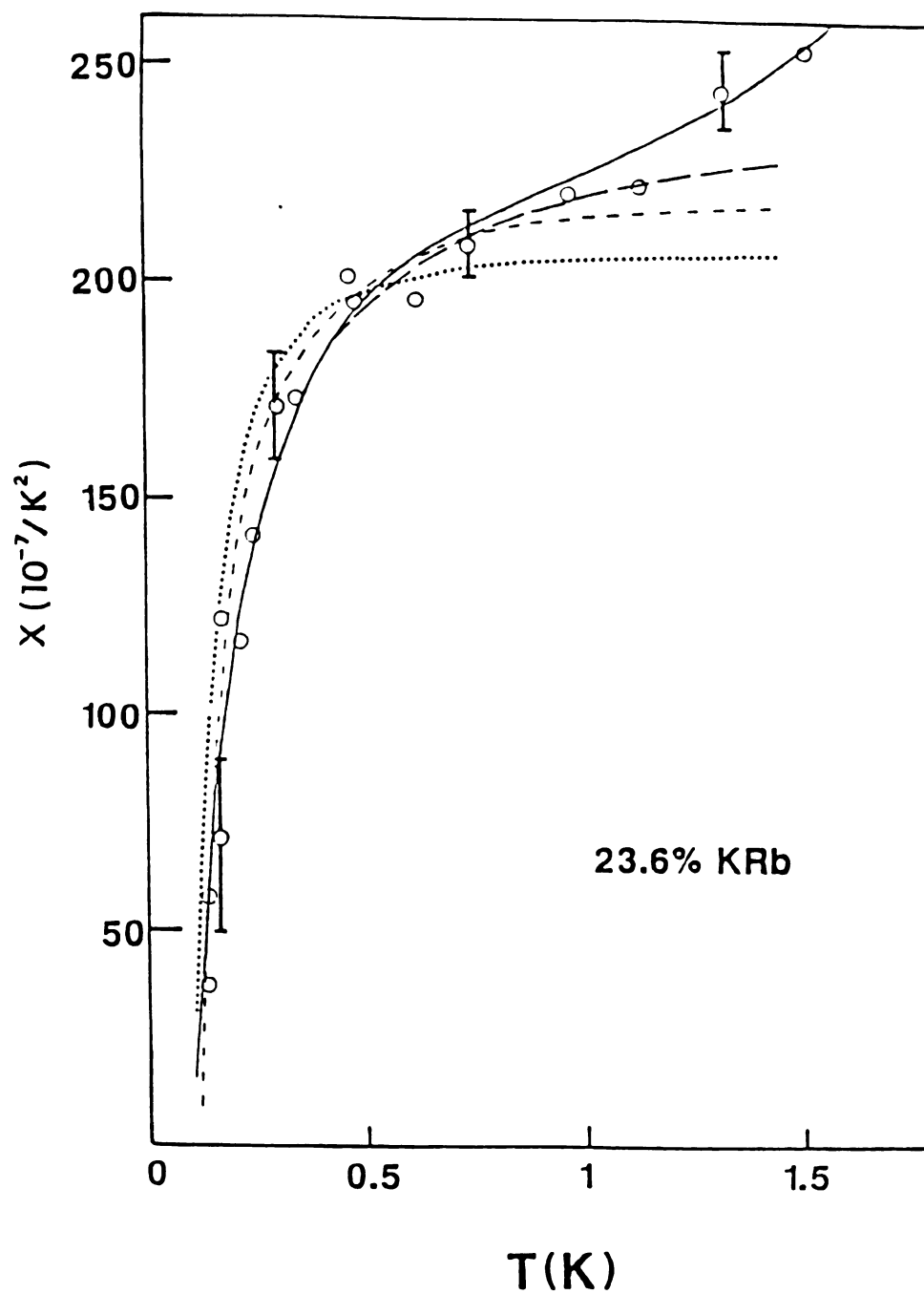


Figure.11:  $X$  versus  $T$  for 23.6%  $\text{KRb}$ . The long dashed, dashed, and dotted curves are fit to Eqs.4.7, 4.6, and 4.8 respectively. The solid curve is fit to Eq.4.6 along with an additional  $T^5$  term.



If we choose two high-temperature terms (i.e:  $T^5$  and an exponential) to adjust, we can fit the entire range of data for each alloy--to within experimental uncertainty--using each of the three forms given in Eq.4.6, 4.7, 4.8. We thus cannot absolutely rule out any one of these three alternatives. In the absence of detailed knowledge of the magnitudes of these two high temperature terms, we choose to parameterize our results using the low temperature form which, by itself, fits the data over the widest temperature range. This is  $f \propto T$ , Combining this best fit with the fact that  $f \propto \rho_0$  we offer as an approximate empirical equation for our data at low temperature

$$\rho = \rho_0 + AT^2 + B\rho_0 T^2 - C\rho_0 T \quad (4.9)$$

If Eq.4.9 is correct, then plots of  $d\rho/dT$  versus  $T$  for the data should give straight lines which do not pass through the origin. The intercept with the abscissa should give the coefficient  $C\rho_0$ . Such plots are given in Figs.12 and 13. We see that for KRb, KNa, and dilute LiMg the data appear to be consistent with straight lines, corresponding to a resistivity anomaly of the form  $f \propto T$ . Fig.13 also shows that the data begin to deviate from a straight line for LiMg alloys with Mg concentration higher than 10%. Fig.14 contains the coefficient  $C\rho_0$  versus  $\rho_0$ . We see that for all alloys with  $\rho_0 < 10^{-7} \Omega m$ , the data are consistent with a  $\rho_0$  dependence to within the uncertainties. On the other hand, when the LiMg alloy data are extended to  $\rho_0 > 10^{-7} \Omega m$ , the data increase faster than  $\rho_0$ . Therefore, both the temperature dependences and the residual resistivity dependences of the low temperature resistivity anomaly of LiMg alloy system seems to be

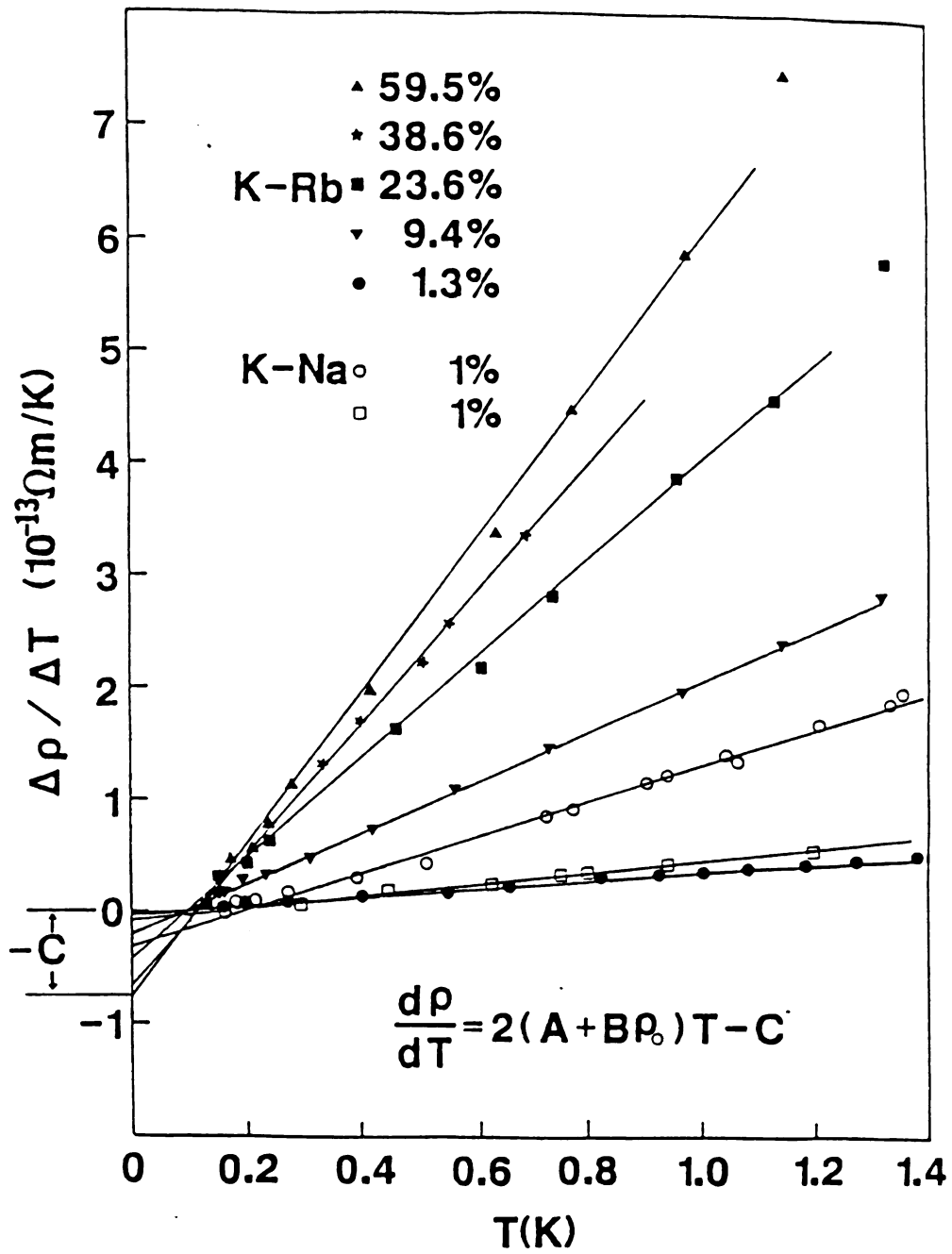


Figure.12:  $dp/dT$  versus  $T$  for  $\underline{\text{K}}\underline{\text{Rb}}$  and  $\underline{\text{K}}\underline{\text{Na}}$  alloys.

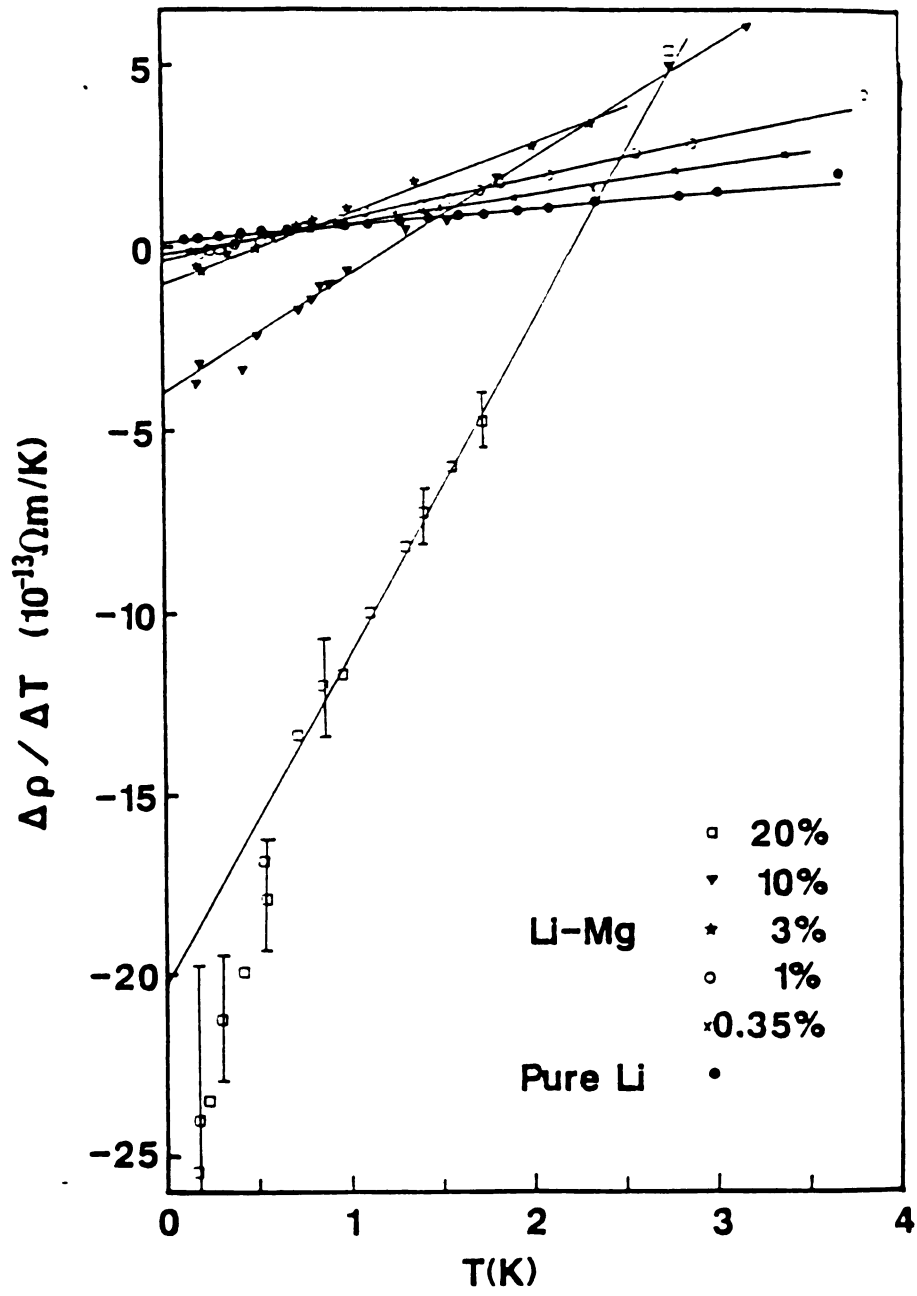


Figure.13:  $d\rho/dT$  versus  $T$  for LiMg alloys.

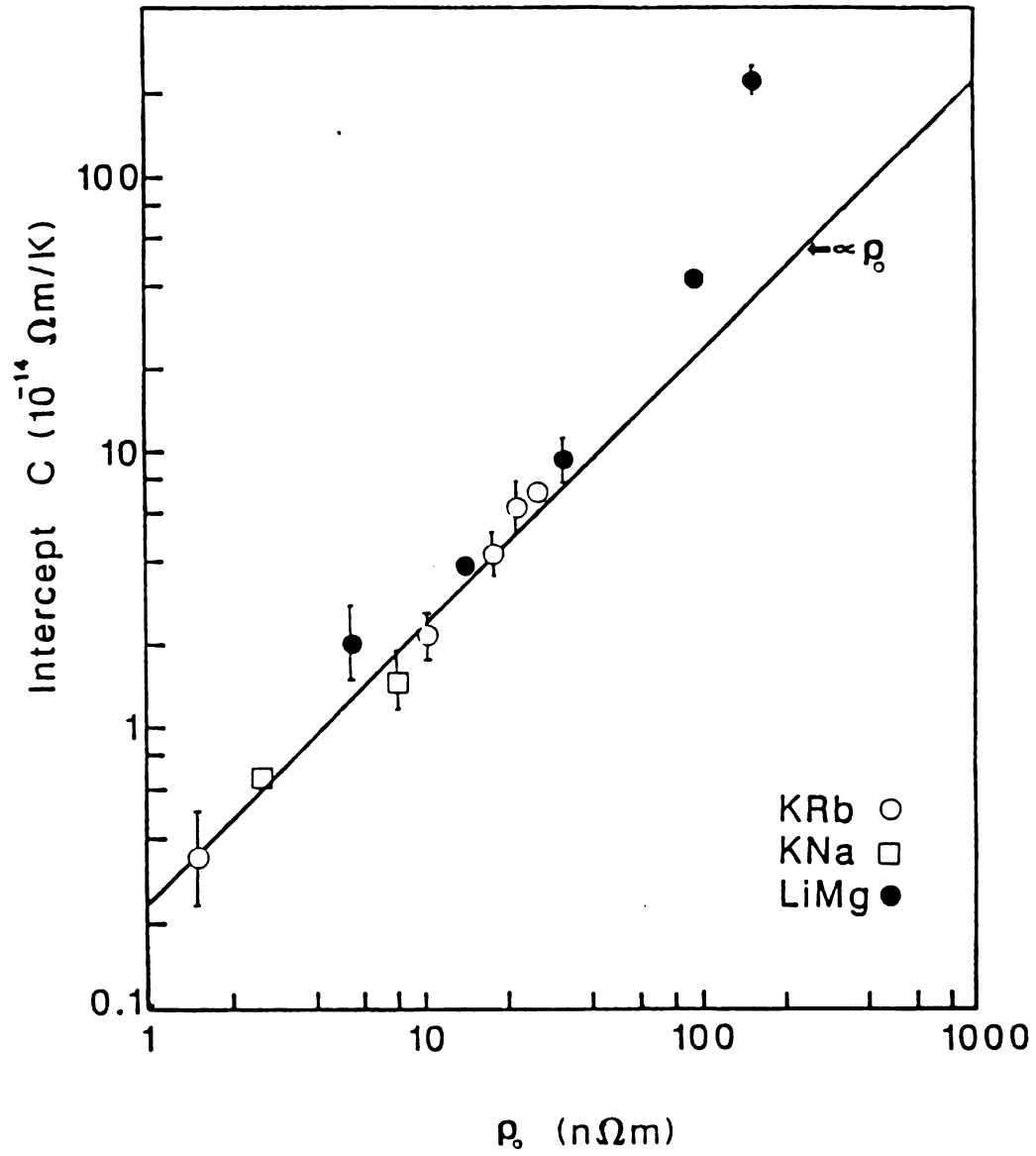


Figure.14:Intercepts of the data in Fig.11 and Fig.12 versus  $\rho_0$ .

separable into two categories by  $\rho_0 \approx 10^{-7} \Omega\text{m}$ . To see both the  $T$  and  $\rho_0$  dependences of the anomaly for high concentration LiMg alloys, we plot the  $(1/T)d\rho/dT$  data versus  $T^{-3/2}$  and  $T^{-1}$  in Fig.15. This shows that the  $T^{-3/2}$  form becomes a better fit as the Mg concentration increases. Fig.16 is a plot of the coefficients of the  $T^{-3/2}$  term in  $(1/T)d\rho/dT$  versus  $\rho_0$  for all samples (i.e. the data for  $\rho_0 < 10^{-7} \Omega\text{m}$  are forced to this form). We see how the data change from a  $\rho_0$  dependence (dashed line) to  $\rho_0^{5/2}$  (solid line) as  $\rho_0$  increases.

To summarize the experimental data, we rewrite the best fit form for the low temperature resistivity anomaly as

$$\rho_a = f = -C\rho_0 T \quad \text{for } \rho_0 < 10^{-7} \Omega\text{m}, \quad (4.10)$$

$$\rho_a = f = -D\rho_0^{5/2} T^{-3/2} \quad \text{for } \rho_0 > 10^{-7} \Omega\text{m} \quad (4.11)$$

where the power of the temperature dependence in Eq.4.10 can only be determined to between 1/2 and 2, due to the uncertainties.

For the 32% LiMg samples we found that heat treatment begins to affect the resistivity anomaly; annealing always reduces the magnitude of the anomaly. Also a K cold-welding technique was necessary for making the potential leads of the 32% LiMg samples, since the soldering technique was found to sometimes cause anomalous behavior. Thus we only consider the 32% LiMg sample which was well annealed and with good potential leads, a detailed discuss of the other 32% LiMg data is in Ap.2.

#### 4.1.4.b Comparison with Theoretical Models

As discussed above, the anomaly contributes a negative resistivity term at low temperatures, and its magnitude grows with increasing  $\rho_0$ . In the following we compare the data with models which might explain such behavior. These models are (a) the Kondo effect,

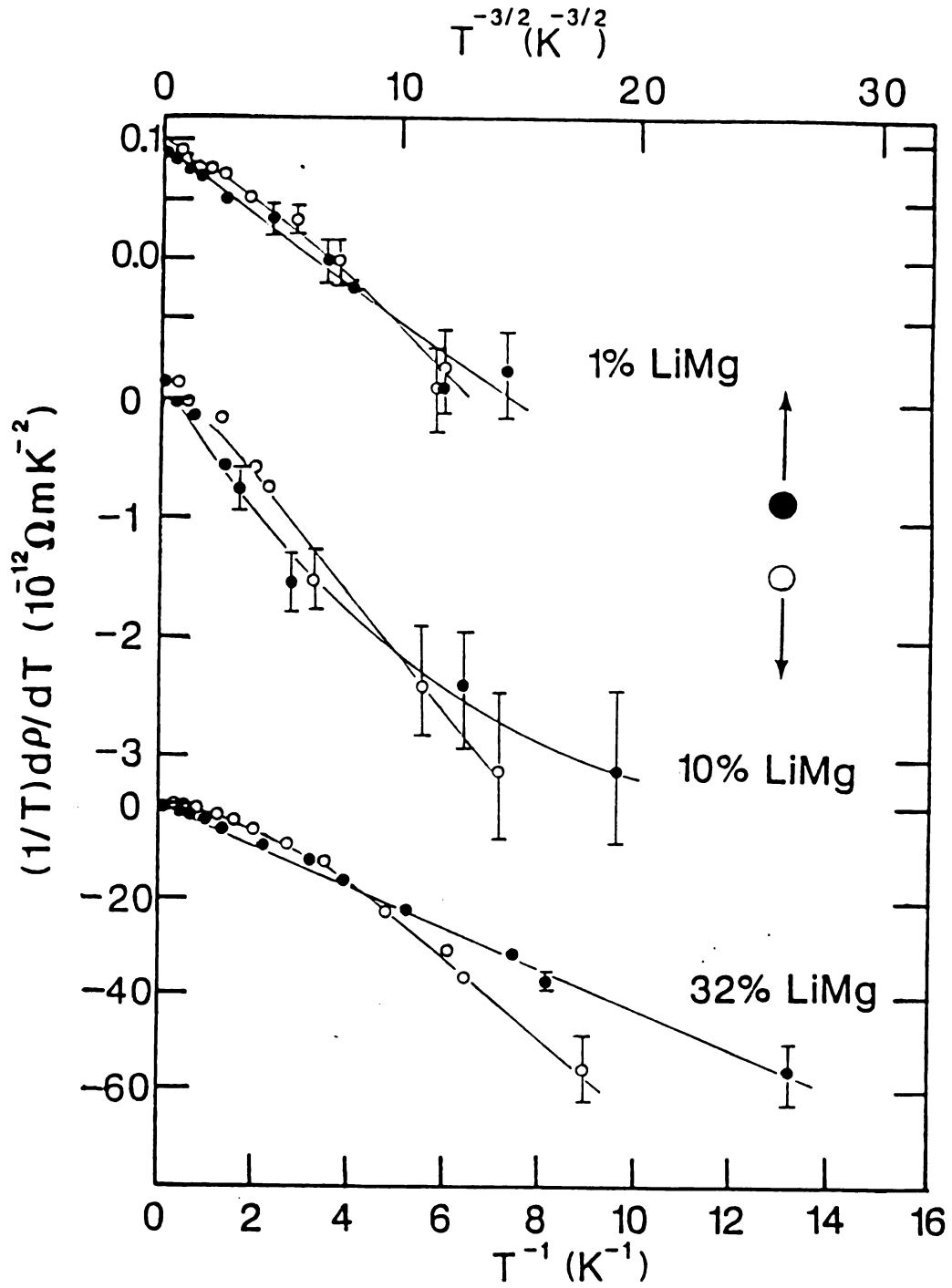


Figure.15:  $(1/T)d\rho/dT$  versus  $T^{-1}$  and  $T^{-3/2}$  for 1%, 10%, and 32% LiMg alloys.

(b) two level systems, (c) ineffectiveness condition for electron-phonon scattering, (d) localization and interaction. The detailed descriptions of these models are given in Ch.2.

(a) The Kondo effect

To test if the anomaly is caused by the Kondo effect, we<sup>63</sup> measured the magnetic field dependence of the anomaly. In Fig.17 the open symbols are with no external magnetic field and the filled ones are with a 0.2 Tesla field. Both the 9.7% KRb and 1% LiMg alloy data show essentially no magnetic field dependence. Applying the theory mentioned in ch.2, a field of 0.2 T should decrease the Kondo temperature by about  $0.3K^{48}$ , which means approximately the patterns of filled symbol should move towards low temperature by about 0.3K. Therefore, the Kondo effect seems to be ruled out. Moreover, as we will describe later, we find no Kondo-type anomalies in the thermoelectric properties.

(b) Two level system

Two level systems were, for a while, proposed to explain the negative logarithmic temperature dependent resistivities in structurally disordered metals.<sup>49</sup> The anomaly for TLS is expected to be independent of magnetic field. Moreover, the extra parameter  $T_K$  in the TLS logarithmic temperature dependent form permits an improvement in the logarithmic fit to the  $\rho(T)$  of our alloy data. However, our samples are crystalline, and it is difficult to see how isolated Rb impurities in crystalline K could be free to tunnel between two alternative positions.

(c) Ineffectiveness of electron-phonon scattering

A postulate on the electron-phonon interaction, that phonons with wavelength exceeding the electron mean free path are ineffective electron scatters, has been applied to the calculation of  $\rho(T)$  for amorphous metals<sup>62</sup>

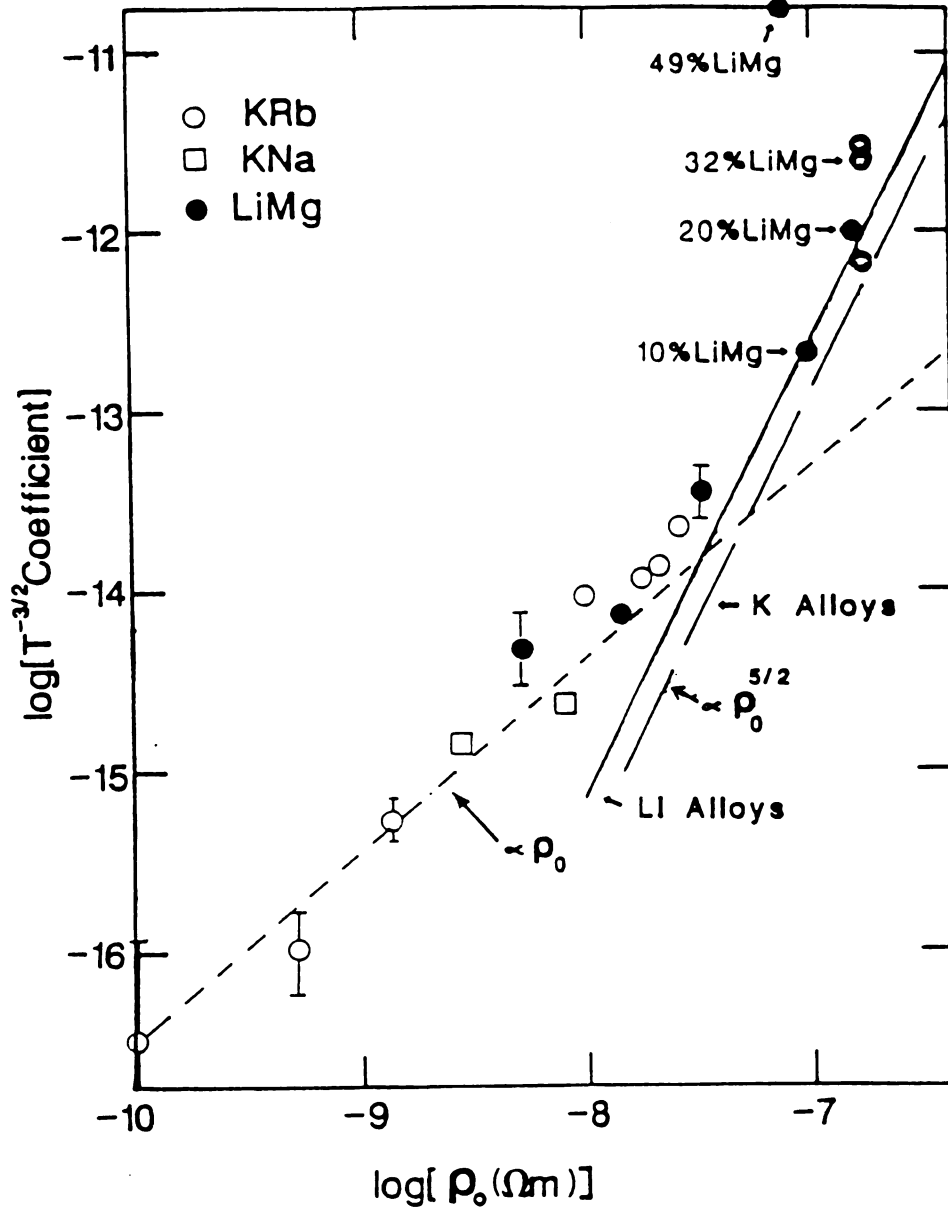


Figure.16: The coefficients of the corresponding  $T^{-3/2}$  term in  $(1/T)dp/dT$  versus  $\rho_0$  for all alloy samples. The dashed line is a  $\rho_0$  dependence. The solid and long dashed lines are  $\rho_0^{5/2}$  dependences for Li and K based alloys, respectively, from electron-electron interaction theory.



which have high  $\rho_0$ . Very recently Kaveh and Wiser<sup>45</sup> applied this postulate to inelastic electron-impurity scattering in KRb alloys at low temperatures. By assuming a phonon cut off wave vector  $q_{\min} = \pi/l$ , they modified Taylor's expression for inelastic electron-impurity scattering and found that it fit the KRb data up to 23.6%, as shown in Fig.18. When we attempt to repeat this calculation using the same formulae they used and the best available value for sound velocity, we do not obtain the fit they show. However, if we treat  $q_{\min}$  as a fitting parameter, we find that we can approximately fit the dilute KRb and LiMg data with  $q_{\min} = (1/4)\pi/l$  and  $q_{\min} = (1/5)\pi/l$  respectively. Fig.19 illustrates the fits (solid lines) to 0.35% and 1% LiMg data. Considering the approximations involved in these calculations, (isotropic Debye model, choice of pseudopotentials, approximation of sound velocities), such a discrepancy in  $q_{\min}$  might be possible. Thus if  $q_{\min}$  is treated as a fitting parameter, the Kaveh and Wiser model can give good fits to the dilute KRb and LiMg data, with values of  $q_{\min}$  within an order of magnitude of that postulated. However, since the postulate has not been generally used in calculating electron-phonon scattering, it seems more theoretical and experimental evidence is needed to make this theory convincing.

#### (d) Localization and interaction

As the electron mean free path becomes short, quantum corrections to the Boltzmann transport theory may no longer be neglected. Our samples are in the weak localization regime(WLR). In the WLR there is interference between scattered partial waves, and this interference can be significant in very short mean free path samples. There are two sources of corrections; a) the localization effect, which involves quantum interference, and b) the interaction effect, which involves modification of

the electron-electron interaction. We compare our data with the theoretical calculations given by Lee and Ramakrishnan<sup>7</sup>. As discussed in Ch.2, if we assume that the "normal" contribution to  $\rho(T)$  is dominated by inelastic electron-impurity scattering, then for our values of  $\rho_0$  the theory predicts that the interaction term should predominate, and  $(1/T)d\rho/dT$  should vary as  $T^{-3/2}\rho_0^{5/2}$ . As summarized in Eq.4.11, such a formula is consistent with LiMg data with  $\rho_0 > 10^{-7} \Omega m$ . To compare the predicted magnitude of interaction effects with the experimental data, the coefficients of the  $T^{-3/2}$  term have been estimated for our KRb, KNa, and LiMg alloys from plots such as the one shown in Fig.10.

We plot these coefficients versus  $\rho_0$  on a log-log plot in Fig.16. The solid line and the broken solid line in Fig.16 are the predicted behavior for interaction effects in Li and K based alloys respectively. For small values of  $\rho_0$  the data in Fig.16 are consistent with a linear dependence on  $\rho_0$ , as indicated by the dashed line, and the data fall well above the solid and broken lines. This shows that the quantum effects are too small to account for the anomaly in these samples. As  $\rho_0$  increases above about  $10^{-7} \Omega m$ , the data break away from the dashed line, and appear to approach the solid line, although the high concentration alloys show large variations from sample to sample for a given Mg concentration. These variations are associated with different heat treatments, which suggests that microscopic differences within these alloys affect the data.

The 49% LiMg alloy has a much bigger magnitude than the prediction. Changing the electron density due to alloying can also affect the magnitude of the interaction effect, however, as estimated in Ch.2 such density changes should only turn the solid line up a little at large  $\rho_0$  in Fig.16.

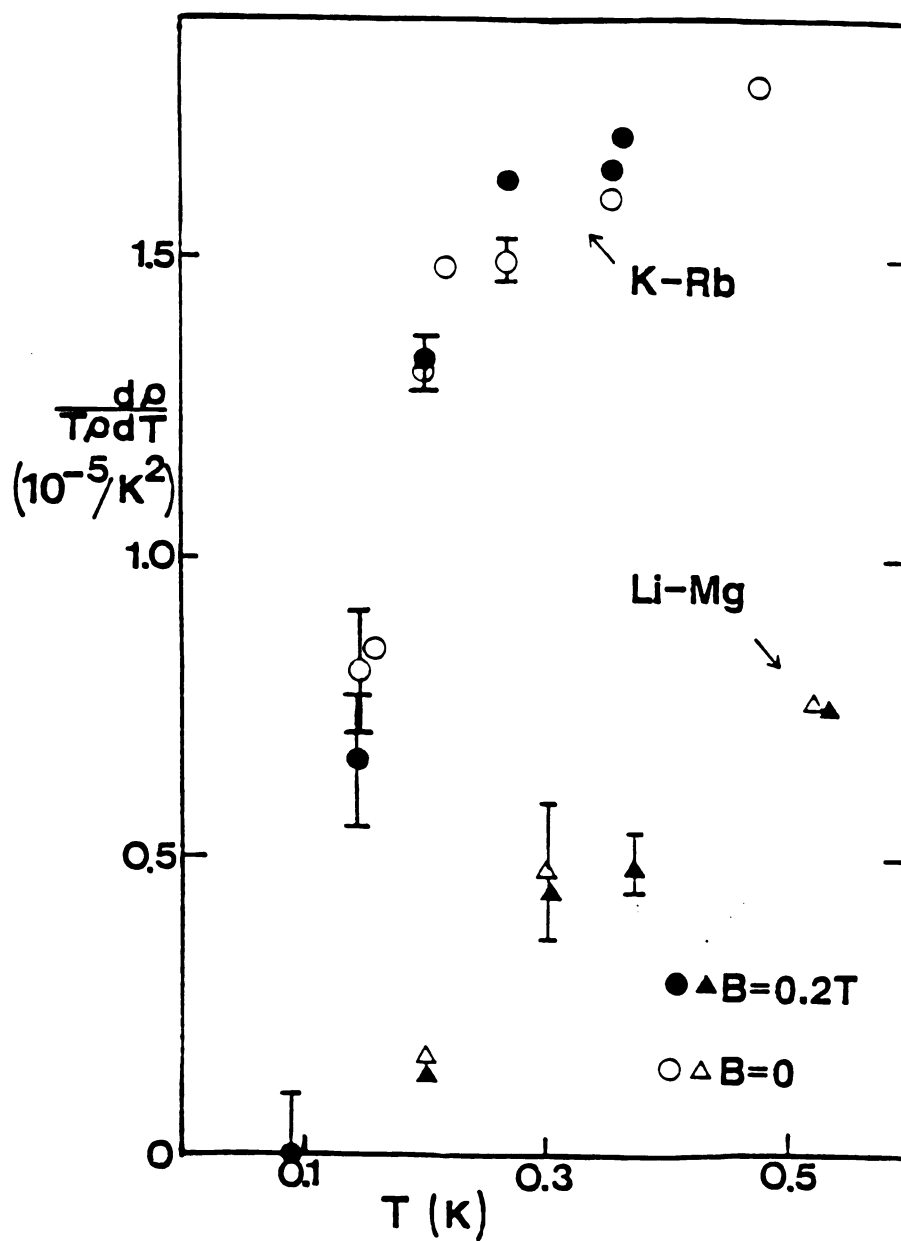


Figure.17:  $(1/T)d \ln \rho / d T$  versus  $T$  for 9.7% K-Rb and 1% Li-Mg alloys for magnetic fields of  $B = 0$  (open symbols) and  $B = 0.2 T$  (filled symbols) .

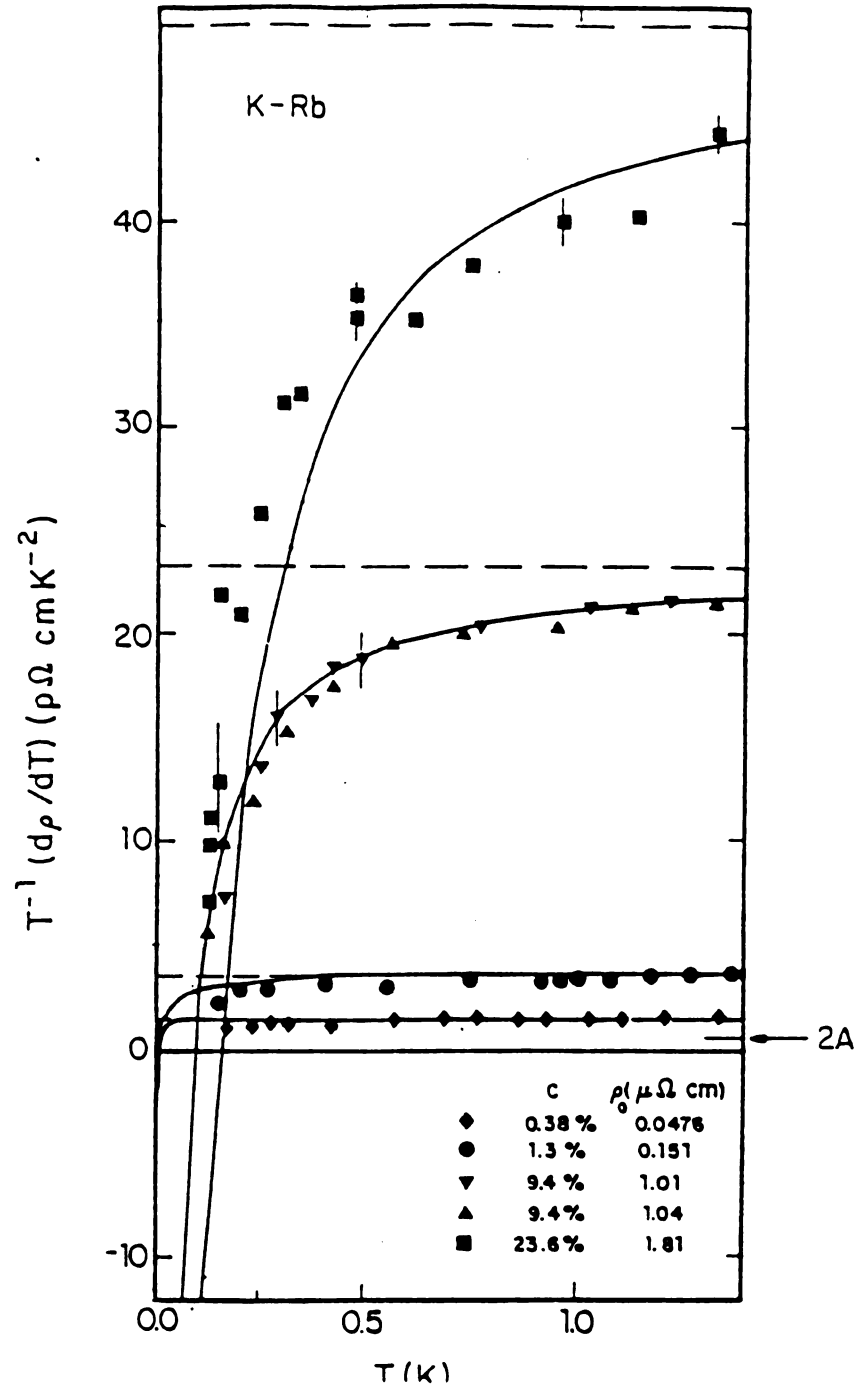


Figure.18:  $(1/T)d\rho/dT$  versus  $T$  for KRb alloys with the solid lines fit to the ineffectiveness of electron-phonon scattering model by Kaveeh and Wiser. The dashed lines indicate the behavior expected from the standard theory. This figure is taken from ref.45.

Other possibilities for increasing the anomaly magnitudes in the high concentration LiMg alloys are: a) since annealed samples always show smaller magnitudes than do unannealed samples, while their  $\rho_0$ 's differ not much, (Ap.2) the disorder formed in the very high concentration alloys seems to enhance the electron-electron interaction over the simple theory. b) the solid line in Fig.16 completely neglects the localization effect. However, localization might become important in very high concentration LiMg alloys, since the argument that the localization effect in LiMg alloys is smaller than the interaction effect is based on the assumption that the "normal" resistivity is dominated by the Koshino-Taylor  $T^2$  term. This assumption may no longer be true in the very high concentration LiMg alloy, especially in the sample with 49% Mg.

#### 4.1.4.c Conclusions Concerning the Low Temperature Resistivity Anomaly

We conclude that a change in the low temperature resistivity of our data takes place at  $\rho_0 \approx 10^{-7} \Omega\text{m}$ .

(A) For KRb, KNa, and LiMg samples with  $\rho_0 < 10^{-7} \Omega\text{m}$ , the resistivity anomaly is approximately proportional to  $\rho_0 T$ , and is not sensitive to an applied magnetic field, nor to the spatial distribution of the impurities. The anomaly is not due to the Kondo effect, or to localization and interaction effects. The anomaly can be fit by the Kaveh and Wiser ineffectiveness electron-phonon scattering model, if substantial variation in the cutoff phonon wave vector is allowed. However, it is not yet clear whether the anomaly might be caused by two-level effects or by other mechanisms.

(B) For LiMg samples with  $\rho_0 > 10^{-7} \Omega\text{m}$ , the anomaly approximately varies as the form predicted for the interaction effect, ( $\propto \rho_0^{5/2} T^{-3/2}$ ), and its magnitude is about what would be expected from electron-electron

interaction theory. For very high concentration LiMg alloys the details of the microscopic structure of the samples seem to affect the anomaly. This behavior is not understood.

#### 4.2 Thermoelectric ratio G

In addition to the resistivity, we also always measured the thermoelectric ratio  $G$ . As described in the above section, when the temperature is low enough,  $L = L_0$  ( $L_0 = 2.44 \times 10^{-8} \text{ V}^2/\text{K}^2$ ), and measuring  $\rho$  and  $G$  provide complete information about electron transport properties. This is true for most of our samples at temperatures below 1K. As discussed in ch.2, the thermoelectric ratio arises fundamentally in two different ways when a temperature gradient is applied to a metal: either because of the thermal "diffusion of the conduction electrons, or because of direct transfer of momentum from excited lattice wave (phonons) to the conduction electrons, the latter being known as "phonon-drag". The free electron theory predicted that

$$G = (L_0/L)[G_0 - bT^2 + c(1/T)\exp(-\theta^*/T)] \quad (4.12)$$

where  $G_0$  is a contribution from thermal diffusion of conduction electrons,  $-bT^2$  is due to normal phonon drag, and the last term is an Umklapp phonon drag term appropriate to the alkali metals with bcc lattice structure. At low temperatures where  $L \approx L_0$  and the exponential term becomes negligible, Eq.4.12 reduces to a simple form

$$G = G_0 - bT^2. \quad (4.13)$$

In the following section we present our experimental data of pure alkali metals and their alloys, and discuss the results in terms of Eq.4.12 and Eq.4.13.

#### 4.2.1 The Lorentz ratio L

As shown in Fig.20, several Ls of different samples were measured to ascertain the general temperature dependence of  $L(T)$ . The values of  $L$  are determined from the Wiedemann-Franz law

$$L = \frac{\kappa}{\sigma T} = \frac{QR}{T\Delta T} \quad (4.14)$$

where  $\kappa$  and  $\sigma$  are the thermal and electrical conductivities respectively,  $Q$  is the heating power,  $R$  is the sample resistance, and  $\Delta T$  is the temperature gradient caused by  $Q$ . From Fig.20 we see that for pure K and KRb samples at low temperatures below about 1.1K,  $L(T)$  is very close to  $L_0$ ,  $1.03 \leq L(T)/L_0 \leq 0.97$ . For quantitative analysis of  $G$  of K and K based alloys we thus concentrate upon  $T \leq 1.1K$ . Above 1K the values of  $L(T)$  for K and KRb samples turn down, as shown in Fig.20. This can be explained<sup>70</sup> as due to the fact that at these intermediate temperatures, electron-phonon interactions produce changes in electron energy which are large compared to  $kT$ , and but changes in electron momentum that are relatively small; thus the thermal conductivity is reduced much more than the electrical conductivity. The  $L(T)$  of the 32%LMg alloy approaches  $L_0$  at very low temperatures and has a different behavior at high temperatures than expected from the above simple electron-phonon scattering consideration. Apparently the electron behavior in very concentrated LiMg alloys is more complex. However, as we will display later, for not very high concentration LiMg alloys the electron behavior seems simple.

#### 4.2.2 G Data

Figs. 21, 22, 23 illustrate the G data for KRb, KNa, and LiMg alloys. Several points are immediately obvious. For Pure K and Rb samples, the data behave as expected from Eq.4.12. The solid lines are fit to Eq.4.12. with  $L=L_0$ . The deduced parameters from the fit are  $G_0 = -0.08V^{-1}$ ,  $b = 0.48V^{-1}K^{-2}$ ,  $c = 6200 V^{-1}K$ , and  $\theta^* = 23K$  for K and  $G_0 = 1.06V^{-1}$ ,  $b = 0.21V^{-1}K^{-2}$ ,  $c = 561 V^{-1}K$ , and  $\theta^* = 9.7K$  for Rb. For pure Li and LiMg samples with Mg concentration up to 20 at%, to within the uncertainty one hardly sees phonon drag effects, due to the high Debye temperatures of the samples. The flat data means that the electron diffusion effect  $G_0$  in Eq.4.12 is dominant in all of those samples. For samples with Mg concentrations up to 32% in Li we begin to see deviation from horizontal line at low temperatures, and the deviation becomes prominent in 49% LiMg sample. The deviation at low temperatures indicates that the electron behavior no longer can be described by simple free-electron theories, and such behavior also show in  $L(T)$  and the resistivity behavior as discussed in the above section.



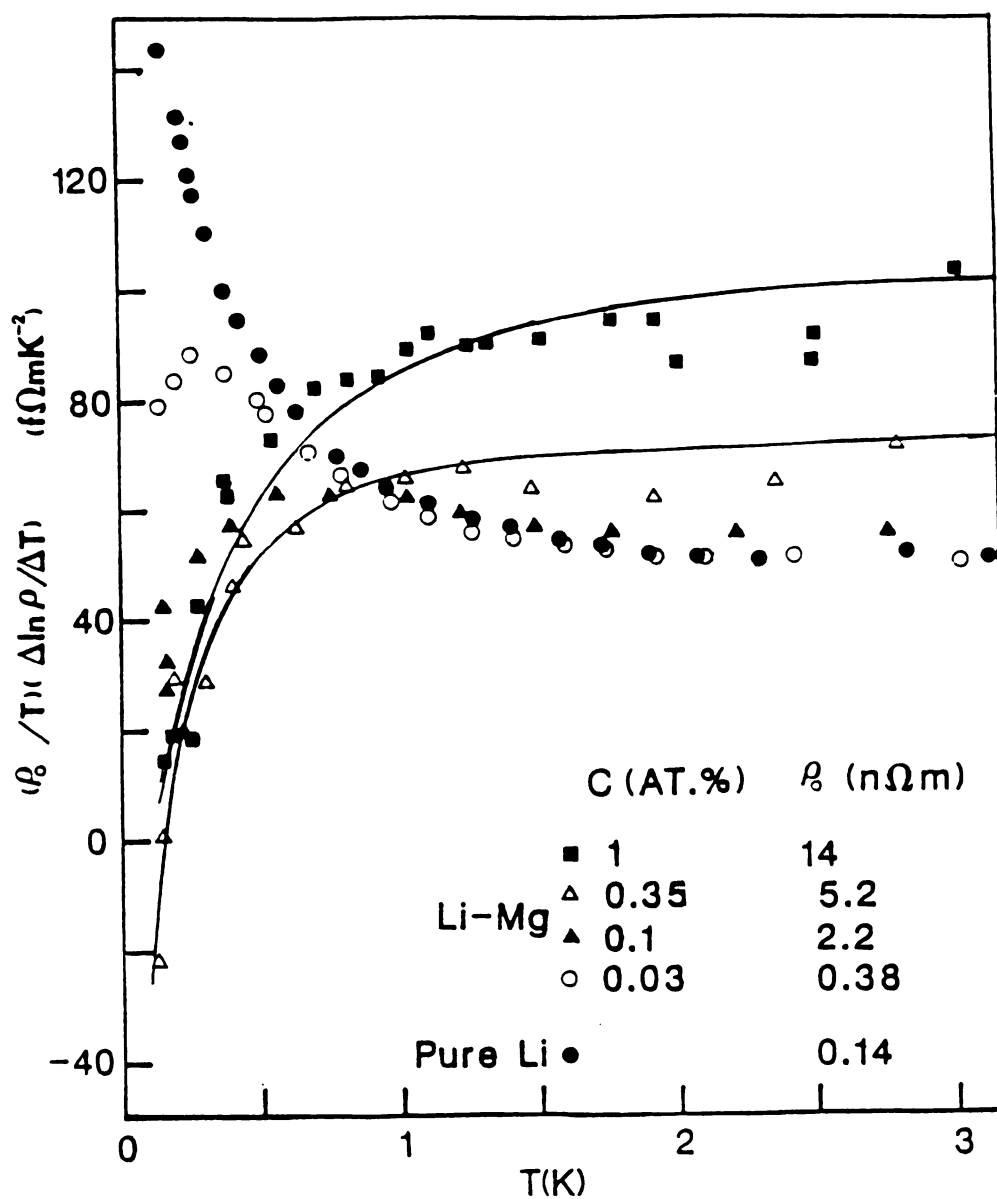


Figure.19:  $(1/T)d\rho/dT$  versus  $T$  for dilute LiMg alloys with the solid lines fit to the ineffectiveness of electron-phonon scattering model.

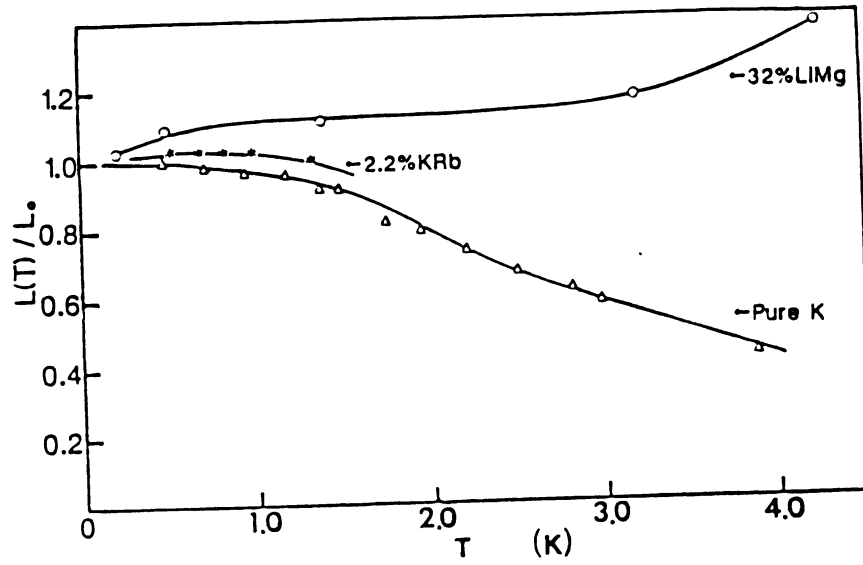


Figure.20: The Lorentz ratio  $L$  versus  $T$  for 32% LiMg and 2.2% KRb alloys, and pure K.

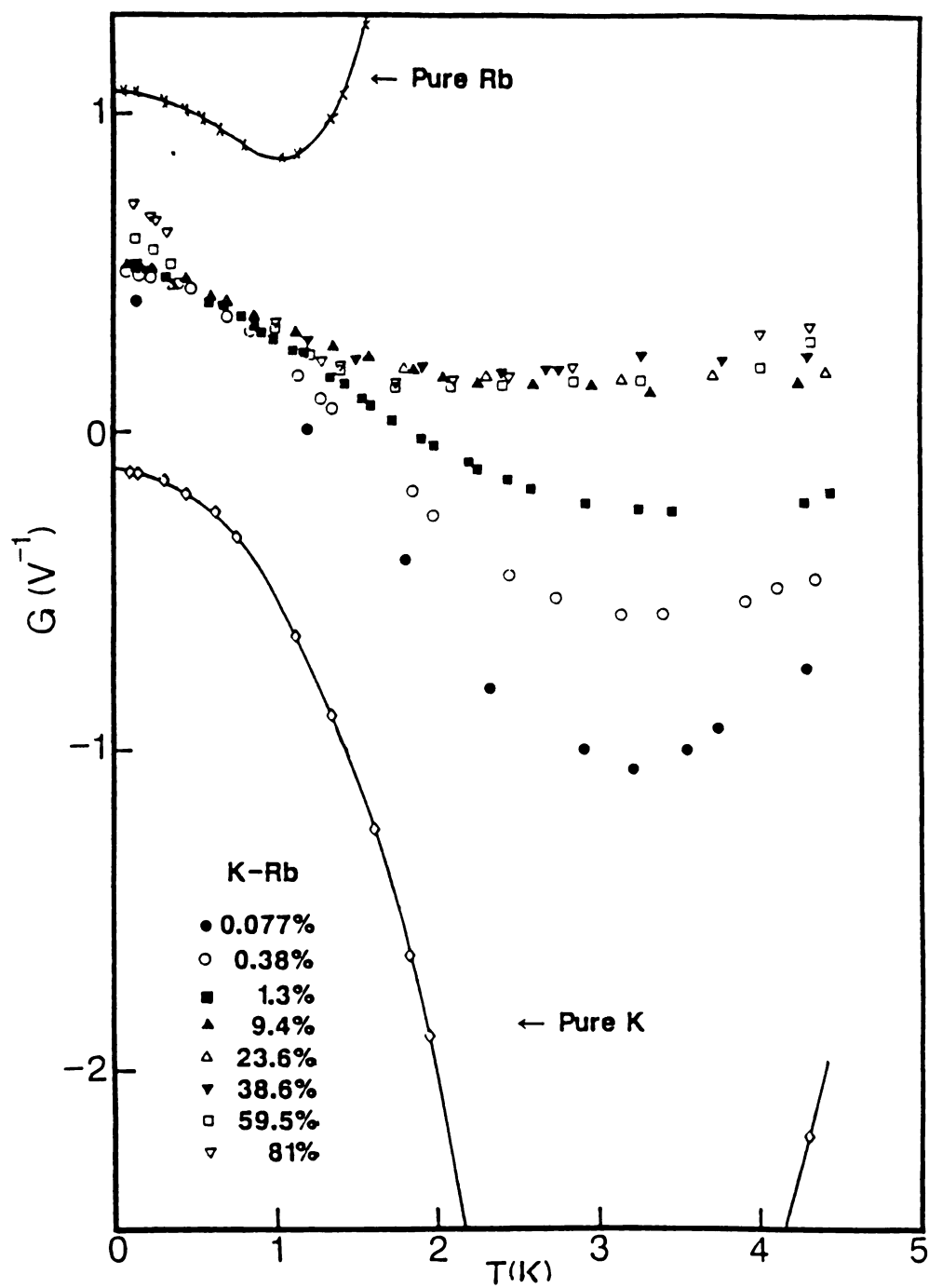


Figure.21:  $G$  versus  $T$  for all  $K_{\underline{R}b}$  alloys, and pure K and Rb .

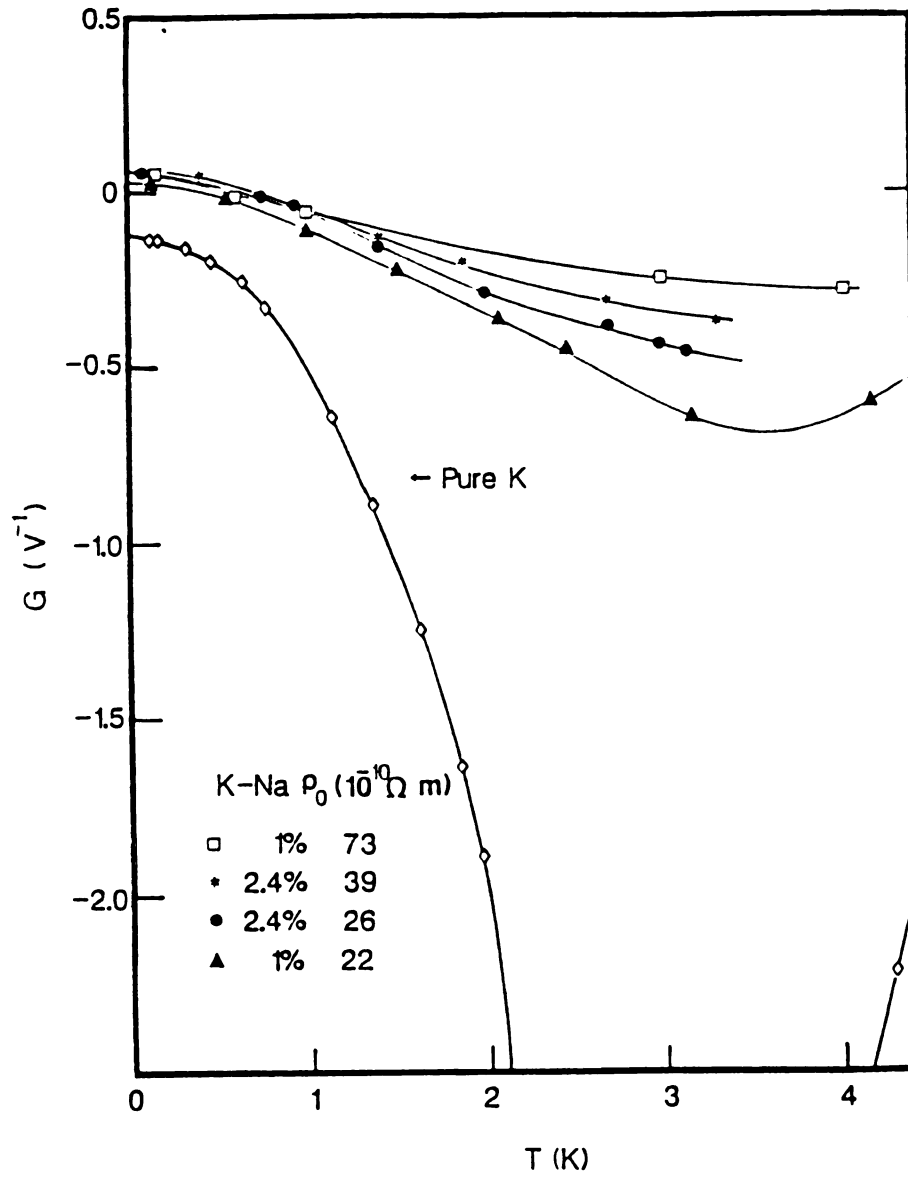


Figure.22:  $G$  versus  $T$  for all  $KNa$  alloys, and pure  $K$ .

#### 4.2.3 The electron diffusion component $G_0$

We determined  $G_0$  by extrapolating the data in Figs.21, 22, and 23 to zero temperature. Generally,  $G_0$  can be written as

$$G_0 = (e/\epsilon_f)\xi. \quad (4.14)$$

Here  $e$  is the electron charge. (which give a negative sign in Eq.4.14) The dimensionless parameter for free-electron like metal (essentially spherical Fermi surface) has the form

$$\xi = 1 + d \ln \ell / d \ln \epsilon \big|_{\epsilon_f} + \Delta \xi \quad (4.15)$$

where  $\ell$  is the electron mean free path and  $\Delta \xi$  is the many-body contributions. Thus  $G_0$  is determined essentially by the properties of the Fermi surface of the conduction electrons and the electron scattering processes. The electron diffusion component  $G_0$  of free-electron like metals can be separated into different scattering contributions by the Gorter-Nordheim relation

$$G_0 = (\rho_a G_0^a + \rho_p G_0^p) / \rho_0 \quad (4.16)$$

where the subscripts  $a$  and  $p$  represent the two different scatterers e.g. the alloy impurity "a" and the impurities and defects in the relatively pure samples "p".  $\rho_0 = \rho_a + \rho_p$ . Due to the lack of detail knowledge of the residual impurities and defects inside the relatively pure K, Rb, and Li, here we only focus on  $G_0$  arising from electron scattering by the deliberately added impurities. Eq.4.16 can be rewritten to eliminate the variable  $\rho_a$ .

$$G_0 = G_0^a + (\rho_p / \rho_0) (G_0^p - G_0^a) \quad (4.17)$$

Since  $G_0^a$ ,  $G_0^p$ , and  $\rho_p$  are assumed constant for a alloy system made from the same purity host metal, a plot of  $G_0$  versus  $(1/\rho_0)$  should yield a straight line with intercept  $G_0^a$  and slope  $\rho_p(G_0^p - G_0^a)$ , and this is displayed in Fig.24. For dilute alloys the data show a linear behavior. It is easy to see from the above equations that a straight line relationship suggests the Fermi surface of the host metal has not been affected by the amount of alloying solute involved. Hence, from Fig.21 we can conclude that the K Fermi surface appreciably begins to change at Rb concentrations about 39 at% , and from Fig.23, Li Fermi surface changes take place at Mg concentrations up to about 3%. It is interesting to note that no significant Fermi surface changes even up to this high concentration of Rb in K. Rb appears to fit very well into the K lattice; for the atomic volumes of the two metals do not differ much and the two metals form a continuous range of solid solution with a very narrow liquid + solid region in the phase diagram. The  $G_0$  due to KRb, KNa, and LiMg alloying are listed in table 2, which are obtained from the intercepts in Fig.24.

Table 2  $G_0(V^{-1})$ 

Alloy	$G_0(\text{exp.})$	$\xi(\text{exp.})$	$\xi(\text{N\&T})$
<u>KRb</u>	$+0.50 \pm 0.05$	$-1.1 \pm 0.1$	$-0.3 \pm 0.5$
<u>KNa</u>	$+0.07 \pm 0.05$	$-0.2 \pm 0.1$	$+0.9 \pm 0.5$
<u>LiMg</u>	$-0.2 \pm 0.1$	$+1.0 \pm 0.5$	

N&T--Nielsen and Taylor<sup>37</sup>

From Eq.4.15 we see that without the many-body effect correction  $\xi$  is explicitly dependent on the scattering, namely  $(d\ln\ell/d\ln\epsilon)_{\epsilon_f}$ . For elastic scattering one would expect that the electron mean free path  $\ell$  would increase with  $\epsilon$ . For example, with unscreened Coulomb scattering,  $\ell$  is proportional to  $\epsilon^2$ , and for perfect screening or hard sphere scattering,  $\ell$  is independent of  $\epsilon$ . Thus the value of  $\xi$  should be in the range of 1 ~ 3. From the experiment results and Eq.4.15, we see that the effects of the many-body dominate the sign as well as the magnitude of the thermal diffusion effects. The signs of  $\Delta\xi$  were estimated by Nielsen and Taylor<sup>37</sup> to be negative, which is in agreement with the experimental results. However, the predicted magnitudes are not quite agree, which be may due to, as emphasized by Nielsen and Taylor, the large uncertainty arising from the choice of potential, since no accurate pseudopotentials for Rb and Na

impurities inside K seem available. It should be pointed out that the listed theoretical values were fit to the experimental results of the thermoelectric power of KRb and KNa alloys at 3K measured by Guenault and MacDonald<sup>36</sup>. From Figs.21, 22, we see that  $G_0$  obtained by the data at 3K are a very rough approximation, which neglect the effect of phonon-drag below 0.3K. Such an approximation decreases the values of  $G_0$  by about  $0.3V^{-1}$  for KRb and KNa alloys, and this will makes  $\xi$  close to the listed theoretical values.

#### 4.2.4 The Phonon Drag Components

The effects of alloying on the phonon drag components of KRb and KNa alloys can be seen from Figs.21 and 22. Both Normal and Umklapp phonon drag (in terms of Eq.4.12) are quenched more and more as the impurity concentration increases, i.e., the magnitudes of these two terms decrease as  $\rho_0$  increases (this is also true for the segregated KNa samples). A more detailed illustration of the Normal phonon drag component of pure K and KRb is shown Fig.25, where we plot  $G$  versus  $T^2$  for the low temperature data. We see that for both pure K and dilute KRb alloys the data fall nicely on straight lines as expected from Eq.4.13, and the slope decreases as the impurities concentration increases as expected from impurity quenching phonon drag. Fig.25 also illustrates that the Normal phonon drag component deviates from the simple  $T^2$  behavior by the 9.4% KRb sample. The observation of impurity quenching phonon drag is consistent with the resistivity measurements as discussed in section 1.



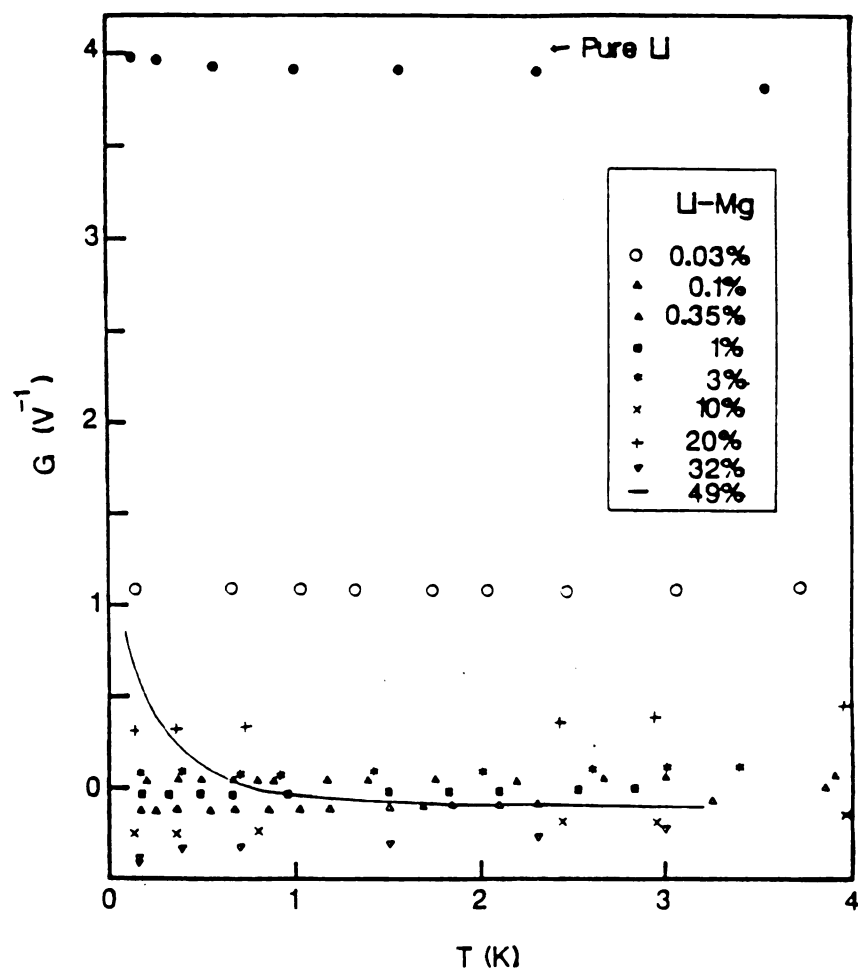


Figure.23:  $G$  versus  $T$  for all  $\underline{\text{LiMg}}$  alloys, and pure Li.

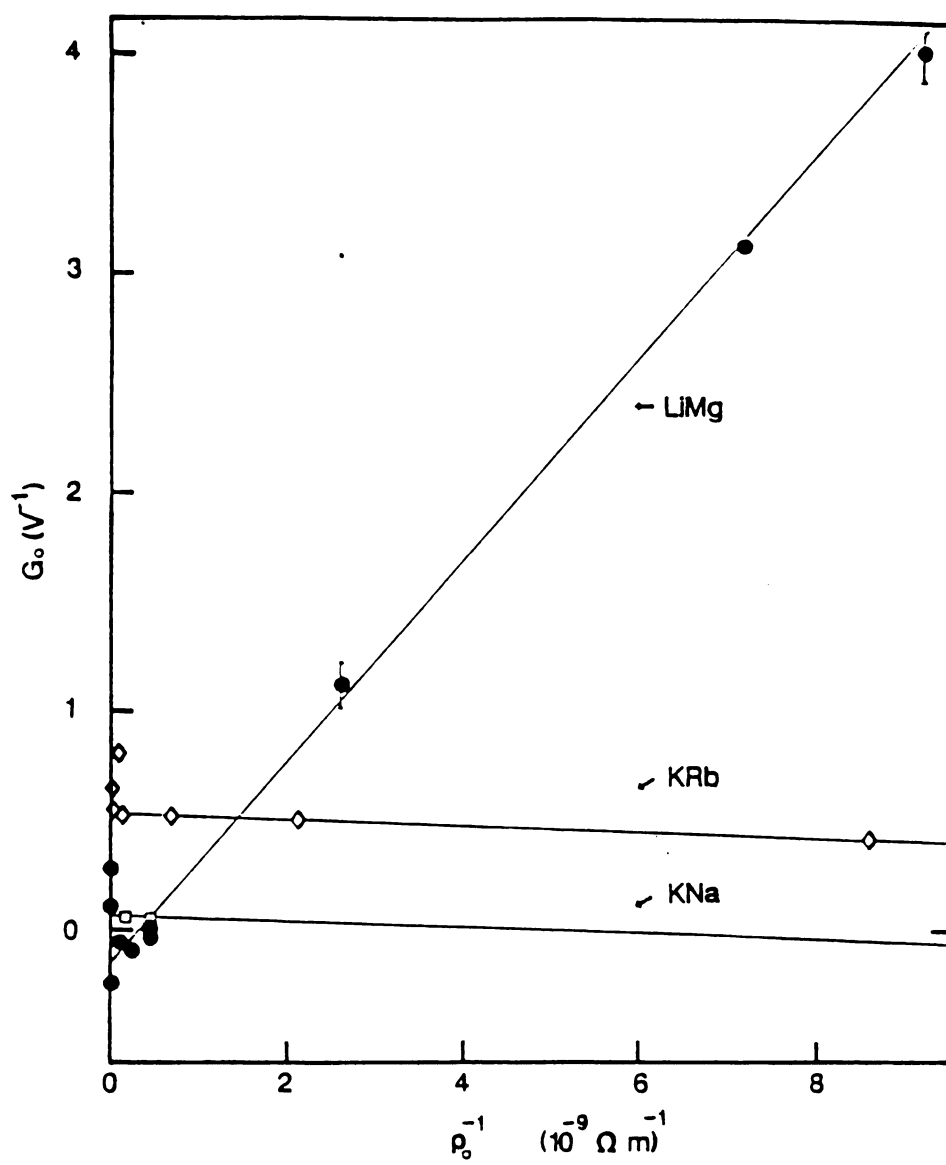


Figure.24:  $G_0$  versus  $\rho_0^{-1}$  for all alloy samples.

#### 4.2.5 Conclusions

(1) We obtained reliable values of electron thermal diffusion components  $G_0$  for KRb, KNa, and LiMg alloys.

(2) The thermoelectric properties of dilute KRb, KNa, and LiMg alloys are simple, as expected from the free-electron theories. For LiMg samples with Mg concentrations higher than about 30%, the thermoelectric properties become much more complicated.

(3) Alloying dose not significantly change the Fermi surfaces of the host for impurity concentrations up to about 39% in KRb and 3% in LiMg alloys.

(4) The many-body effects dominate the sign as well as the magnitudes of the thermal diffusion component.

(5) Adding impurities to K quenches both N-phonon-drag and U-phonon-drag.

## Chapter 5

## ELECTRON-ELECTRON SCATTERING

There has been considerable interest in the past few years in electron-electron scattering in very pure metals at low temperatures. As discussed in Ch.2, the electron-electron scattering contribution to the resistivity  $\rho_{e-e}(T)$  in alkali metals is predicted to be dominated by U-scattering and to have the form:

$$\rho_{e-e}(T) = AT^2 \quad (5.1)$$

The experimental data and the best theoretical calculations are listed in table.3, where the experimental values of A for K and Li are obtained from Fig.8 and A for Na from Fig.2.

Table 3      A ( $\text{f}\Omega\text{mK}^{-2}$ )

metal	A(MD) (bcc alkali) fcc Al	A(exp.)
Li	2.1	27±2
Na	1.4	1.7±0.3
K	1.7	2.4±0.4
Al	4.3	2.7(Rt)

MD --MacDonald et al. 1981<sup>64</sup>

Rt --Ribot et al. 1981<sup>65</sup>

In K, Na, and Al, the values of  $A$  for freely hanging bulk samples are in satisfactory agreement with the latest calculations and are insensitive to small amounts of impurities or defects.<sup>24,23,65</sup>

The unexpectedly large value of  $A$  in very pure Li, on the other hand, is a puzzle. Although this  $A$  appears to be insensitive to small amounts of impurities or defects,<sup>34,23</sup> it is about an order of magnitude larger than the predicted value. As we mentioned in Ch.1 Li has the most distorted spherical Fermi surface among the alkali metals, and it undergoes a 75%-complete martensitic transformation at about 75K to a more complex structure,<sup>67</sup> for which the Fermi surface either contacts or nearly contacts several Brillouin zone boundaries that have substantial energy gaps. The discrepancy between experiment and theory is surely related to the fact that the prediction was made for Li in BCC crystal structure with a nearly spherical Fermi surface which does not contact Brillouin zone boundaries. There are two very different ways in which the phase transformation might produce a value of  $A$  larger than predicted: (A) indirectly or (B) directly.

(A) The argument for an indirect mechanism was made by Sinvani et al.,<sup>34</sup> as follows. As derived in Ch.2, for a metal with a spherical Fermi surface which does not contact Brillouin zone boundaries and in which the dominant (e.g. impurity) scattering mechanism is isotropic in  $k$ -space, normal electron-electron scattering does not contribute to  $\rho(T)$ . The only contribution is due to Umklapp electron-electron scattering which, as listed in table 3, is estimated for BCC Li at  $2.1 \text{ f}\Omega \text{ mK}^{-2}$ . If, instead, the dominant scattering mechanism is anisotropic in  $k$ -space, then normal electron-electron scattering can contribute to  $A$ , (i.e. Eq.2.24 does not vanish), and  $A$  is the sum of Umklapp and Normal terms,  $A = A^U + A^N$ . Sinvani et al. argued that there should be two sources of anisotropy in Li;

1) Due to the large deviation of the Fermi surface of Li from sphericity in the 110 direction, it seems necessary to use a multiple plane-wave pseudo-wavefunction, which leads to a mildly anisotropic  $\tau(\vec{k})$  even for the scattering of an electron by an isotropic impurity. They calculated this "impurity-scattering dominated"  $A_i^N$  to be about  $0.8 \text{ f}\Omega \text{ mK}^{-2}$ . 2) A large "effective dislocation density" might be introduced into Li during its transformation, and might produce highly anisotropic scattering. This would put  $A^N$  into its anisotropic limit  $A_a^N$ , they estimated  $A_a^N$  to lie between  $10$  and  $40 \text{ f}\Omega \text{ mK}^{-2}$ . Therefore, they argued that  $A_a^N$  is the explanation of the large experimental value of  $27 \text{ f}\Omega \text{ mK}^{-2}$ . Using their estimates, the impurity-scattering dominated  $A = A^U + A_i^N$  would be about  $3 \text{ f}\Omega \text{ mK}^{-2}$ .

(B) The argument for a direct mechanism is that the large value of  $27 \text{ f}\Omega \text{ mK}^{-2}$  for  $A^U$  arises from greatly increased Umklapp electron-electron scattering associated with the complex Fermi surface of Li at low temperatures. That is, that the  $A^U$  calculated for bcc lattice is just not relevant to real Li at low temperatures.

To discriminate between these two mechanisms, we have measured the temperature-dependent resistivities of pure Li and several dilute LiMg alloys from 4K down to 0.1K. LiMg alloys with concentrations up to 20 at.% undergo martensitic transformations upon cooling<sup>69</sup> similar to that for pure Li. As noted before, except at the lowest temperatures, addition of Mg to Li should add to equation 5.1 an inelastic impurity scattering term of the form  $B\rho_0 T^2$  to give

$$\rho(T) = AT^2 + B\rho_0 T^2 \quad (5.2)$$

As is true for most impurities in most host metals, we would expect Mg to scatter electrons nearly isotropically in Li, consistent with the estimate of Sinvani et al. for impurity-dominated scattering. Addition of Mg to Li should then lead to one of two possible outcomes:

(i) Indirect. An earlier paper by Kaveh and Wiser<sup>68</sup> (1982) indicated that  $A^N$  should decrease rapidly as isotropic impurity scattering increases. Using information given by Sinvani et al (1981), we estimate that addition of only about 0.05% of Mg to Li would reduce  $A^N$  from  $\sim A_a^N$  to  $\sim A_i^N$ , and that extrapolation of  $A+B\rho_0$  for more concentrated LiMg alloys back to the Mg-free limit should yield  $A=A^U + A_i^N \sim 4f\Omega m K^{-2}$ .

(ii) Direct. If the effects of anisotropic scattering are small, then  $A=A^U$  will be large, and will hardly change upon addition of a small amount of Mg to Li. In this case, a linear extrapolation should yield a coefficient  $A$  of about  $27 f\Omega m K^{-2}$ .

In figure 26 we replot, from figure 7, the  $T^2$  coefficient of  $\rho(T)$  against  $\rho_0$  for pure Li and the LiMg alloys, along with the broken curve which represents our estimate for the indirect mechanism using the parameters of Sinvani et al. The alloy data are plotted as open triangles and the pure Li as a full triangle. We see that the alloy data extrapolate linearly back to the pure Li value of  $A=27f\Omega m K^{-2}$ . The data thus follow the form of equation (5.2) with a constant value of  $A$ , and not the broken curve estimated for the indirect mechanism of Sinvani et al.

We conclude that the unexpectedly large  $A$  in Li is due not to dominance of anisotropic scattering, but rather to the change in Fermi surface which accompanies the transformation that Li undergoes at about 75K. We note that the  $T^2$  coefficients for dilute  $\underline{K}Rb$  and dilute  $\underline{K}Na$  alloys (see figure 7) also extrapolate directly to the coefficient for pure bulk

K. It thus appears that anisotropic scattering is not needed to explain the behaviour of the  $T^2$  components of the resistivities of either Li or K in the vicinity of 1K.

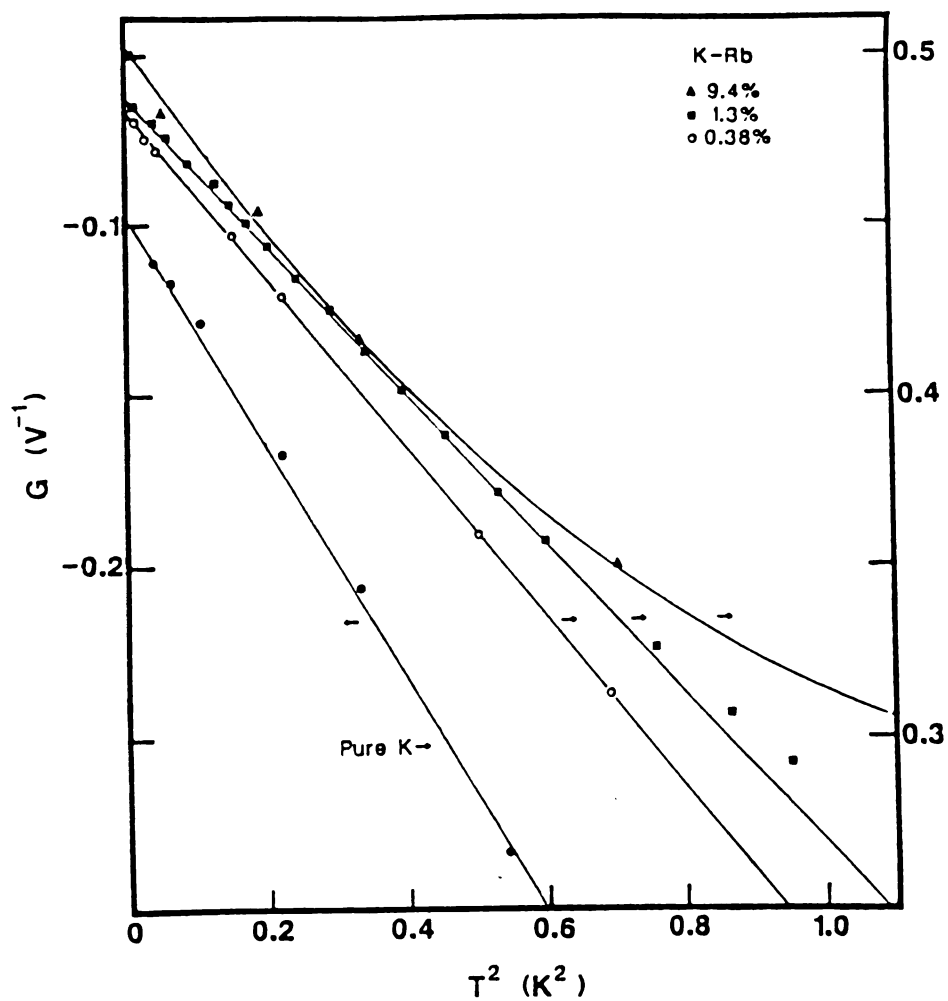


Figure.25:  $G$  versus  $T^2$  for  $K_{\underline{R}b}$  alloys.



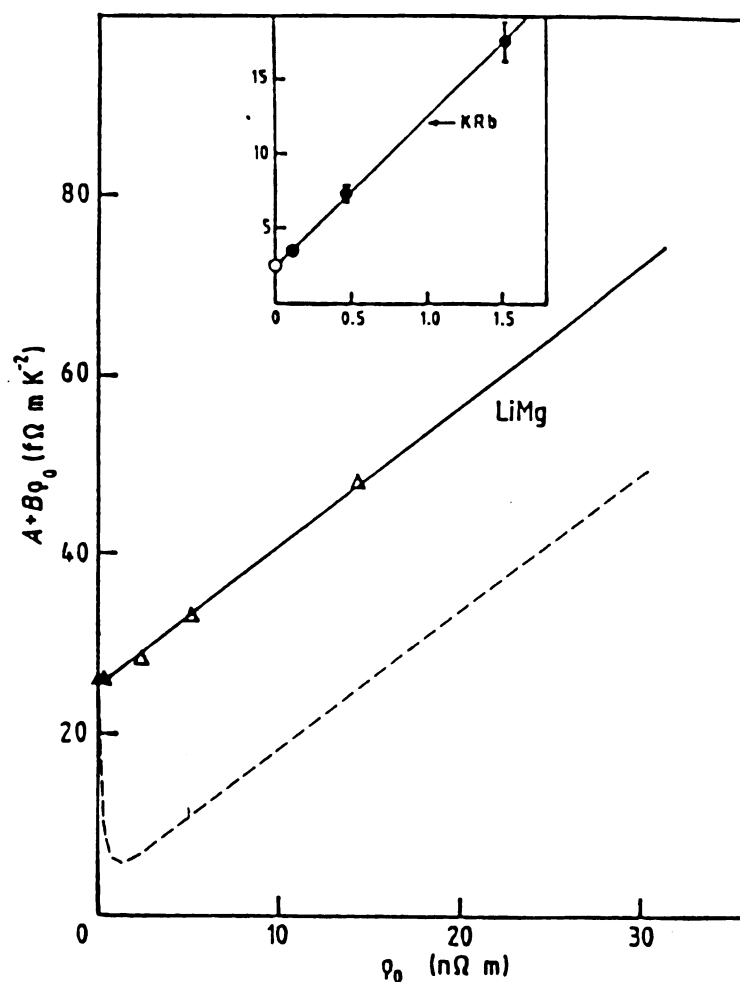


Figure.26: The values of  $A + B\rho_0$  determined from figure 7 against  $\rho_0$  for LiMg alloys (open triangles) and pure Li (full triangle). The broken curve represents the expected behavior for LiMg with anisotropic scattering, using the parameters suggested by Sinvani et al. Data for KRb alloys (full circles) and for pure K (open circle) are given in the same units in the inset. Note that both the LiMg and KRb data extrapolate linearly to their respective pure metal data points.

## REFERENCES

(Chapters 1 - 5)

1. R. Taylor, C.R. Leavens, and R.C. Shukla, Solid State Comm.19, 809 (1976); C.R. Leavens and R. Taylor, J.Physis. F.8, 1969 (1978).
2. H. van Kempen, J.S. Lass, J.H. Ribot, and P. Wyder, Phys. Rev. Lett. 37, 1574 (1976).
3. J.A. Rowlands, C. Duvvury, and S.B. Woods, Phys. Rev. Lett. 40, 1201 (1978)
4. C.W. Lee, W.P Pratt Jr., J.A. Rowlands, and P.A. Schroeder, Phys. Rev. Lett. 45, 1708 (1980).
5. C.W. Lee, M. M. Haerle, V. Heinen, J.A. Rowlands, . Bass, W.P. Pratt Jr., and P.A. Schroeder, Phys. Rev. B25, 1411 (1982).
6. A.W. Overhauser, Adv. in Phys. 37, 343 (1978).
7. P.A. Lee and T.V. Ramakrishnan, Rev. Mod. Phys. 57, 287 (1985).
8. M.J.G. Lee CRC Crit. Rev. Sol. t. Sc. 2, 85 (1971).
9. M. de Podesta, and M. Springford, J. Phys. F. 16, L131 (1986).
10. T.M. Giebultowicz, A.W. Overhauser, S.A. Werner, Phys. Rev. Lett. 56, 1485 (1986).
11. J.A. Wilson and M. de Podesta, J. Phys. F. 16, L121 (1986).
12. J. M. Ziman, Electrons and Phonons, Oxford niversity Press, London,(1960).
13. L. Landau and I. Pomeranchuk Phys. Sowjetunion 10, 649, (1936).
14. A.H. MacDonald, R. Taylor and D.W. Geldart Phys. Rev. B 23, 2718,(1981).
15. S. Koshino, Prog. Theor. Phys., 24, 484 (1963); Ibid., 24, 1049 (1960).

16. P. L. Taylor, Proc. Phys. Soc., 80, 755 (1960); Proc. R. Soc. A275, 209 (1963); Phys. Rev. A135, 1333 (1964).
17. J. A. Rowlands, C. Duvvury, and S. B. Woods, Phys. Rev. Lett. 40, 1201 (1978).
18. N. Wiser, Contemp. Phys., 25, 211 (1984).
19. H. van Kempen, J. S. Lass, J. H. J. M. Ribot, and P. Wyder, Phys. Rev. Lett. 37, 1574 (1976).
20. M. F. Bishop and A. W. Overhauser, Phys. Rev. B, 23, 3638 (1981); Ibid., 18, 2447 (1978).
21. M. Kaveh and N. Wiser, J. Phys. F, 10, L37 (1980).
22. B. Levy, M. Sinvani, and A. J. Greenfield, Phys. Rev. Lett. 43, 1776 (1979).
23. Z.-Z. Yu, Ph.D. thesis, Michigan State University, 1984.
24. C. W. Lee, M. L. Haerle, V. Heinen, J. Bass, W. P. Pratt, Jr., J. A. Schroeder, Phys. Rev. B, 25, 1411 (1982).
25. M. L. Haerle, Ph.D. thesis, Michigan State University, 1983; M. L. Haerle, W. P. Pratt Jr., and P. A. Schroeder, J. Phys. F 13, L243 (1983).
26. S. Yin, Ph.D. thesis, Michigan State University, 1987.
27. M. E. Farrell, M. F. Bishop, N. Kumar, and W. E. Lawrence, Phys. Rev. Lett. 55, 626 (1985).
28. M. Kaveh and N. Wiser, J. Phys. F, 15, L195 (1985).
29. S. DeGennaro and A. Rettori, J. Phys. F, 14, L237 (1984); *ibid.* 15, (1985).
30. C. W. Lee, W. P. Pratt, Jr., J. A. Rowlands, and P. A. Schroeder, Phys. Rev., 45, 1708 (1980).
31. F. W. Kus and D. W. Taylor, J. Phys. F 10, 1495 (1980).

32. J.Bass, M.L.Haerle, W.P. Pratt, Jr., P.A. Schroeder, and Z.-Z. Yu, LT-17 U.Eckern, A.Schmid, W. Weber, H. Wuhl (eds) Elsevier Science Publisher B.V.,(1984).
33. G.Krill, Solid State Comm. 9, 1065, (1971).
34. M. Sinvani, A.J. Greenfield, M. Danino, M.Kaveh and N. Wiser, J. Phys., F 11 L73 (1983).
35. G. Oomi, M.A.K. Mohamed and S.B. Woods J. Phys. Rev. B 23,2718 (1981).
36. D.K.C MacDonald, W. B. Pearson, and I.M. Templeton, Proc. R. Soc. A,248, 107 (1958); *ibid.*, 256, 334 (1960). A.M. Guenault and D.K.C. MacDonald, Proc. R. Soc. A,264, 41 (1961); *ibid.*, 274, 154 (1963).
37. P.E. Nielsen and P.L. Taylor, Phys. Rev. Lett. 10, 4061, (1974).
38. C. W. Lee, Ph.D. Thesis, Michigan State University, 1980.
39. Hansen, Constitution of Binary Alloys, McGraw-Hill Book comp. 1958.
40. A.H. MacDonald Phys. Rev. Lett. 44, 489, (1980).
41. Z. -Z. Yu, M.Haerle, J.W. wart, J.Bass, W.P.Pratt,r., and P.A.Schroeder,Phys. Rev. Lett. 52, 368 (1984).
42. P.G. Coulter and W.R. Datars, J. Phys. F.14, 911 (1984).
43. A. Faldt and L. Wallden, J. Phys. C.13, 6429 (1980).
44. J.S.Dugdale, The Electrical Properties of Metals and Alloys, Edward Arnold, London, 1977.
45. M.Kaveh and N.Wiser, Phys. Rev. B 36, 6339, (1987).
46. S.P.Hu and A.W. Overhauser, Bull. Am. Phys. Soc. 30, 261(1985). S.Hu,Ph.D Thesis Purdue University, 1987.
47. J. Kondo, Progr. heoret. Phys.32,37 (1964).
48. W.A. Harrison, Solid State Theory, Dover Publications, Inc. 1979.
49. R.W. Cochrane and .O. Strom-Olsen, Phys. Rev. B 29, 1088 (1984)
50. P.W. Anderson, Phys. Rev. 109,1492, (1958).

51. D.Y. Sharvin and Y.V.Sharvin. JETP Lett. 34, (1981).
52. D.J. Thouless, Phys. Rev. Lett. 39, 1167, (1977).
53. B.L. Altshuler and A.G. Aronov, ETP Lett.30, 514 (1979).
54. W.E.Lawrence and J.W.Wilkins, Phys. Rev. B,7, 2317 (1973).
55. P.G.Klemens, Handb.Phys.14, 198, (1956).
55. D.L.Edmunds, W.P.Pratt, Jr., and J.A.Rowlands, Rev. Sci. Instrum.51, 1517, (1980).
56. M.A.Howson and D.Greig, J.Phys.F16, 989, (1986); *ibid.*, Phys.Rev.B, 30, 4805, (1984).
57. C.C. Tsuei, Phys.Rev.Lett. 57, 1943, (1986).
58. T.F.Rosenbaum, K.Andres, G.A.Thomas, and P.A.Lee, Phys.Rev.Lett. 46, 568, (1981).
59. J.Bass, Landolt-bornstein New Series, Group III, Vol.15a, Metals: Electronic Transport Phenomena", Springer Verlag, Berlin, 1982.
60. M.L.Haerle, W.P.Pratt, Jr., and P.A.Schroeder, J.Low temp. Phys.62, 397, (1986).
61. Y. Kagan and A.P. Zhernov, Soviet Phs. JETP 23, 737, (1966).
62. P.J. Cote and L.V. Meisel, Phys.Rev. Lett.39, 102 (1977); 40, 1586 (1978)
63. J.Bass, .L.Haerle, W.P.Pratt, Jr., Y.J.Qian, P.A.Schroeder, S.Yin, Z.-Z.Yu, and J.Zhao, Phys.Rev.Lett. 56, 957, 1986.
64. A.H.MacDonald, R.Taylor and D.J.W. Geldart, Phys.Rev.B23, 2718 (1981).
65. J.H.J.M.Ribot, J.Bass, H.van Kempen and P.Wyder, J.Phys.F,9, L117, (1979); Phys.Rev.B 23, 532 (1981).
67. A.W. Overhauser, Phys.Rev.Lett.53, 64 (1984).
68. M.Kaveh and N.Wiser, J.Phys.F 12, 935 (1982).
69. G.Oomi and S.B.woods, Solid State Commun.53, 223 (1985).

70. George Terence Meaden, "Electrical Resistance of Metals", Plenum Press, 1965. 71. N. Wiser, Contemp. Phys. 25, 211 (1984).

## Chapter 6

## ELECTRONIC TRANSPORT PROPERTIES OF THIN POTASSIUM WIRES BELOW 1K

6.1. DERIVATIVE OF ELECTRICAL RESISTIVITY,  $d\rho/dT$ 6.1.1 Introduction.

We recently published<sup>1</sup> measurements of the temperature dependent electrical resistivities  $\rho(T)$  below 1K of thin, high purity potassium (K) wires prepared and cooled to low temperatures in the presence of He gas. As shown in Fig. 1, wires thinner than diameter  $d \approx 1$  mm showed anomalous deviations from the simple  $T^2$  variation expected for electron-electron scattering. Wires thinner than the elastic bulk mean-free-path for impurity scattering ( $\ell \approx 0.2$  mm) displayed negative values of  $d\rho/dT$ , the temperature derivative of the resistivity. When Rb was added to the K to reduce  $\ell$  to  $\sim 0.02$  mm, a  $d = 0.25$  mm wire of the dilute alloy showed a much smaller anomaly, as we discuss below. We concluded that we were seeing a size-effect, and tentatively attributed the anomalous behavior to the Gurzhi effect,<sup>2</sup> a reduction in electron-surface scattering due to normal electron-electron scattering. It was noted<sup>1</sup> that wires prepared and cooled in Ar gas, or prepared in He but cooled in vacuum, displayed anomalies having the same form as those prepared and cooled in He, but with magnitudes generally representative of thicker wires and with more variation from wire to wire of a given thickness. This somewhat different behavior, illustrated in Fig. 2, was rationalized<sup>3</sup> as being due to the different atmospheres. Indeed, part of the stimulus for the investigation in ref. 1 of the behavior of thin K wires cooled in He gas was the apparent

contradiction between observations by Rowlands et al.<sup>4</sup> of anomalous behavior in  $d = 0.8$  mm K wires cooled in He, and those by Lee et al. of little or no such anomalies in  $d = 0.9$  mm K wires cooled in Ar.<sup>5</sup>

The measurements of ref. 1 stimulated proposals of three alternative models for the anomalous behavior: (1) localization effects;<sup>6</sup> (2) reduction in electron-surface scattering due to electron-phonon scattering;<sup>7</sup> and (3) interference between electron-surface scattering and electron-electron scattering.<sup>8</sup> The authors of these models, as well those of a more recent paper,<sup>9</sup> all challenged the applicability of the Gurzhi effect to the data of ref. 1.

Of particular interest was the localization model,<sup>6</sup> which predicted that when  $dp/dT < 0$ , the anomalous behavior should be proportional to  $L^2$ , the square of the length of the wire, provided that a parameter  $\nu$ , defined as the number of distinct conduction channels in the thin wire, is constant. This model stimulated us to make new measurements on thin wires with diameter  $d \leq 0.1$  mm, but with different lengths. The new samples had bulk resistance ratios  $RRR = R(295K)/R(0K)$  which differed from that for the old samples. We were thus able to investigate the effects of different bulk electron mean-free-paths on the behavior of thin K wires. This paper is a report of the results of our measurements. In addition to our measurements of  $dp/dT$ , we also routinely measured the thermoelectric ratio  $G$  of our samples, which provides information that complements  $dp/dT$ . The behavior of  $G$  is generally compatible with the patterns described in the



current paper. Details of the behavior of  $G$  are given in the following paper.<sup>10</sup>

This paper is organized as follows. In section II we briefly review the various models proposed to explain the original size-effect data on  $dp/dT$ . In section III we discuss experimental details, focussing upon sample characterization and modifications of previous procedures. In section IV we present our data and some data analysis. Section V contains a summary of the most important features of the data and a more detailed analysis, as well as comparisons with various theories. Section VI contains our conclusions.

#### 6.1.2 Theoretical Background.

For a simple nearly-free-electron metal such as K (neglecting, for the moment, the possibility of a Charge-Density-Wave (CDW) ground state<sup>11</sup>), we would expect<sup>1</sup> the very low temperature electrical resistivity of a thick sample to have the form:

$$\rho = \rho_i + \rho(T) = \rho_i + AT^2 + B\rho_i T^2 + \rho_{e-ph}. \quad (1)$$

Here  $\rho_i$  is the temperature independent residual resistivity due to impurities in the sample and  $\rho(T)$  is composed of an electron-electron component  $AT^2$ , an inelastic electron-impurity component  $B\rho_i T^2$ , and an electron-phonon component  $\rho_{e-ph}$  that drops off exponentially with

decreasing temperature.<sup>12</sup> In bulk K,  $\rho_{e-ph}$  is negligibly small below about 1K.

We can eliminate the unknown constant term  $\rho_i$  by measuring  $d\rho/dT$ , the temperature derivative of  $\rho$ . If we neglect  $\rho_{e-ph}$ , then from Eqn. 1 we expect  $d\rho/dT$  to have the form

$$d\rho/dT = 2(A + B\rho_i)T, \quad (2)$$

so that a plot of  $d\rho/dT$  versus  $T$  should yield a straight line passing through the origin. Indeed, as illustrated by the +-symbols in Fig. 1, Eqn. 2 is closely obeyed for bulk samples of high purity K. However, for thin wires we find large deviations from this equation. It is these deviations which we call the "anomaly".

The model originally proposed to explain the data in Fig. 1 is the Gurzhi effect.<sup>2</sup> In this effect, normal electron-electron scattering (NEES) (which, by itself, cannot contribute to the electrical resistivity in a metal with a spherical Fermi surface and isotropic scattering) reduces the probability that a typical electron will reach the sample surface where it is diffusely scattered, compared to this probability in the absence of NEES. In ref. 1, we noted that our data were not in the regime where the Gurzhi effect predominates, but we suggested that the effect might persist down to where our data lay. Subsequent theoretical work, both numerical,<sup>9</sup> and analytical,<sup>13</sup> has shown that this suggestion is incorrect.

The next model, proposed by de Gennero and Rettori,<sup>8</sup> involved an interference between NEES and surface scattering. This model predicted an anomaly in  $\rho(T)$  that was proportional to  $T^2$ , and that passed through a maximum value as a function of  $l/d$  at  $l/d \approx 1$ . The anomaly was a complex function of  $l/d$ , the form of which had to be determined numerically for the range of values of  $l/d$  of interest. The predicted  $T^2$  temperature dependence disagreed with the data of Fig. 1. In addition, recent theoretical analysis<sup>9</sup> calls into question the validity of this model.

Kaveh and Wiser<sup>7</sup> proposed an alternative explanation for the anomaly in terms of a reduction in the effectiveness of electron-surface scattering due to electron-phonon scattering. This model predicted the form:

$$\rho_{\text{anom}}(T) \propto -3(\rho_0^2/\rho_s\rho_i)(2l/d)T^5 \quad (3)$$

where  $\rho_s$  is the residual resistivity due to surface scattering, and  $\rho_0 = \rho_i + \rho_s$  is the total residual resistivity of the wire. In the "thin wire" limit we expect  $\rho_s \propto \rho_i(l/d)$ , and this model predicts  $\rho_{\text{anom}} \propto (1 + l/d)^2$ , provided that no contaminants are introduced into the sample during thinning. The predicted temperature dependence of  $T^5$  was much too rapid to explain the data of Fig. 1.

Finally, Farrell et al.<sup>6</sup> proposed that the data of ref. 1 were due to a combination of Charge-Density-Wave (CDW) effects for thicker wires,<sup>14</sup> plus localization effects for sufficiently thin, high purity wires. The CDW

model was used to describe the data when  $dp/dT > 0$ , and the localization effects were assumed to take over for  $dp/dT < 0$ . This model predicted that localization would predominate for  $l/d > 1$ , provided that certain other conditions were also satisfied. The model also predicted a variation of  $dp/dT$  with  $L^2$  in the localization regime, provided that the number of parallel conducting channels remained constant. Our new data allow us to investigate whether two different phenomena are present, but we were not able to obtain enough data on samples with different lengths and negative values of  $dp/dT$  to convincingly test for an  $L^2$  variation of the anomaly under the conditions predicted.

### 6.1.3 Sample Characterization and Experimental Procedure.

#### A) Samples and sample preparation

The samples were prepared from high purity (99.95%) K purchased from Mine Safety Appliances (MSA) Division of Gallard Schlesinger Corp. The K was supplied in 5 gm or 20 gm glass ampoules filled with argon gas. Different batches of K from MSA contain different amounts of trace impurities, as shown by the different impurity tables supplied by the manufacturer. For example, the Na content of the K studied in ref. 1 and the purer K in the present study were both listed as containing 15 ppm Na, while the less pure K in the present study was listed as 48 ppm Na. The typical bulk  $RRR = R(295K)/R(OK)$  (or bulk residual resistivities  $\rho_i$ ) for the three different batches of K were also different. To account for these differences, we compare the data for thin samples against data for thick ("bulk") samples prepared from the same batch. This procedure is not

perfect, since thick samples prepared from different ampoules can show different values of  $\rho_1$ , as can, in some cases, even samples prepared from the same ampoule. Variations from within a single ampoule are normally only 10-20% (see table 3.1 in ref. 3), but variations between ampoules can be much larger. These variations can produce significant scatter in the inferred thin sample behavior.

The samples in ref. 1 were made from material taken from several different 5 gm ampoules purchased at the same time. The data of ref. 3 show that the bulk RRR varied somewhat from ampoule to ampoule. Based upon all of the available data, we assume a bulk RRR = 7300 for both the samples prepared in He and those prepared in Ar. The samples used in the current study were made from two different sets of K. The first set of new samples was fabricated from a single 20 gm ampoule. The data from this set are shown below in Fig. 6. Measurements on one thick sample from this ampoule gave RRR = 4800, which we take as the bulk RRR. The second set of new samples was fabricated from several 5 gm ampoules purchased together at a later time. The data from this set are shown in Fig. 5 below. From measurements on two different samples which were in close agreement, the bulk RRR for the set is taken as RRR = 1700. We show in ref. 10 that the behavior of G supports this division of our samples into batches having three different bulk purities. For simplicity, we refer to samples as being from batches labelled by K(7300), K(4800), and K(1700).

From Eqn. 2, we would expect the  $T^2$  coefficient of  $\rho(T)$  for bulk samples to vary linearly with  $\rho_1$  (i.e. inversely with RRR). Such behavior is illustrated in Fig. 3 for samples prepared in both He and Ar. Note

especially the substantial variations in  $\rho_i$  (and the associated values of  $A + B\rho_i$ ) for the samples of K(7300) from different ampoules. The filled symbols in Fig. 3 indicate the values of  $A + B\rho_i$  used as the reference "bulk" behavior in Figs. 1, 2, 5, and 6.

The sample wires were extruded at room temperature from stainless steel presses through stainless steel dies. As in ref. 1, two wires were extruded and mounted together in a sample can inside a He filled glove box. The sample can was sealed with an In o-ring and transferred to a dilution refrigerator, with which the samples were cooled. When the sample can was filled with He gas at atmospheric pressure, molecular sieve was used to absorb the residual He gas in the can at low temperatures. In the current measurements, the sieve was freshly baked in vacuum at  $300^{\circ}\text{C}$  for each sample pair, except in one case noted below. To better clean the sieve, this temperature was  $100^{\circ}\text{C}$  higher than that used in ref. 1.

Although the surfaces of the samples were still shiny when the sample can was sealed, by the time the thin samples had been measured and brought back up to room temperature their surfaces were normally covered with a thin film of white material. To check whether this white material was essential to the anomalous behavior, for the last few thin samples studied we further cleaned the atmosphere in the sample can by wrapping a thin copper foil freshly coated with K around the inside surface of the can. This foil was inserted into the can along with the freshly baked sieve and the can was initially sealed a day before the samples were extruded and mounted. The large area of fresh K cleaned the He atmosphere in the sample can both before and after the samples were mounted. For the first time,

this procedure yielded surfaces of thin wires ( $d \leq 0.1$  mm) that were still shiny when the samples were warmed back to room temperature after being measured.

The lengths of the thinnest wires in ref. 1 were about 10 mm, although length measurements were not generally recorded. The carefully measured lengths of the new wires varied from 2 mm to 14 mm. For wires of diameter  $d \geq 0.25$  mm, the sample length was determined by two K potential leads of the same diameter as the sample. Thinner wires were connected between 1 mm diam. wires as described in ref. 1.

#### B) Measuring System and Procedures.

The basic measuring system and procedures are described elsewhere.<sup>1,15</sup> We note here only one important improvement upon previous procedure, namely that we were able to extend our experimental resolution from a part in  $10^7$  to a few parts in  $10^8$  using computer averaging of the last digit of our current comparator.

#### C) Sample Thickness Determination.

It is important for this study to know the diameters of the samples. For samples with  $d \geq 0.25$  mm, measurements of sample length  $L$  (with an uncertainty of  $< 10\%$ ) and room temperature resistance  $R(295K)$  (with an uncertainty of  $< 1\%$ ), combined with the known  $\rho(295K)$  for K, showed that the diameters of the sample wires were closely equal to the diameters of the dies through which the samples were extruded. For samples with  $d \leq 0.1$  mm, however, surface corrosion usually caused the effective diameter of the

sample to decrease between the time when the sample was mounted on the sample holder in the glove box and when it was cooled to liquid Nitrogen temperature. We estimated the diameters of these thinnest samples as follows.

For the samples of ref. 1, where the sample lengths were not generally recorded, there is no independent way to evaluate the diameters of most of the thinnest wires. We thus retain the values listed in ref. 1, except for one sample pair where the lengths are known, and for those samples where the room temperature resistance  $R(295K)$  changed significantly before and after measuring. In these latter cases, we reduced the diameter listed in ref. 1 by the ratio  $[\bar{R}(295)/R(295K)]^{1/2}$ . Here  $R(295K)$  is the resistance before the low temperature measuring run, and  $\bar{R}(295)$  is the average of the resistances before and after the run. This procedure assumes that the samples thinned somewhat due to corrosion between the time they were mounted and when they were measured at low temperatures.

For our new samples, we defined  $d$  by the equation

$$d = [4\rho(295K)L/\pi\bar{R}(295K)]^{1/2} \quad (3)$$

where  $\rho(295K) = 71.9 \text{ n}\Omega\text{m}$ .  $R(295K)$  normally changed by  $\leq 10\%$  over a single cooling cycle, but changes of 20%-50%--and once even 90%--were occasionally observed. Large changes were always observed when the samples were held at room temperature for several days or weeks before being cooled down again. We note that the use of Eqn (3) is strictly valid only when the sample diameter is uniform along the sample length. To check for uniformity of corrosion, we cut open some highly corroded thick samples, and found that



the corrosion was not uniform along the sample length, as will be discussed in more detail below. Non-uniformities are likely to be largest in the thinnest samples and in those which were corroded most. The effect of non-uniform corrosion should be to produce an anomaly characteristic of a sample thinner than the diameter given by Eqn. 3.

A check for internal consistency of the sample thicknesses inferred from Eqn. 3 can be obtained from a plot of  $\rho_0$  versus  $1/d$  as shown in Fig. 4. If surface scattering is purely diffuse, if the sample diameter is uniform, and if no additional contamination is introduced during sample thinning, then the residual resistivities of thin wires of a given bulk purity should be given to good approximation by the Nordheim Eqn.<sup>16</sup>

$$\rho_0 = \rho_i + (3/4)(\rho_i l/d), \quad (4)$$

where for K we expect<sup>16</sup>  $\rho_i l = 2.9 \times 10^{-14} \Omega m$ .

For the new, K(1700) samples, all but three of the thicker wire data points fall around the expected line down to about  $d = 0.08$  mm, and the data for thinner wires rise only slightly above this line. Perhaps the two K(1700) samples which fall below the nominal bulk values came from an ampoule with lower residual impurity content. This is, however, only speculation, since, as we show below and in ref. 10, both the  $dp/dT$  anomaly and the thermoelectric properties of these two samples are indistinguishable from those for similar samples from this batch with values of  $\rho_0$  that fall on the expected line. For the  $d = 0.8$  mm K(1700)

sample corroded in air, we believe that portions of the sample have cross-sections much less than the average diameter, as we discuss below. For the new K(4800) samples, the data for wires thicker than 0.1 mm fall around the expected line, but for  $d \leq 0.1$  mm the data rise well above this line. For the old K(7300) samples, the data for  $d \geq 0.25$  mm fall around the expected line, but for thinner wires the data begin to rise above this line, and by  $d = 0.1$  mm, the data lie well above the line. The data for the Ar and Vacuum cooled K(7300) samples approximately follow those for the He K(7300) samples. It appears from Fig. 4 that the purer the starting K, the thicker the wire for which the data begin to rise above the expected line. Finally, we note that the data in Fig. 4 for wires with shiny surfaces (indicated by the letter "s") are similar to those for wires of equivalent diameter with white surfaces.

Taken together, these data show that independent measurements of sample length and room temperature resistance permit reasonably accurate determinations of the diameters of the extruded thin K wires down to  $d \approx 0.1$  mm. Below this value, the samples must either be thinner than we estimate--because of non-uniform corrosion, or else their values of  $\rho_0$  must be higher due to internal contamination leading to shortening of the bulk mean-free-path. If we assume that they are only thinner, then we should get an estimate of the correct diameters by moving the high data points in Fig. 4 to the right until they lie on the appropriate full lines. From Eqn. 4 we see that this is equivalent to defining a new inverse diameter,  $(1/d') = (4/3)(\rho_0 - \rho_i)/\rho_i l \propto (\rho_0 - \rho_i)$ . Below we will analyze our data in terms of both  $1/d$  and  $\rho_0 - \rho_i \propto (1/d')$ .

#### 6.1.4 Experimental Data and Analysis.

##### A. Data from Reference 1.

Fig. 1a contains the data from Fig. 1 of ref. 1 (along with some additional samples of K(7300) not shown in ref. 1), replotted as  $(\rho_0/\rho)\Delta\rho/\Delta T$  instead of the original  $(\rho_{4.2K}/\rho)\Delta\rho/\Delta T$ . This replotting eliminates a sample-dependent normalization factor  $\rho_{4.2}/\rho_0$  present in ref. 1. For the temperature range considered in this paper, we have  $(\rho - \rho_0)/\rho_0 < 0.1\%$ . Thus the quantity plotted in Fig. 1 and the other figures is essentially  $d\rho/dT$ , and for simplicity we use  $d\rho/dT$  to label the ordinates of our figures. For ease of comparison, the symbols of Fig. 1 of ref. 1 have been retained. In Fig. 1b, we replot selected data from Fig. 1a in integrated form to give  $\rho(T)$ .

For bulk, high purity K, in which simple electron-electron scattering with  $\rho = AT^2$  is dominant, we would expect  $d\rho/dT = 2AT$ , corresponding to a straight line passing through the origin. The +-symbols in Fig. 1 indicate that the behavior of the 1.5 mm thick sample chosen as the reference wire for this set of samples conforms to this expectation. However, very different behavior is found as the wire thickness decreases below 1 mm, and for  $d \leq 0.2$  mm we find negative values of  $d\rho/dT$ . The arrows show how the sizes of the anomalies increased when the wires were thinned inside the sample can by surface corrosion. To see whether substantially shortening the electron mean-free-path would eliminate the anomaly, we prepared a  $d = 0.25$  mm wire of K(0.08 at% Rb) with  $\ell \approx 0.02$  mm. As illustrated by the dashed curve of Fig. 1, because of inelastic impurity scattering, the value of  $A + B\rho_i$  for this wire was larger than that for the thick pure K wires.

It was, however, only a little smaller than the value for a thick wire of the same Rb concentration (not shown), and showed no evidence of deviations from straight line behavior. Any anomaly was thus quite small (see Figs. 8-11 below).

Fig. 2 contains data similar to that in Fig. 1, but for wires prepared and cooled in Ar, or prepared in He and cooled in partial vacuum ( $\approx 10$ -100 micron of He) without molecular sieve. These data were noted but not shown in Ref. 1. Fig. 2 contains data from both samples of all of the pairs studied, and we have retained the symbols used in Fig. 4.8 of ref. 3 for the three sample pairs shown there. We see that the data of Fig. 2 display the same anomalous form as those in Fig. 1. However, while the data for the pair of  $d = 0.25$  mm wires show the same size anomaly as  $d = 0.25$  mm wires in Fig. 1, the data for the  $d \leq 0.1$  mm samples show smaller anomalies than in Fig. 1, and also much more variation from wire to wire, especially for the wire pair designated by inverted triangles. This pair of wires was unusual, in that instead of the normal few minutes between the mounting of the two paired samples, the sample designated by the open inverted triangles was mounted an hour before its pair. Additional surface corrosion of this sample as it sat in the glove box certainly contributed to its larger anomaly. As noted in the introduction, the somewhat different behavior between the thinnest samples in Fig. 2 and those in Fig. 1 was originally<sup>1</sup>, attributed to differences in the atmospheres. We shall see below that most of these anomalies in Fig. 2 agree rather well with the anomalies for our new sample sets K(4800) and K(1700).

### B. New Data.

In Figs. 5 and 6 we present collected data for the new pairs of K wires examined in this study, most of which were extruded through 0.1 mm dies. These two figures contain a wealth of data, which must be considered in detail to develop an understanding of the behavior of thin K. Wires prepared together are indicated by brackets. For these two figures, in each wire pair the sample designated by the open symbol was prepared first. The figures contain listings of the sample diameters  $d$ , lengths  $L$ , and values of  $\rho_0$ , as well as brief notes with other important information. These samples were all prepared and cooled in He gas. The + and x symbols in each figure represent assumed bulk behavior (see filled symbols in Fig. 3), determined as described above.

#### a. K(1700)

Fig. 5 contains data for the thin K(1700) samples. Their bulk RRR corresponds to an elastic mean-free-path of  $\ell \approx 0.05$  mm, about half the  $d \approx 0.1$  mm of our smallest die. Three pairs of  $d \approx 0.1$  mm wires were prepared; they are designated by stars, squares, and triangles, and are listed on the figure in the order measured. As initially extruded, all six samples showed only relatively small anomalies. These anomalies were essentially independent of sample length, and approximately the same size for all six samples, independent of their values of  $\rho_0$ . The stars and squares were measured in two different sample cans; we thus conclude that the sample can is not a major issue.

To see whether, and how, these anomalies increased in size as the samples became still thinner, we thinned one pair of samples (the triangles) two times by surface corrosion at room temperature. The circles

are after corrosion for 22 days, and the diamonds are after a total of 35 days. As indicated by the arrows, the anomalies in both samples became larger by similar amounts as the sample diameters decreased.

To test whether surface corrosion would affect a thicker wire, we corroded a  $d = 1$  mm sample (+ 's) until its apparent average diameter decreased by 20%. As shown by the arrow, a significant anomaly appeared. Since this sample was thick, it was possible to section it and check the uniformity of corrosion with a microscope. The corrosion was highly non-uniform; in some places, the surface was deeply corroded and fingers of corrosion extended into the center of the sample; in other places, the corrosion was so great that the sample could best be described as three or four thin cylinders of K embedded in a wire of corroded material.

To check whether the presence of some surface corrosion is essential to the appearance of an anomaly, we cleaned the atmosphere in the the sample can with a large area of fresh K on a Cu foil, as described above. This procedure yielded, for the first time,  $d \leq 0.1$  mm samples which remained shiny when reexamined after being measured. For the K(1700) sample set, the samples with shiny surfaces (squares in Fig. 5) showed anomalies similar in magnitude to those for samples with the typical white surfaces. This means either that surface corrosion is not essential to the anomaly, or that only an extremely thin film of surface corrosion is sufficient to produce an anomaly if the wire is sufficiently thin. Since we see little or no anomaly in thick high purity wires, or in thin wires of dilute K(Rb) alloys, surface corrosion alone apparently cannot produce an anomaly.

To recheck that greatly reducing  $\ell$  does indeed greatly reduce the anomalous behavior, we measured a K(0.1 at.%Rb) sample made from K(1700) material. In agreement with our previous results (see Fig. 1 and Fig. 8-10 below), the data were very close to bulk behavior for such a dilute alloy.

Finally, to see what effect introducing corroded material into the body of a sample would have, we first corroded some K(1700) material, and then mixed the white product with new pure K(1700), all in an Ar-filled glove box. Ar was chosen to eliminate the need for sieve. A  $d = 1$  mm wire extruded in Ar from this composite material had an RRR of 1800, and its anomaly fell between bulk behavior and that found for  $d = 0.1$  mm wires (see Fig. 5). Corrosion in the body of the sample thus apparently produced a small anomaly in the Ar atmosphere. We then corroded the surface of this wire by taking it out into the air. Its  $\rho_i$  increased by 60%, and the magnitude of  $A + B\rho_i$  increased approximately as expected for the observed increase in the bulk  $\rho_i$  (see Fig. 3). The effect of surface corrosion on this  $d = 1$  mm wire prepared and measured in Ar was thus quite different from that of the  $d = 1$  mm wire prepared and measured in He described above.

#### b. K(4800).

Fig. 6 contains data for the K(4800) samples, for which  $\ell \approx 0.15$  mm. Here the anomalies in freshly prepared  $d = 0.1$  mm samples were generally slightly larger than those in Fig. 5, but not as large as those in Fig. 1. Again data are shown for several sample pairs of different lengths, and for one pair subjected to additional corrosion. The sample designated first by an open inverted triangle and then by an open square, broke before it became an open erect triangle; it was replaced by a fresh sample, which is

designated by the open circle. K(4800) samples with shiny surfaces also showed anomalies, but these were smaller than for white-surfaced samples.

### C. Synthesis of Information from Figs. 1, 2, 5, and 6.

We ask first whether the anomalous behavior we see can be due to a combination of two different phenomena. If these phenomena had different temperature dependences, then we would expect the temperature dependence of an anomaly of a given magnitude to change when different conditions led to different ratios of the two phenomena. Fig. 7 shows, however, that for an anomaly of a given size, very different samples produce data having exactly the same temperature dependence--independent of sample length, sample diameter, or whether the samples were prepared in He or Ar. This fact strongly suggests that our "size effects" are the result of a single physical phenomenon.

Since the temperature dependence of an anomaly of a given size is unique, it is worth parameterizing. We focus upon the data below 1.2K, since here electron-phonon scattering should be very small. Most of the published theories assume that the anomaly simply adds to the bulk  $T^2$  behavior predicted by Eqn. 2. We thus take  $\rho(T)$  to consist of a  $T^2$  term plus an anomaly which varies as  $T^n$ . Neither additivity nor a power law dependence is necessarily correct, but requiring both behaviors makes the parameterization unique. When we plotted  $d\rho/dT - 2(A + B\rho_1)T$  versus  $T^{n-1}$  and looked for a value of  $n$  that led to straight lines, we found, in agreement with ref. 3, a best fit of  $n \approx 2.33$  for all anomaly sizes. The solid curves going through the data in Fig. 7 were determined with this form. Both  $n = 2$  and  $n = 2.5$  gave significantly worse fits. Note that the



fits go above the minima in the various curves. This suggests the need for an additional negative contribution before the rapidly rising, positive Umklapp electron-phonon term sets in.

The second major feature of interest is that, with only one exception (the open and filled diamonds in Fig. 6), the size of the anomaly in a given sample pair does not vary significantly with the sample length. Rather, for a given pair, the anomaly is practically independent of sample length, and a larger anomaly always occurs in the sample prepared first. We attribute this latter behavior to extra surface corrosion in the sample prepared first, since this sample sat unprotected in the glove box for several minutes while the second sample was extruded and mounted. The only case where a longer sample had a substantially larger anomaly than its shorter mate (the diamonds in Fig. 6), occurred when the molecular sieve was not freshly cleaned before the samples were mounted. Both the room temperature resistance and  $\rho_0$  for the longer sample (which was mounted first) indicate that it corroded considerably more than the shorter one. We believe that additional thinning of the longer sample due to surface corrosion contributed importantly to its larger anomaly.

The next important issue is whether we are seeing a "size-effect". To try to answer this question quantitatively, we define the quantity  $\Delta$  as the difference at  $T = 1.0\text{K}$  between the value of  $dp/dT$  for a given thin sample and the value of  $dp/dT$  for the reference bulk sample for the same batch of K.  $1.0\text{K}$  was chosen as the highest temperature for which we can safely neglect effects of electron-phonon scattering. Because of the uncertainties noted above concerning the thicknesses of our thinnest samples, we analyze the data in two different ways, one involving the

inverse diameters  $1/d$  determined from the diameters of the extrusion dies and measurements of the sample lengths and room temperature resistances as described above, and the other involving the "effective" inverse diameter,  $\rho_0 - \rho_i \propto (1/d')$ , defined via Eqn. 4. This latter alternative "corrects" the sample diameters of thin wires which do not fall on the straight lines in Fig. 4.

If the anomaly is due primarily to surface scattering, then for each sample set,  $\Delta$  should increase as  $1/d$  increases. We see from Fig. 8 that this is true--with two obvious exceptions<sup>17</sup>--within modest scatter for each of the K(7300), K(4800), and K(1700) sample sets. The only possible alternative explanation for an increase of  $\Delta$  with increasing  $1/d$  is that of increasing bulk contamination as the wires become thinner. From Eqn. 2, which is confirmed by our data for thin wires of dilute KRb alloys, we know that adding substitutional impurities to K increases the  $T^2$  coefficient  $A + B\rho_i$ , and thus produces a change in  $d\rho/dT$  that is opposite to the anomaly we see. We can thus rule out such contamination as the source of our anomalies. More complex is the possibility that surface corrosion extends into the body of the sample and contributes to the anomalies we see. We consider this alternative further below.

If we now consider the general patterns in Fig. 8, we see that the K(1700)  $\Delta$ s seem to fall slightly below the K(4800)  $\Delta$ s, but these two sets of data are mutually consistent for all  $1/d$  to within their experimental uncertainties. In contrast, the K(7300)  $\Delta$ s, and the  $\Delta$ s for one pair of wires prepared in Ar, fall well above the other data for  $1/d < 10$ . On the other hand, for  $1/d > 12$  the K(7300)  $\Delta$ s approach the others. The remainder

of the Ar and Vacuum cooled data fall among the overlapping K(4800) and K(1700) data sets. If each set of data is separately fit to the form  $(1/d)^n$ , then the K(7300) data suggest  $n = 1/2$ , while the K(4800) and K(1700) data seem to give  $1 \leq n \leq 2$ . The  $\Delta$ s for  $d = 0.25$  mm K(0.1%Rb) and  $d = 0.1$  mm K(0.08%Rb) are the smallest in Fig. 8, and both are consistent with no anomaly at all. Aside from its slightly higher purity, the only treatment of the K(7300) sample set which we know differed from that for the K(4800) and K(1700) sets was the  $100^\circ\text{C}$  lower temperature at which the molecular sieve was baked. Perhaps this lower baking temperature led to greater surface contamination of the K(7300) samples which, in turn, led to larger anomalies in thick samples. The data of Fig. 4 are consistent with somewhat greater surface corrosion in the K(7300) samples.

Since Kaveh and Wiser<sup>7</sup> have predicted that  $\Delta$  should vary with  $l/d$ , we replot  $\Delta$  versus  $l/d$  in Fig. 9. This plot rescales each data set along the abscissa, but leaves the ordinate of each point unchanged. Fig. 9 brings the K(7300) and K(4800) data closer together than in Fig. 8, but separates the K(4800) and K(1700) data.

Because the residual resistivities of the samples in each set are not simple functions of  $1/d$  (see Fig. 4), we examine in Fig. 10 how  $\Delta$  varies with "corrected" sample diameter,  $\rho_0 - \rho_1 \propto (1/d')$ . If the increase in  $\rho_0$  is due mainly to non-uniform thinning of the samples, then the data should vary more nearly as  $(1/d')$  than as  $(1/d)$ . The data for the different samples in Fig. 10 overlap rather like those in Fig. 8. However, the data for the thinner samples clearly lie more to the right in Fig. 10 than in Fig. 8 relative to the thicker sample data, and the data for the purer

samples--K(7300) and K(4800)--lie to the right of the data for the least pure samples--K(1700). There are two alternative interpretations of the data in Figs. 8 and 10. 1) The higher than expected values of  $\rho_0$  in Fig. 4 are due primarily to non-uniform diameters, in which case Fig. 10 indicates that  $\Delta$  increases less rapidly than linearly with  $(1/d')$  and may even be "saturating" for the thinnest wires. 2) The higher than expected values of  $\rho_0$  for the thinnest samples are due in large measure to internal contamination of the thinner wires, leading to less rapid than expected increases in  $\Delta$  with  $(1/d')$ . To test this latter alternative, we compared the increases in  $\Delta$  for wires thinned by extrusion through smaller dies with the increases due to explicit surface corrosion--as indicated by the arrows in Figs. 11a and 11b. We conclude that changes in  $\Delta$  due to corrosion are generally indistinguishable from those due to thinning. The one obvious exception is the  $d = 0.8$  mm sample, for which the effect of corrosion is unusually large in the plot versus  $1/d$ , but unusually small in the plot versus  $\rho_0 - \rho_i$ . Both behaviors are compatible with highly non-uniform thinning, leading to an effective average diameter much smaller than the nominal one.

In the following paper,<sup>10</sup> we examine the behavior of the thermoelectric ratio  $G$  of these same samples. We see from Fig. 5 in ref. 10 that most of our data points fall on three separate lines on a Gorter-Nordheim plot, in a manner consistent with the separation into three different sample sets that we have been assuming in the current paper. Only three data points deviate significantly from the three expected lines in Fig. 5 of ref. 10. Two are for the K(1700) samples which have unusually

low values of  $\rho_0$  in Fig. 4. The deviation in Fig. 5 of ref. 10 is due primarily to these unusual values of  $\rho_0$ . The third is the corroded  $d = 0.8$  mm sample of K(1700)--the six-pointed star in Fig. 5 of the current paper. Its  $G_0$  is consistent with a much smaller effective diameter, as we have just argued.

#### 6.1.5 Summary of Behavior and Comparison with Theories.

From the foregoing experimental data, we summarize the behavior of  $d\rho/dT$  as follows: (1) All of our pure K samples thinner than  $d = 1$  mm show anomalies. (2) The anomalies are generally larger the thinner the wires and the purer the host material, but there are some large variations for thin wires of a given diameter. (3) Both white and shiny surfaces yield anomalies, but anomalies associated with the former are usually larger. (4) If  $\ell$  is greatly reduced by adding small amounts of Rb, the anomalies become too small to reliably isolate. (5) The anomalies all have the same temperature dependence for a given anomaly size, independent of wire thickness, bulk resistivity, or the gas in which the wire is prepared and cooled. (6) Surface corrosion both thins the wires and increases the sizes of the anomalies--as a corollary, the anomaly is invariably larger in the sample mounted first in a given sample pair. (7) There is no systematic length dependence of anomalies for which  $d\rho/dT$  remains positive. We do not have enough data to draw conclusions about length dependence for anomalies for which  $d\rho/dT$  becomes negative. (8) The variation of the anomaly size with  $1/d$  apparently has a different form for the K(7300) samples from that for the K(4800) and K(1700) samples. (9) The data are not unique functions

of any of the following variables:  $1/d$ ,  $l/d$ , or  $\rho_0 - \rho_1$ . (10) Below about 1.2 K, where electron-phonon scattering is small, the anomaly can be parameterized as  $\rho(T) \propto T^{7/3}$  independent of the anomaly size. This form seems to require an additional negative contribution to  $d\rho/dT$  for data in the vicinity of 1.2K.

We now consider whether any of the proposed models can describe these results. We omit the Gurzhi effect, which can be ruled out on theoretical grounds.<sup>6-9,13</sup>

A combination of CDW effects with localization seems unlikely because, as illustrated in Fig. 7, the temperature dependence of the anomaly follows a single pattern. We thus do not seem to have a combination of two quite different phenomena--a CDW effect for thicker samples and localization for thinner ones--which just accidentally smoothly match together.

The model of interference effects between normal electron-electron scattering and surface scattering makes two predictions: (1) a  $T^2$  variation of the anomaly; and (2) that the magnitude of the anomaly passes through a maximum value at  $l/d \approx 1-2$ . The first prediction is at variance with the temperature dependent behavior shown in Fig. 7. The second prediction could be compatible with the behavior shown in Fig. 10 if the maximum occurs for the largest values of  $l/d$  we have been able to produce, i.e.  $l/d \approx 2.5$ . We note that this model has recently been criticized theoretically.<sup>9</sup>

Reduction of the effectiveness of surface scattering by normal electron-phonon scattering can be ruled out as the primary source of the

anomaly by the temperature dependence of the data illustrated in Fig. 7. The anomaly varies approximately as  $T^{7/3}$  rather than the  $T^5$  variation predicted by this model. If this  $T^{7/3}$  term is taken as reliable, then there is need for a small additional negative contribution to  $dp/dT$  in the vicinity of 1.2K, which could be due to this  $T^5$  term.

Finally, we consider what alternatives exist to these models. If we combine the separate contributions of interference effects plus reduction of surface scattering by normal electron-phonon scattering, we can generate a temperature dependence of about  $T^{2.33}$ . But we have the claim<sup>9</sup> that the interference effect model is incorrect. The possibility of a complete explanation in terms of a CDW state coupled with scattering from the sample surface cannot be ruled out. A CDW-based model has the advantages that: (1) it provides for unexpected variations from sample to sample due to differences in orientation of the CDW domains, and (2) it provides for deviations from simple  $T^2$  behavior. It has the disadvantages that: (1) no CDW-based model without localization yet predicts a negative  $dp/dT$ ; (2) it is hard to see why the data for a given bulk purity fall into such generally nice patterns for a given sample purity if the anomaly is sensitively dependent upon the CDW domain structure, and (3) there appears to be no need for a CDW model to explain the behavior of either bulk K or dilute K-based alloys.<sup>1,5</sup>

#### 6.1.6 Conclusions and Suggestions for Further Work.

We have summarized the results of our measurements in the numbered items in the previous section. We conclude that there does appear to be an anomalous "size-effect" in thin K wires, the nature of which is not yet

clear. Especially unclear is the contribution and role of surface corrosion. We know of no theory that seems able to adequately describe all of our data.

Additional measurements which might help clarify the situation include the following. (1) Measurements on still thinner wires with both shiny and corroded surfaces. Such measurements are not easy, because very thin wires take heavy pressure and long times to extrude, so that extrusion is difficult and the wire surfaces will invariably corrode. (2) Measurements with still higher purity bulk K. This will require additional purification of commercial K by vacuum distillation. (3) Incorporating white, corroded material into the body of K wires prepared and cooled in He, to clearly establish whether or not introducing such material into K produces an anomaly.

This work was supported in part by the NSF Division of Materials Research through Low Temperature Physics grants DMR-83-03206, DMR-83-05289, and DMR-8700900. The authors would like to thank Z.-Z. Yu for allowing us to include in this paper some of his unpublished data.



## REFERENCES

(Chapter 6.1 - 6.16)

1. Z.-Z.Yu, M.Haerle, J.W.Zwart, J.Bass, W.P.Pratt,Jr., and P.A.Schroeder, Phys. Rev. Lett. 52, 368 (1984).
2. R.N.Gurzhi, Zh. Eksp. Teor. Fiz. 44, 771 (1963).
3. Z.-Z.Yu, The Electrical Resistivity and The Thermoelectric Ratio of K, Na, Li, Rb, and K-Rb alloys from 0.07K to 4.2K. Ph.D. Thesis, Michigan State University, 1984 (Unpublished).
4. J.A.Rowlands, C.Duvvury, and S.B. Woods, Phys. Rev. Lett. 40, 1201 (1978).
5. C.W.Lee, M.L.Haerle, V.Heinen, J.Bass, W.P.Pratt Jr., and P.A. Schroeder, Phys. Rev. B25, 1411 (1982).
6. M.E.Farrell, M.F.Bishop, N. Kumar, and W.E. Lawrence, Phys.Rev.Lett.55, 626 (1985).
7. M.Kaveh and N.Wiser, J. Phys. F. 15, L195 (1985).
8. S.DeGennaro and A.Rettori, J. Phys. F.14, L237 (1984); *ibid.* 15, 2177 (1985).
9. D.Movshovitz and N.Wiser, J. Phys. F. 17, 985 (1987).
10. J.Zhao, Z.-Z.Yu, W.P.Pratt Jr., P.A.Schroeder, and J.Bass, Phys. Rev. B (1988), Following Paper.
11. A.W.Overhauser, Adv. in Phys. 27, 343 (1978).
12. H.van Kempen, J.S.Lass, J.H.Ribot, and P. Wyder, Phys. Rev. Lett. 37, 1574 (1976).
13. D.A.Stump (Unpublished).

- 14 M.F.Bishop and W.E.Lawrence, Phys. Rev. B32, 7009 (1985).
15. D.L.Edmunds, W.P.Pratt Jr., and J.A.Rowlands, Rev. Sci. Inst. 51, 1516 (1980).
16. J. Bass, Landolt-Bornstein New Series, Group III, Vol. 15a, "Metals: Electronic Transport Phenomena", Springer Verlag, Berlin, 1982.
17. The two exceptions to the pattern of increasing  $\Delta$  with increasing  $(1/d)$  in Fig. 8 are the corroded  $d = 0.8$  mm K(1700) wire and one shiny K(4800) wire. As noted above, we believe that the  $d = 0.8$  mm K(1700) wire has portions much thinner than its average diameter. The reason for the unexpectedly small  $\Delta$  for the one shiny K(4800) wire is less clear, but may involve accidental internal contamination.

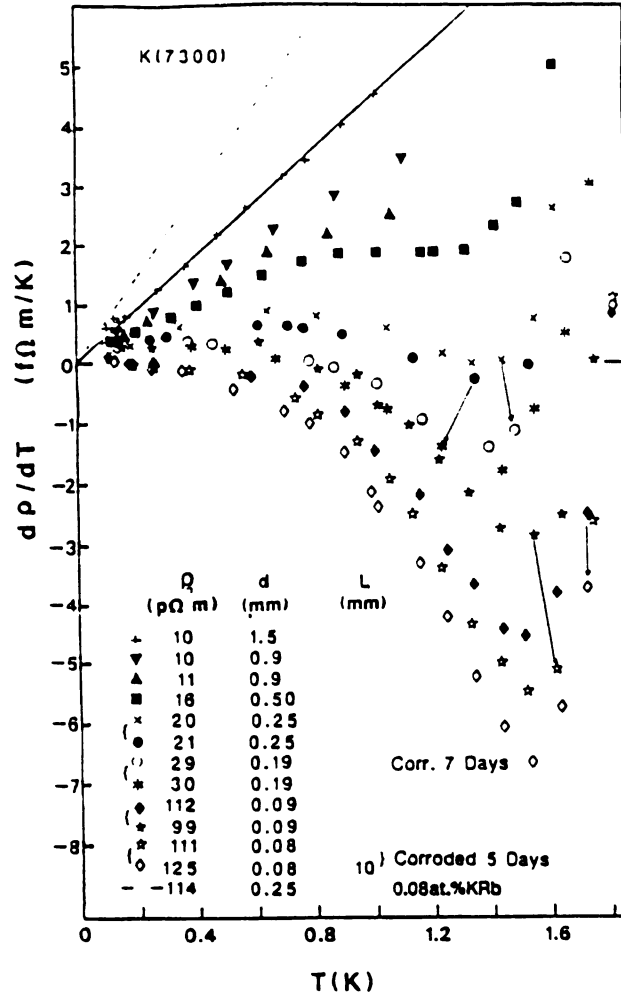


Figure 1: a)  $dp/dT$  versus  $T$  for the K(7300) samples, which were prepared and cooled in a He atmosphere. This figure is taken from Ref. 1, but the data have been renormalized as described in the text, a few plotting errors have been corrected, some of the nominal sample diameters have been revised as described in the text, and some additional samples from ref. 3 have been added. Two nearly identical samples were always prepared and measured together; for the samples in Fig. 1, the data for both wires in a pair was always fairly close. For simplicity, we omit the pairs of the thicker samples; paired samples are indicated by brackets. Two pairs of samples were annealed at room temperature to thin them further after their initial measurements; the arrows indicate the changes which occurred due to these annealings.

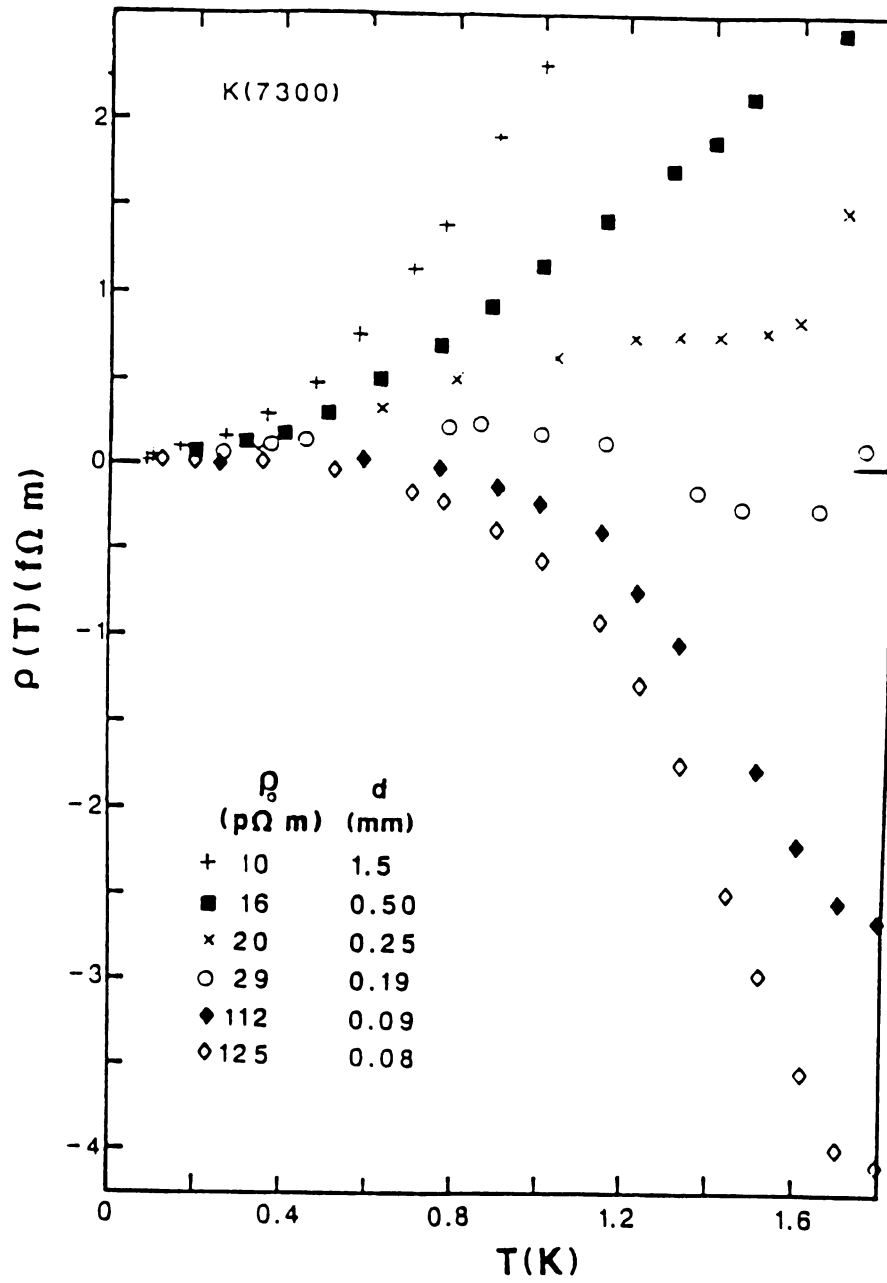


Figure 1: b)  $\rho(T)$  versus  $T$  for selected data from Fig. 1a. The data of Fig. 1a were integrated by hand. Note that the integrated data have qualitatively similar form to the data of Fig. 1a.

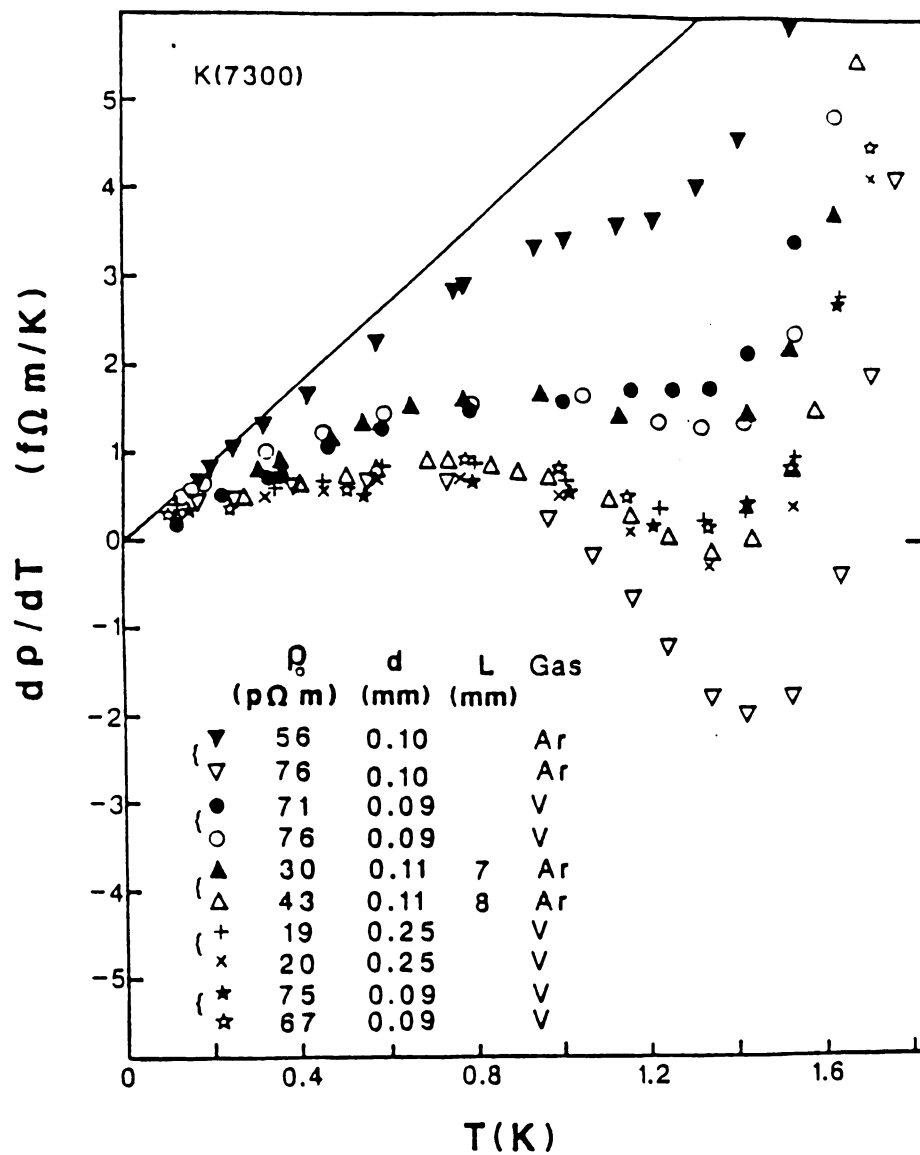


Figure 2:  $dp/dT$  versus  $T$  for thin K(7300) wires cooled in an Ar atmosphere or in partial vacuum. This figure is taken from ref. 2, but the data have been renormalized as described in the text. The straight line indicating bulk behavior is the same line as in Fig. 1. The samples connected by brackets were prepared and measured together.

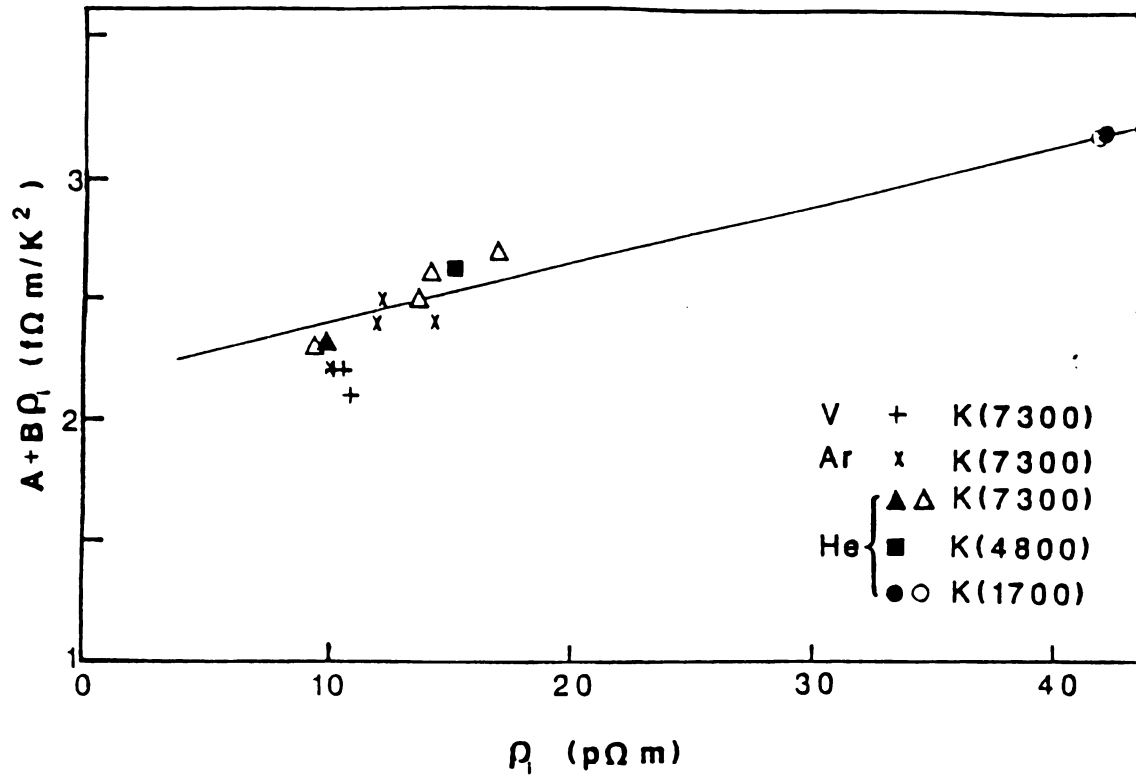


Figure 3: The  $T^2$  coefficient  $A + B\rho_i$  for "bulk" ( $d \geq 1 \text{ mm}$ ) samples of K as a function of residual resistivity  $\rho_i$ . The filled symbols indicate the data used to determine "bulk" behavior for K(7300), K(4800), and K(1700) (for definitions see text) in Figs. 1, 2, 5, and 6, respectively. The K(7300) wires had  $d = 1.5 \text{ mm}$ , the K(4800) and K(1700) wires had  $d = 1.0 \text{ mm}$ . The straight line is a best fit to all of the data. Its slope of  $2.5 \times 10^{-5} \text{ K}^{-2}$  is somewhat larger than those for Rb ( $1.3 \times 10^{-5} \text{ K}^{-2}$ ) and Na ( $0.8 \times 10^{-5} \text{ K}^{-2}$ ) impurities in K.

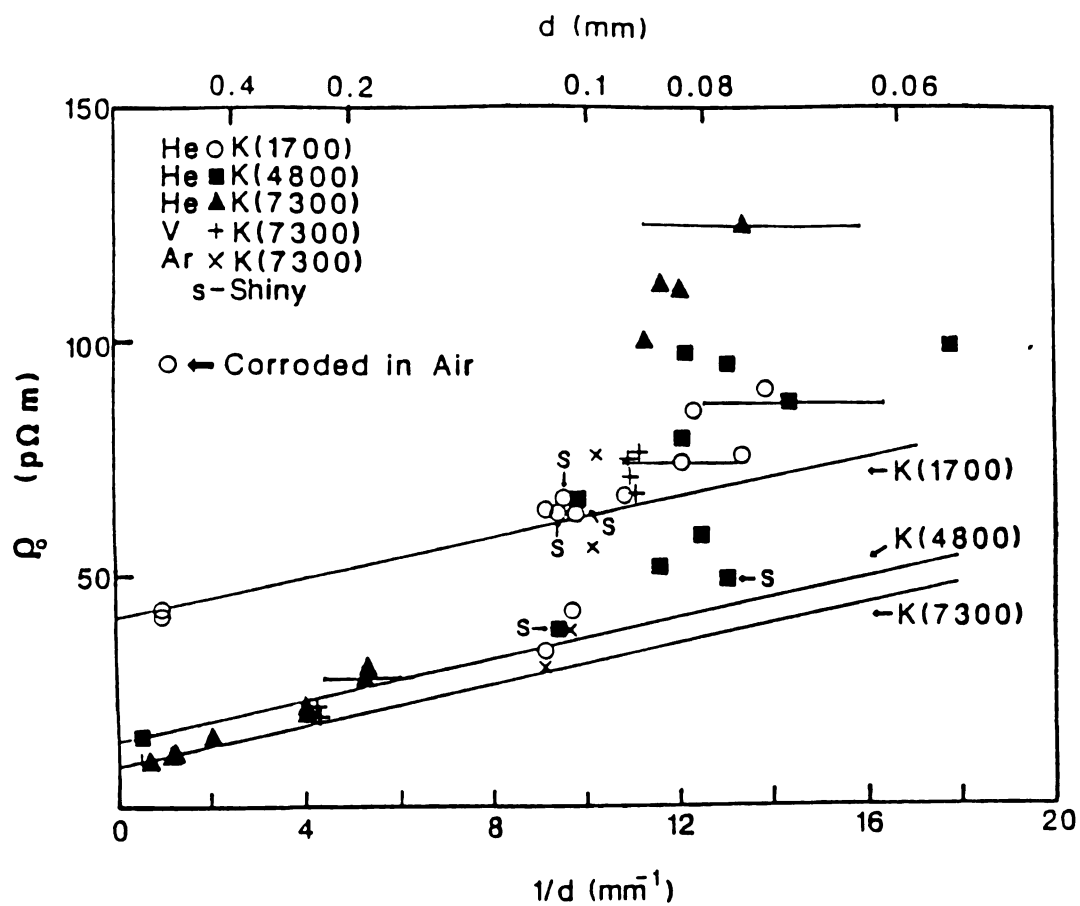


Figure 4:  $\rho$  versus  $1/d$  for K wires of different diameter and different bulk purity. The solid lines have a slope taken from ref. 16. The letter "s" indicates samples with shiny surfaces.

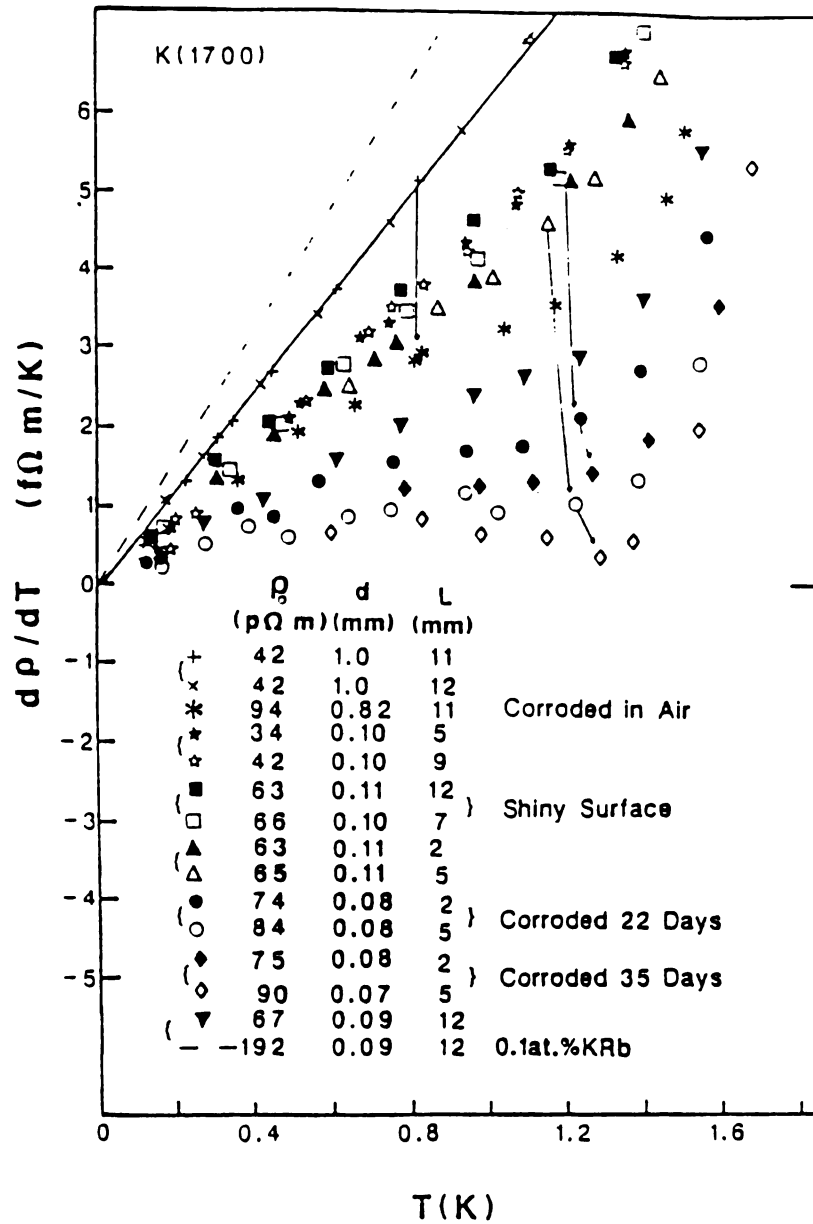


Figure 5:  $d\rho/dT$  versus  $T$  for the K(1700) samples. Pairs of samples prepared together are designated by identical symbols, with the open symbol designating the sample prepared first. Note that in each pair the anomaly is always larger for the sample prepared first, and the anomaly is independent of sample length. After their initial cooling, some of the samples were given room temperature anneals and then cooled and measured again. The progression of behavior after such anneals is indicated by the arrows.



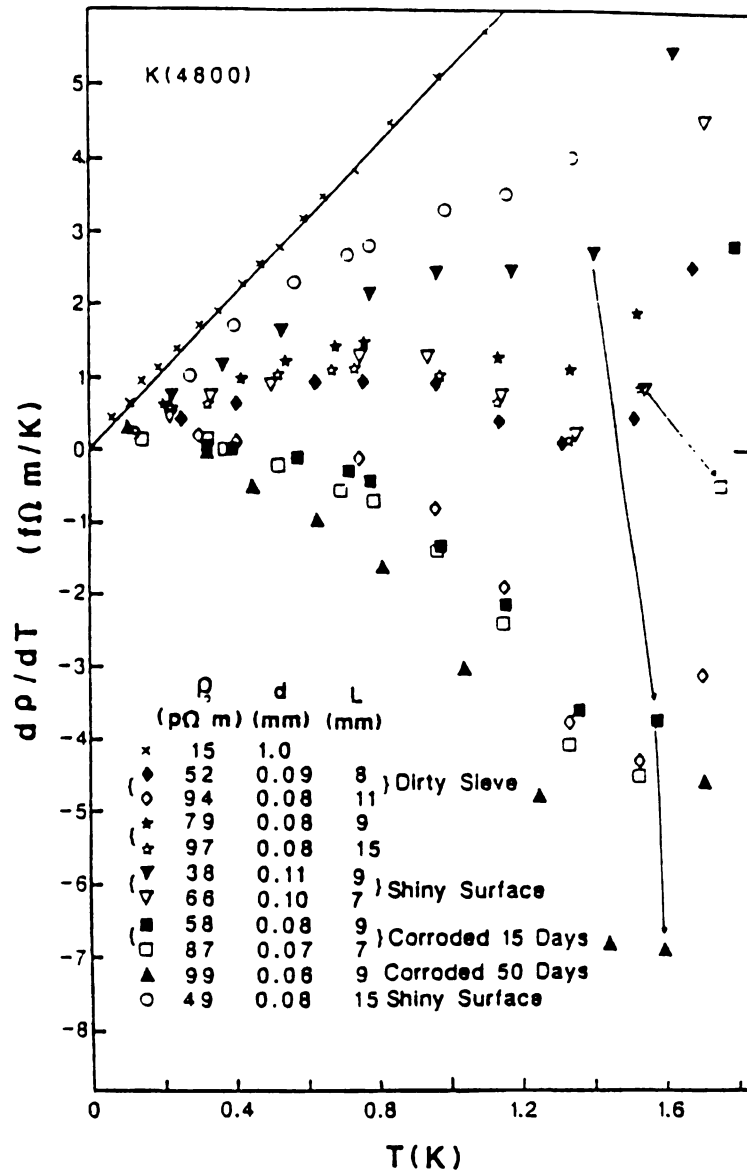


Figure 6:  $dp/dT$  versus  $T$  for the K(4800) samples. Pairs of samples prepared together are designated by identical symbols, with the open symbol designating the sample prepared first. Note that in each pair the anomaly is always larger for the sample prepared first, and the anomaly is independent of sample length, except for the sample pair denoted by diamonds. This pair was the only one that showed a length dependence approximately proportional to  $L^2$ . After their initial cooling, some of the samples were given room temperature anneals and then cooled and measured again. The progression of behavior after such anneals is indicated by the arrows.

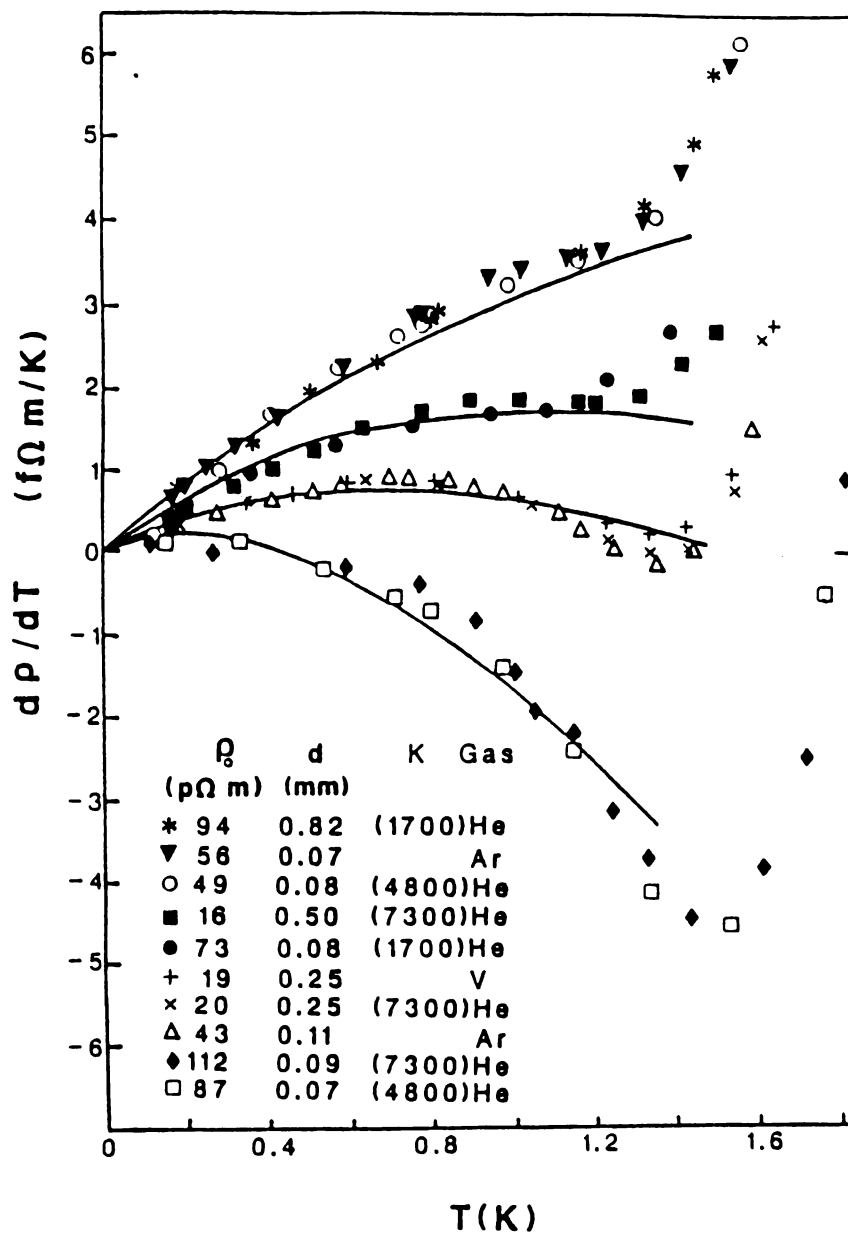


Figure 7: Intercomparison of data sets with four different size anomalies involving wires having different thicknesses, different bulk RRRs, and/or cooled in different gases. The curves through the low temperature data are fits up to 1.2K to an equation of the form  $\rho(T) = (A + B\rho_1)T^2 - CT^{7/3}$  where  $(A + B\rho_1)$  is determined by the behavior of thick K wires.

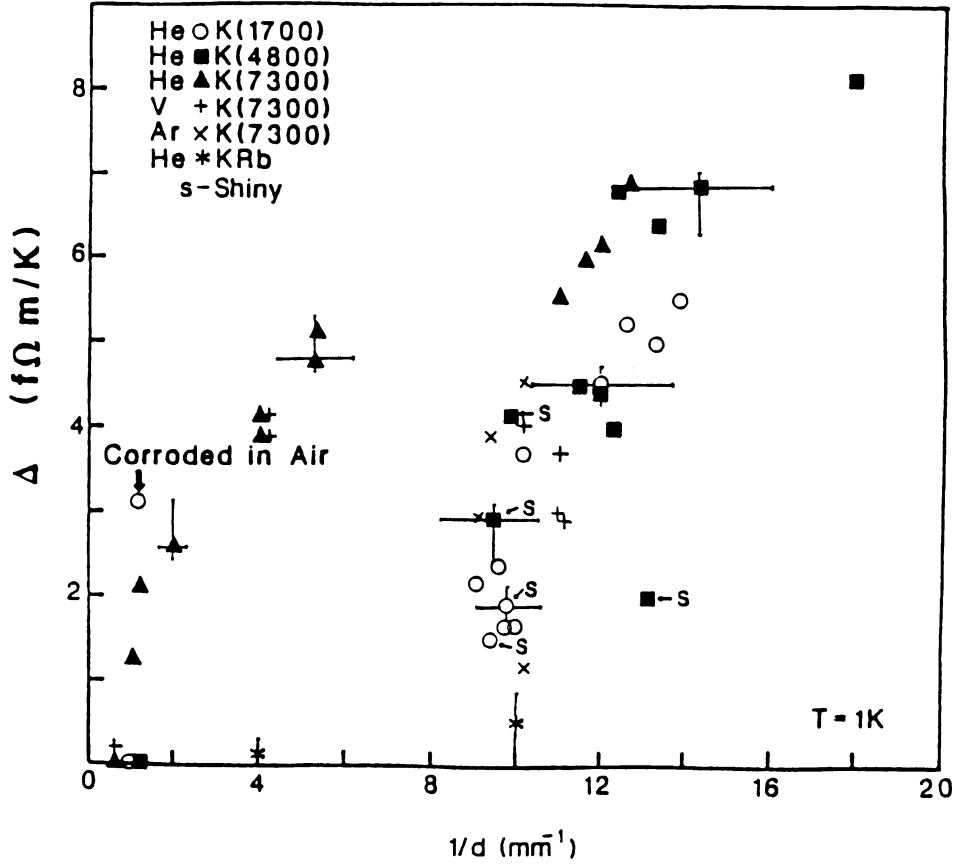


Figure 8:  $\Delta$  versus  $1/d$  for the data of Figs. 1, 2, 5, and 6.  $\Delta$  is the deviation at 1.0K of the anomalous values of  $dp/dT$  in Figs. 1, 2, 5, and 6 from the bulk behavior shown in each figure. The letter "s" indicates samples with shiny surfaces.

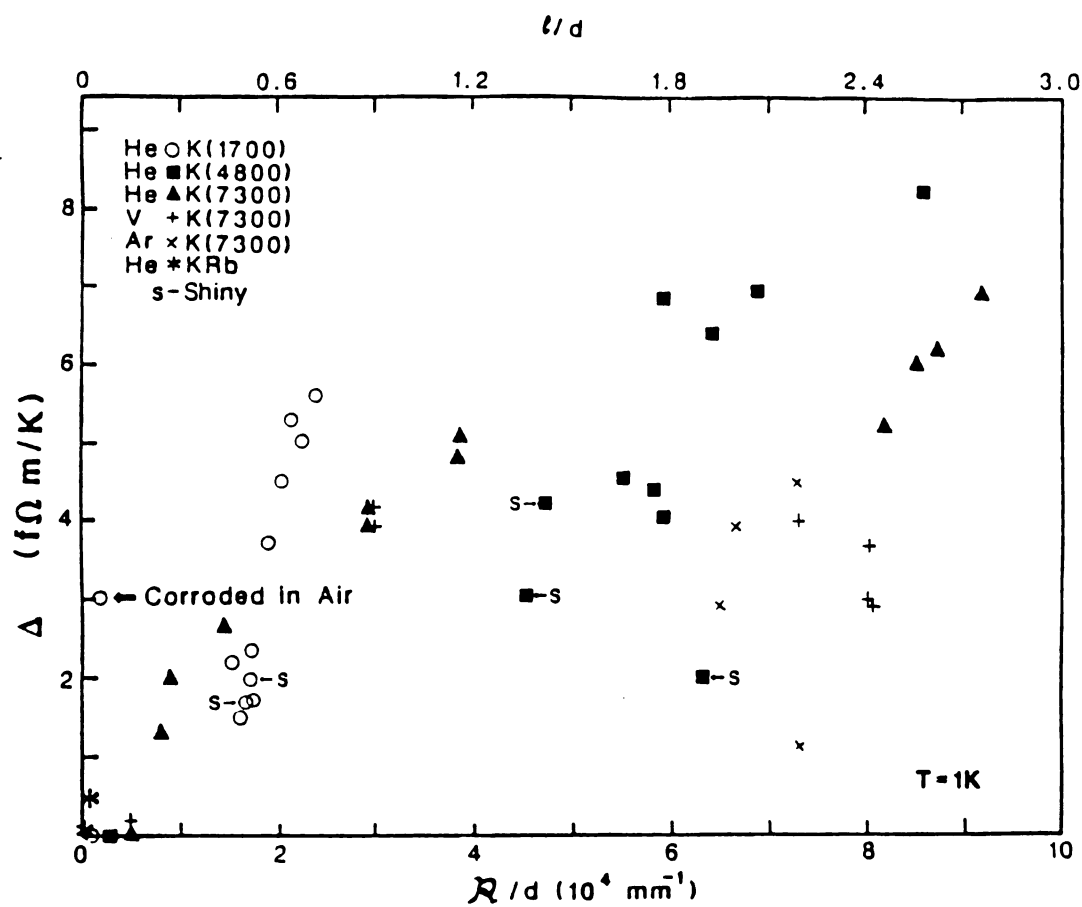


Figure 9:  $\Delta$  versus  $(RRR/d)$  for the data of Figs. 1, 2, 5, and 6. The scale for  $\Delta$  versus  $l/d$  is given at the top of the graph. The letter "s" indicates samples with shiny surfaces.

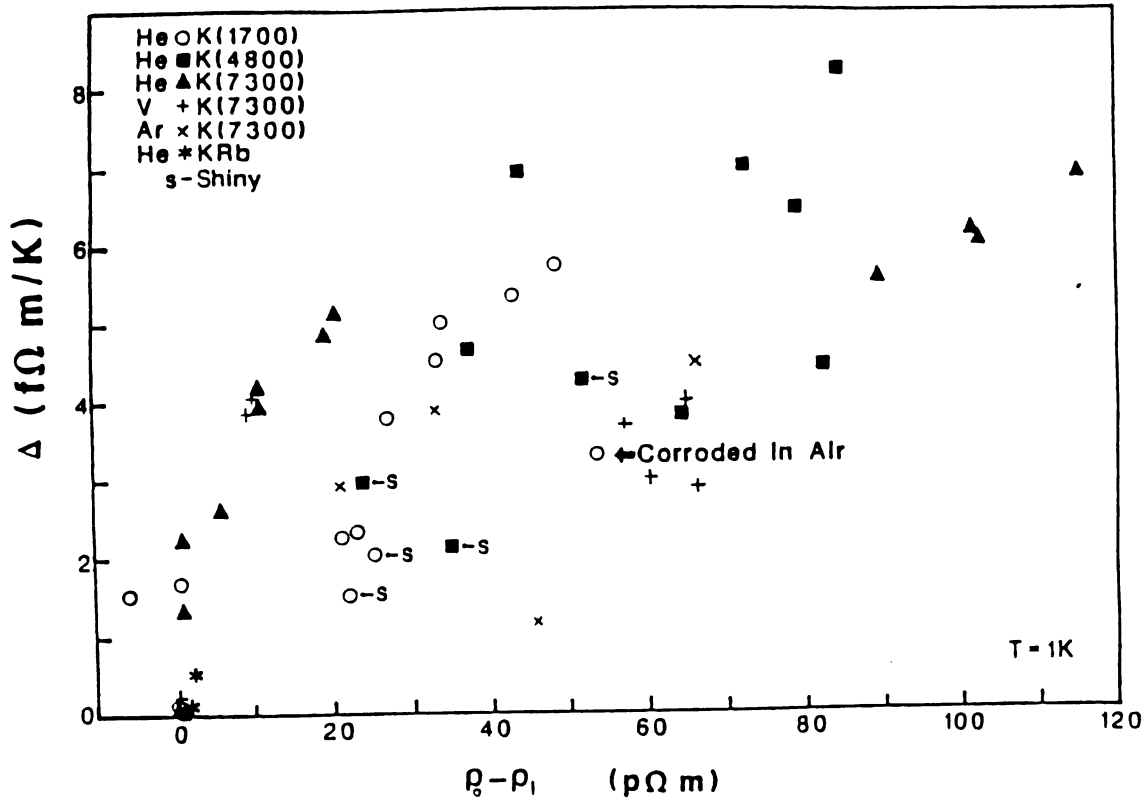


Figure 10:  $\Delta$  versus  $\rho_0 - \rho_1$  for the data of Figs. 1, 2, 5, and 6. The letter "s" indicates samples with shiny surfaces.

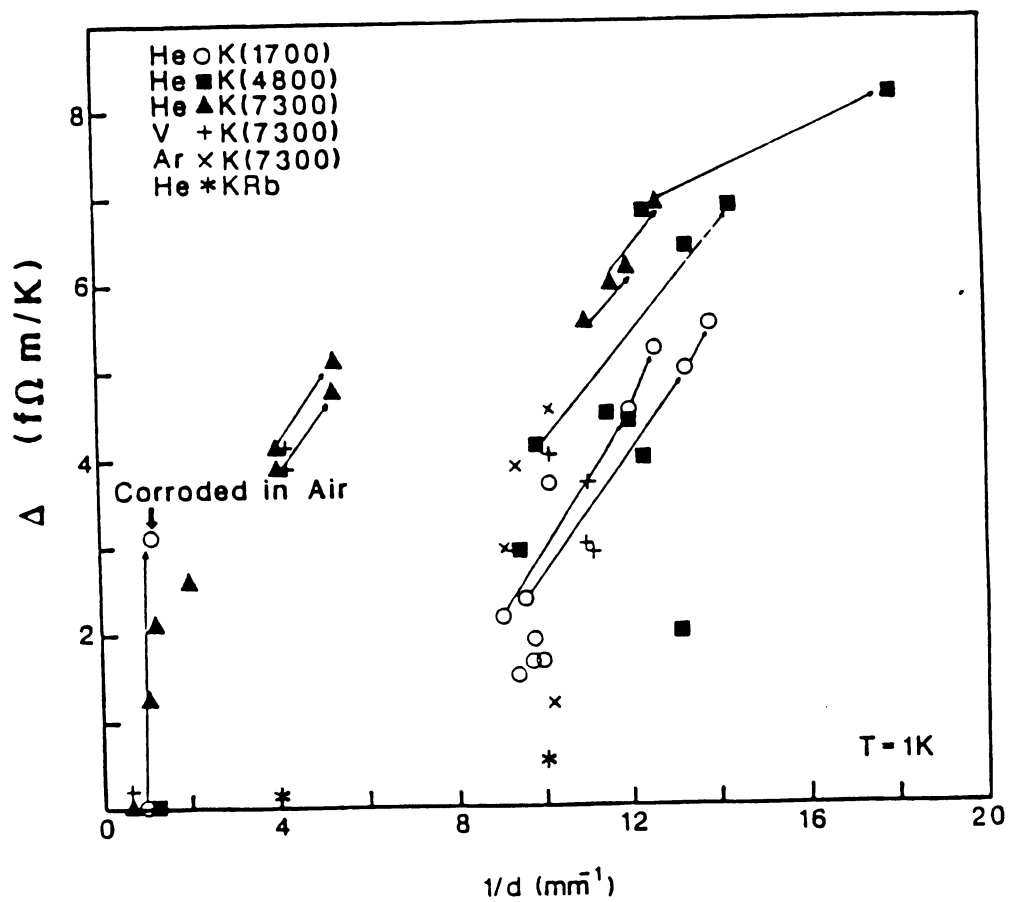


Figure 11:a) Figure 8 with arrows indicating changes in  $\Delta$  which occur upon corrosion.

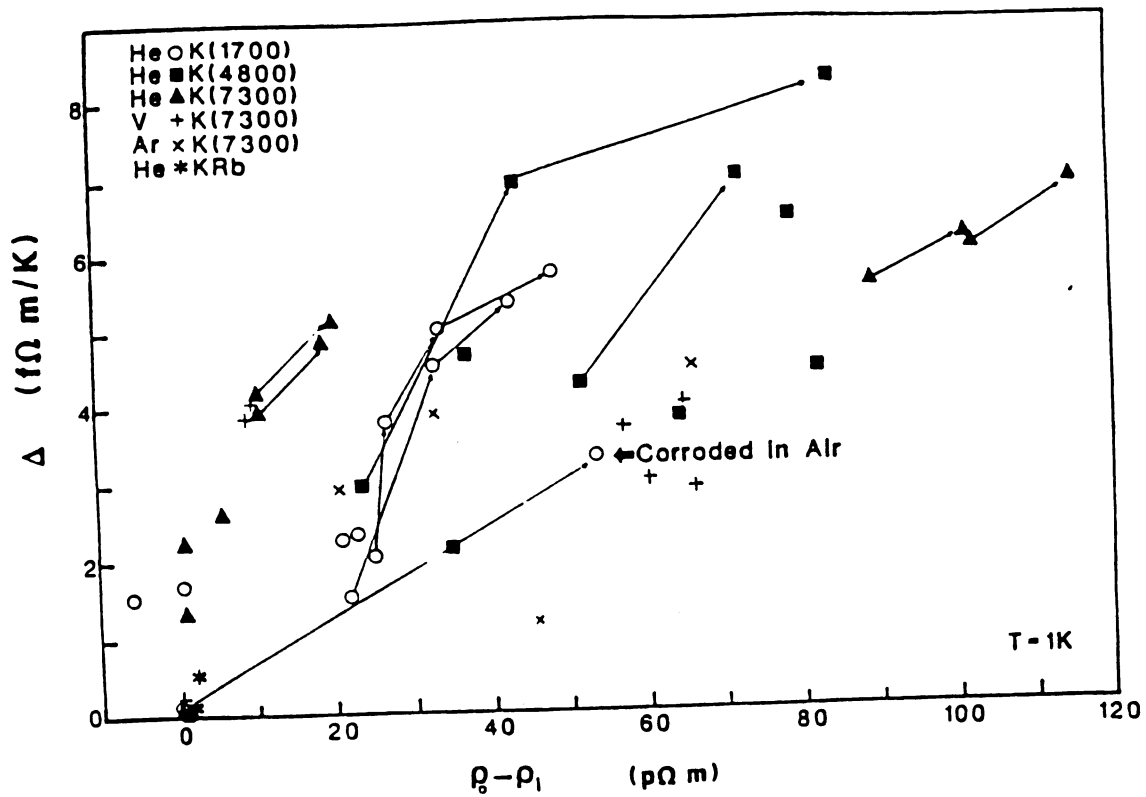


Fig.11 b) Figure 10 with arrows indicating changes in  $\Delta$  which occur upon corrosion.

## 6.2 THERMOELECTRIC RATIO G.

### 6.2.1 Introduction.

In the process of studying the low temperature electrical resistivity  $\rho(T)$  of thin Potassium (K) wires,<sup>1,2</sup> we also measured the thermoelectric ratio  $G$  of these same wires. In this paper we describe the results we obtained, which shed additional light upon the behavior of thin K wires. As we discuss below,  $G$  provides information complementary to that obtained from  $\rho(T)$ .

We know of only one prior set of studies of the low temperature thermoelectric properties of thin K wires, the pioneering measurements by the Canadian group of D.K.C. MacDonald. MacDonald, Pearson, and Templeton<sup>3</sup> measured the thermopower  $S$  of K wires with diameters ranging from  $d = 0.8$  mm to  $0.07$  mm. These samples were not made from the same stock, and they found no systematic variation of properties of  $S$  with  $d$ . We will summarize their results below.

This paper is organized as follows. In section II we review the results obtained by MacDonald et al. on the low temperature thermoelectric properties of high purity K and describe the expected behavior for  $G$ . In section III we present and analyze our data. Section IV contains a summary and conclusions.

### 6.2.2 Review of Previous Work and Background Information.

MacDonald et al.<sup>3</sup> fit their thermopower data for high purity K below about 3K to the equation:



$$S = AT + BT^3 + C \exp(-\Theta/T). \quad (1)$$

The form of this equation was based upon the predicted behavior for a simple, free electron metal with a spherical Fermi surface that does not contact the Brillouin Zone boundary.<sup>4</sup> The first term was attributed to the electron diffusion component of  $S$ , the second term to the Normal portion of the phonon-drag component, and the third term to the Umklapp portion of the phonon-drag component. They found values of  $A = (+ 0.5 \rightarrow -1.0) \times 10^{-8} \text{ V/K}^2$  and  $B = (-0.15 \rightarrow -0.30) \times 10^{-8} \text{ V/K}^4$  for samples with RRRs ranging from 4000 to 10,000 and  $0.07 \text{ mm} \leq d \leq 0.8 \text{ mm}$ . Above about 1.5K, both the second and third terms in Eqn. 1 are significant, and they combine to produce a minimum in  $G$  at  $\sim 3.3\text{K}$ . Below 1K, where we will examine our data quantitatively, the third term in Eqn. 1 is completely negligible.

The thermoelectric ratio  $G$  is related to  $S$  by the Eqn.

$$G = S/LT \quad (2)$$

where  $L$  is the Lorenz ratio.<sup>4</sup> Experimentally we have found<sup>5</sup> that  $L$  is equal to  $L_0$  (the Sommerfeld value of the Lorenz ratio,  $2.44 \times 10^{-8} \text{ V}^2/\text{K}^2$ ) only at temperatures below 1K. For quantitative analysis of  $G$  we thus concentrate upon  $T \leq 1\text{K}$ .

From Eqns 1 and 2 we expect  $G$  to have the low temperature form:<sup>4</sup>

$$G = G_0 + DT^2, \quad (3)$$

where  $G_o = A/L_o$  and  $D = B/L_o$ . The MacDonald et al. data described above gave  $G_o \approx (+ 0.2 \rightarrow -0.4) V^{-1}$  and  $D = (- 0.06 \rightarrow - 0.12) V^{-1}K^{-2}$ .

If two different scatterers are present, e.g. impurities "i" and the sample surface "s", then from the Gorter-Nordheim equation<sup>4</sup> we expect the value of  $G_o$  to be:

$$G_o = (\rho_i/\rho_o)G_o^i + (\rho_s/\rho_o)G_o^s. \quad (4a)$$

Here  $G_o^i$  and  $\rho_i$  are, respectively, the bulk thermoelectric ratio and resistivity due to residual impurities,  $G_o^s$  and  $\rho_s$  are the thermoelectric ratio and resistivity due to surface scattering, and  $\rho_o = \rho_i + \rho_s$ . We can eliminate the variable  $\rho_s$  from Eqn. (4a) and rewrite it as

$$G_o = G_o^s + (\rho_i/\rho_o)(G_o^i - G_o^s). \quad (4b)$$

Since  $G_o^s$ ,  $G_o^i$ , and  $\rho_i$  are assumed constant for a set of thin samples from a given batch of K, a plot of  $G_o$  versus  $(1/\rho_o)$  should yield a straight line with intercept  $G_o^s$  and slope  $\rho_i(G_o^i - G_o^s)$ .

Eqns. 3 and 4b will form the basis for analysis of our experimental data. Although Eqn. 3 was initially derived from a simple model involving a free-electron diffusion term plus phonon-drag, we now know that its form is also appropriate to more modern analyses of low temperature thermopower

involving many-body contributions such as the Nielsen-Taylor effects<sup>4,6</sup> and electron-phonon mass enhancement.<sup>4,7</sup> Nielsen and Taylor showed that a many-body contribution which they labelled "virtual recoil", provided a qualitative understanding of the impurity thermopowers produced by Na, Rb, and Cs impurities in K. Another contribution which they labelled "phony-phonon-drag" gave a contribution to the diffusion thermopower in pure metals which mimicked the temperature dependence of phonon-drag. These effects complicate the analysis of experimental data, especially in a case such as ours where the total residual impurity content is small and its detailed composition is not known. We thus concentrate upon presenting our experimental results, deriving values of the quantities in Eqn. 4b, and showing that the contribution of surface scattering to the thermopower is what would be expected if such scattering is completely diffuse. We continue to refer to the two terms in Eqn. 3 as electron-diffusion and phonon-drag components, although the second term in Eqn. 3 may contain a contribution from "phony-phonon-drag".

For a metal with an essentially spherical Fermi surface, like K, one should be able to write the low temperature diffusion term in the thermoelectric ratio to good approximation as:<sup>4</sup>

$$G = (e/E_F) [(d \ln(nv)/d \ln E) - (d \ln \ell / d \ln E)]_{E=E_F} \quad (5a)$$

Here  $e$  is the electronic charge,  $n$  the electronic density of states,  $v$  the Fermi velocity,  $\ell$  the electron mean-free-path, and the logarithmic

derivatives are to be evaluated at the the Fermi energy  $E_f$ . If the "nv" term is evaluated for a free-electron model, we obtain:

$$G = -0.5[1 + d\ln\ell/d\ln E]_{E_f} v^{-1}. \quad (5b)$$

We will use Eqns. 4b and 5b to find values of  $(d\ln\ell/d\ln E)$  for both residual impurities in our samples and the sample surface.

Eqn. 1 of ref. 1 and Eqn. 4 of the present paper demonstrate both the complementary nature of  $\rho$  and  $G$ , and an important fundamental difference between them. Eqn. 1 of ref. 1 shows that the contributions to  $\rho$  from two different sources of scattering are additive. For each scatterer,  $\rho$  increases linearly with the concentration of that scatterer, until the two concentrations become so large that the individual scatterers interact. In contrast, we see from Eqn. 4 above that, when one scatterer is strongly dominant, the value of  $G$  becomes independent of the concentration of both that scatterer and any minority scatterer.

### 6.2.3 Experimental Data.

We have measured  $G$  on a variety of samples, as described in ref. 1. Following ref. 1, we categorize the samples as follows. Three sets were prepared and cooled in He gas; these sets are designated as K(7300), K(4800), and K(1700), where the numbers refer to the measured residual resistance ratios ( $RRR = R(295K)/R(0K)$ ) of bulk samples from each set. The fourth set contains samples of material from K(7300), but which were either prepared and cooled in Ar gas, or prepared in He and cooled in Vacuum. They will be designated by the symbols Ar or V, respectively.

Fig. 1 shows the  $G$  values for the K(7300) samples. The values of  $dp/dT$  for these samples are given in Fig. 1 of ref. 1. If we examine first the data for the thickest-- $d = 1.5$  mm-- samples (crosses), we find a relatively large, negative phonon-drag minimum with a magnitude  $> 3 \text{ V}^{-1}$  at its lowest point at about 3.3K. Below 3.3K, the data rise smoothly to a low temperature limiting value which is close to zero and usually slightly negative. As the samples become thinner,  $G$  changes systematically; the phonon-drag minimum becomes shallower, and the low temperature limit  $G_0$  becomes more negative.

According to the standard picture of phonon-drag in K, the phonon-drag minimum at  $\sim 3.3\text{K}$  involves a competition between a negative "Normal" component and a positive "Umklapp" component.<sup>4</sup> In this picture, the fact that the phonon-drag minimum becomes shallower with decreasing wire thickness and concurrent increase in  $\rho_0$  indicates that the additional surface scattering in the thinner wires reduces either the Normal component alone, or both the Normal and Umklapp components together. As we noted above, many-body contributions to the temperature dependent portion of the thermopower may complicate this interpretation.

The shift toward more negative values of  $G_0$  with decreasing sample thickness indicates: (a) that the dominant scatterer in the samples is changing from impurity scattering to surface scattering (possibly including effects of surface corrosion) as the sample thickness decreases, and (b) that surface scattering produces a negative contribution to  $G_0$ .

Similar behavior is shown in Figs. 2--Ar and Vac. cooled, 3--K(1700), and 4--K(4800). The behaviors of  $dp/dT$  for these same samples are shown in

Figs. 2, 5, and 6, respectively, in ref. 1. Comparison of Fig. 2 in the current paper with Figs. 1, 3, and 4, shows that the general behavior of  $G$  for samples prepared or cooled in Ar and Vacuum differs little from that for samples of the same diameter and purity prepared and cooled in He.

To determine  $G_O^S$  and  $G_O^i$  as defined in Eqn. 4, we plot  $G_O$  versus  $1/\rho_O$  in Fig. 5. Aside from three data points,<sup>8</sup> the data for the four sets of K fall on three straight lines, with most of the Ar and Vac data falling on the same line as the He data from the K(7300) batch of K. As expected from Eqn. 4, the slopes of these lines are in proportion to the values of  $\rho_i$  for the different sample sets. Within experimental uncertainties, the data for the K(7300) and K(4800) samples determine the same values of  $G_O^S$  and  $G_O^i$ , namely  $G_O^S \approx -0.55 \pm 0.1 \text{ V}^{-1}$  and  $G_O^i \approx -0.1 \pm 0.1 \text{ V}^{-1}$ . The data for the K(1700) samples determine the slightly different values  $G_O^S = -0.65 \pm 0.1 \text{ V}^{-1}$  and  $G_O^i = +0.1 \pm 0.1 \text{ V}^{-1}$ . Within their mutual uncertainties, both sets of data are consistent with the common values  $G_O^S = -0.6 \pm 0.2 \text{ V}^{-1}$  and  $G_O^i = 0 \pm 0.2 \text{ V}^{-1}$ , which we take as our best estimates for  $G_O^S$  and  $G_O^i$ . We note that this value of  $G_O^i$  falls within the range of the values estimated from the data of MacDonald et al.<sup>2</sup>

If we insert these estimates for  $G_O^i$  and  $G_O^S$  into Eqn. 5b, we find that

$$[\mathrm{d}\ln\ell^{\mathrm{i}}/\mathrm{d}\ln E]_{E_{\mathrm{f}}} = -1 \pm 0.3 \quad (6a)$$

and

$$[\mathrm{d}\ln\ell^{\mathrm{s}}/\mathrm{d}\ln E]_{E_{\mathrm{f}}} = +0.2 \pm 0.3. \quad (6b)$$

Here  $\ell^{\mathrm{i}}$  and  $\ell^{\mathrm{s}}$  are the electron mean-free-paths for scattering from impurities and the sample surface, respectively.

The sign of the impurity term (Eqn. 6a) is opposite to that expected for simple elastic scattering of electrons by impurities.<sup>4</sup> This sign discrepancy argues for the presence of the many-body contributions of Nielsen and Taylor.<sup>6</sup>

To within experimental uncertainty, the surface term (Eqn. 6b) is consistent with the value zero. This is exactly what would be expected for completely diffuse surface scattering, in which an electron hitting the sample surface is scattered into a random direction independent of its incoming energy.

According to Eqn. 3, we expect  $G(T)$  to vary as  $T^2$  for temperatures below the phonon-drag peak. This expectation is valid, to within experimental uncertainties, as illustrated in Fig. 6 with a subset of samples chosen to have minimal overlap of data. We have checked how the coefficient  $D$  varies with various parameters such as residual resistivity  $\rho_0$ , nominal sample diameter  $d$ , etc. The best systematic variation was found to be with  $\rho_0^{-1}$ , as shown in Fig. 7.

#### 6.2.4 Summary and Conclusions.

From the foregoing data and analysis, we are able to draw the following conclusions. (1) The general form of  $G$  remains the same as samples are thinned, but the phonon-drag minimum generally becomes less negative and the low temperature electron diffusion limiting value  $G_0$  becomes more negative. (2) The data for all four sets of samples are consistent with the Gorter-Nordheim rule, and mostly fall on three different straight lines, one for each bulk sample purity. These lines determine values of  $G_0^i$  and  $G_0^S$  which are the same for the K(4800) and K(7300) samples, but slightly different for the K(1700) samples. To within an experimental uncertainty of  $\pm 0.2 \text{ V}^{-1}$ , the data for all four sample sets are consistent with the values:  $G_0^S \approx -0.6 \pm 0.2 \text{ V}^{-1}$  and  $G_0^i \approx 0 \pm 0.2 \text{ V}^{-1}$ . This value for the surface term is compatible with completely diffuse surface scattering. (3) Below 1K,  $G$  varies approximately as  $DT^2$ , as expected from Eqn. 3, and the coefficient  $D$  varies approximately as  $\rho_0^{-1}$ .

This work was supported in part by the NSF Division of Materials Research through Low Temperature Physics grants DMR-83-03206, DMR-83-05289, and DMR-87-00900.



## REFERENCES

(Chapter 6.2 - 6.24)

1. J. Zhao, W.P. Pratt, Jr., H. Sato, P.A. Schroeder, and J. Bass, Phys. Rev. B, (1988) (preceding paper).
2. Z.-Z. Yu, M. Haerle, J.W. Zwart, J. Bass, W.P. Pratt Jr., and P.A. Schroeder, Phys. Rev. Lett. 52, 368 (1984).
3. D.K.C. MacDonald, W.B. Pearson, and I.M. Templeton, Proc. Roy. Soc. (London) A256, 334 (1960).
4. F.J. Blatt, P.A. Schroeder, C.L. Foiles, and D. Greig, Thermo-electric Power of Metals, Plenum Press, N.Y., 1976.
5. M.L. Haerle, W.P. Pratt Jr. and P.A. Schroeder, J. Phys. F. 13, L243 (1983).
6. P.E. Nielsen and P.L. Taylor, Phys. Rev. B10, 4061 (1974) and references therein.
7. J.L. Opsal, B.J. Thaler, and J. Bass, Phys. Rev. Lett. 36, 1211 (1976); B.J. Thaler, R. Fletcher, and J. Bass, J. Phys. F. 8, 131 (1978).
8. For the two data points for  $d = 0.10$  mm samples of K(1700) -- see Fig. 6 of ref. 1, the deviation is due to the unusual values of  $\rho_0$  for these two samples (see Fig. 4 of ref. 1). For the datum point of the corroded  $d = 0.8$  mm sample of K(1700)--six-pointed star in Fig. 5 of ref. 1--the deviation is probably related to the especially large amount of both bulk and surface corrosion in this sample.

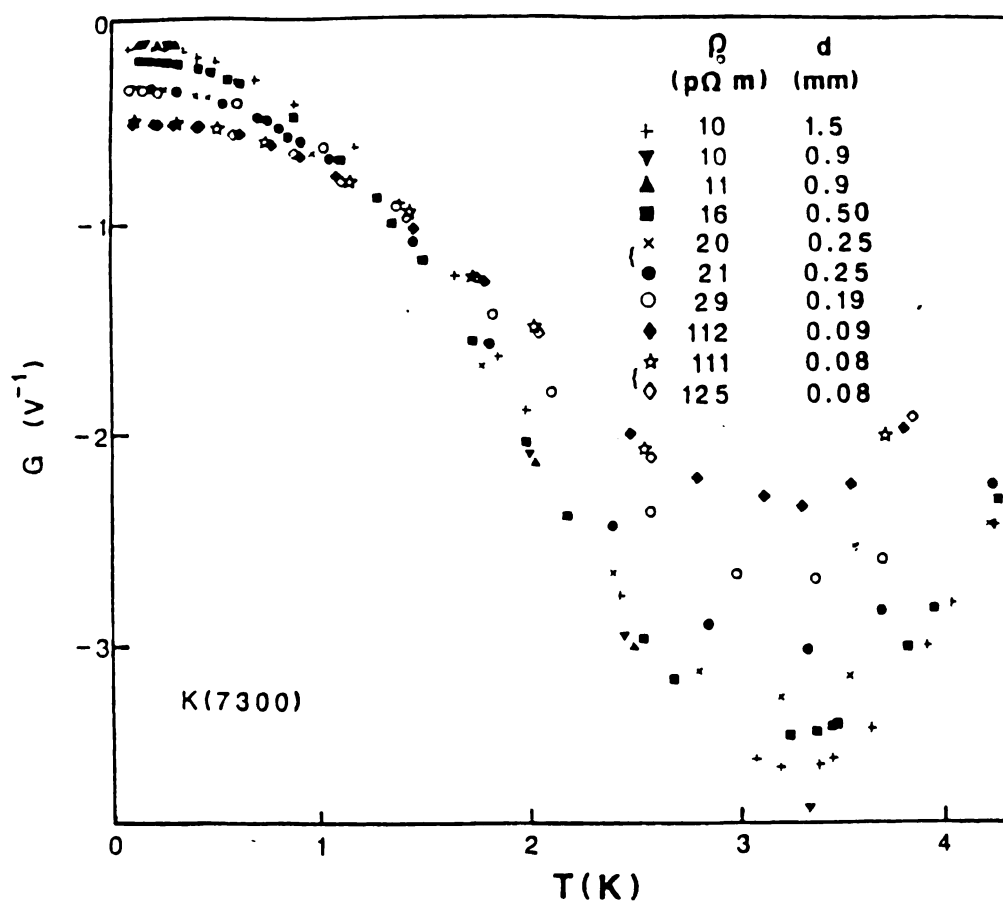


Figure 1: G versus T for He cooled K(7300)

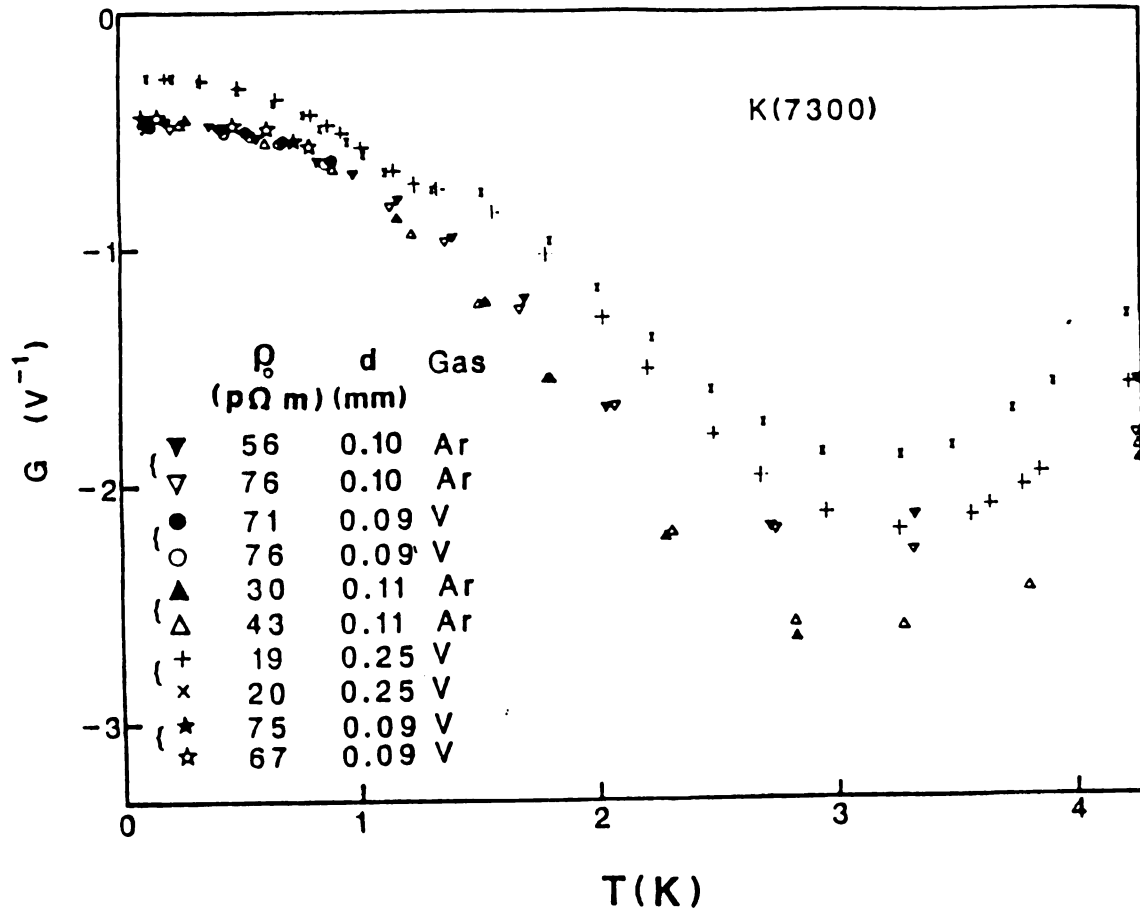


Figure 2:  $G$  versus  $T$  for Ar and Vac cooled K. For the Vacuum cooled samples, about 10 $\mu$ Hg of residual He gas was left in the sample can at room temperature to ensure that the samples would cool properly. This gas affected the  $G$  data above 1K, which is thus not as reliable as the remainder of the data in this paper.

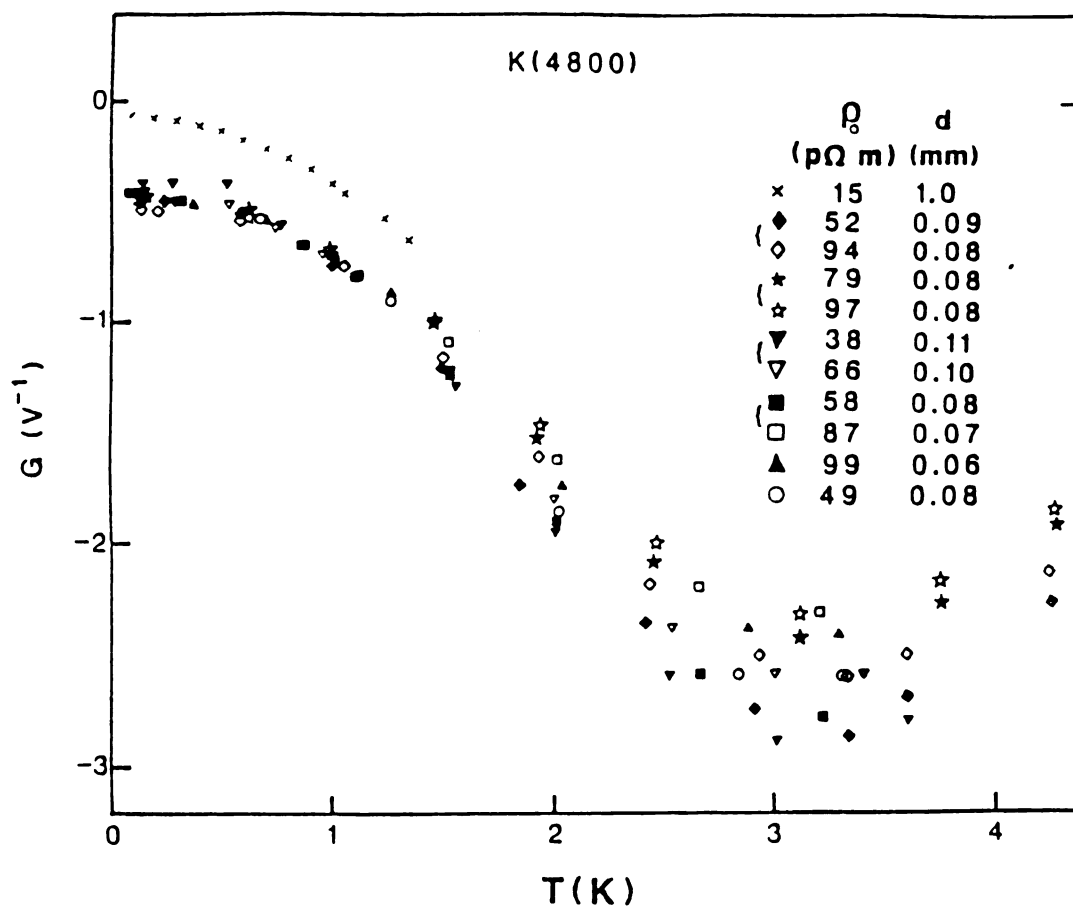
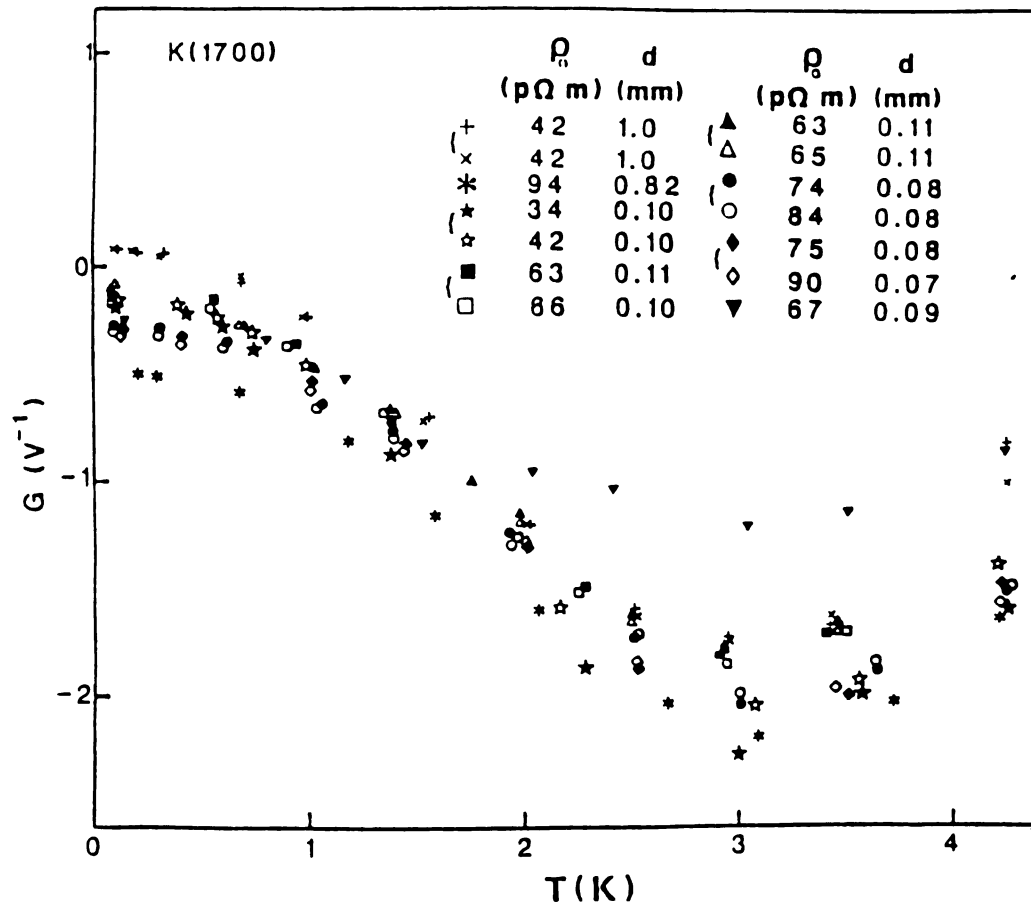


Figure 3: G versus T for He cooled K(4800)

Figure 4:  $G$  versus  $T$  for He cooled K(1700)

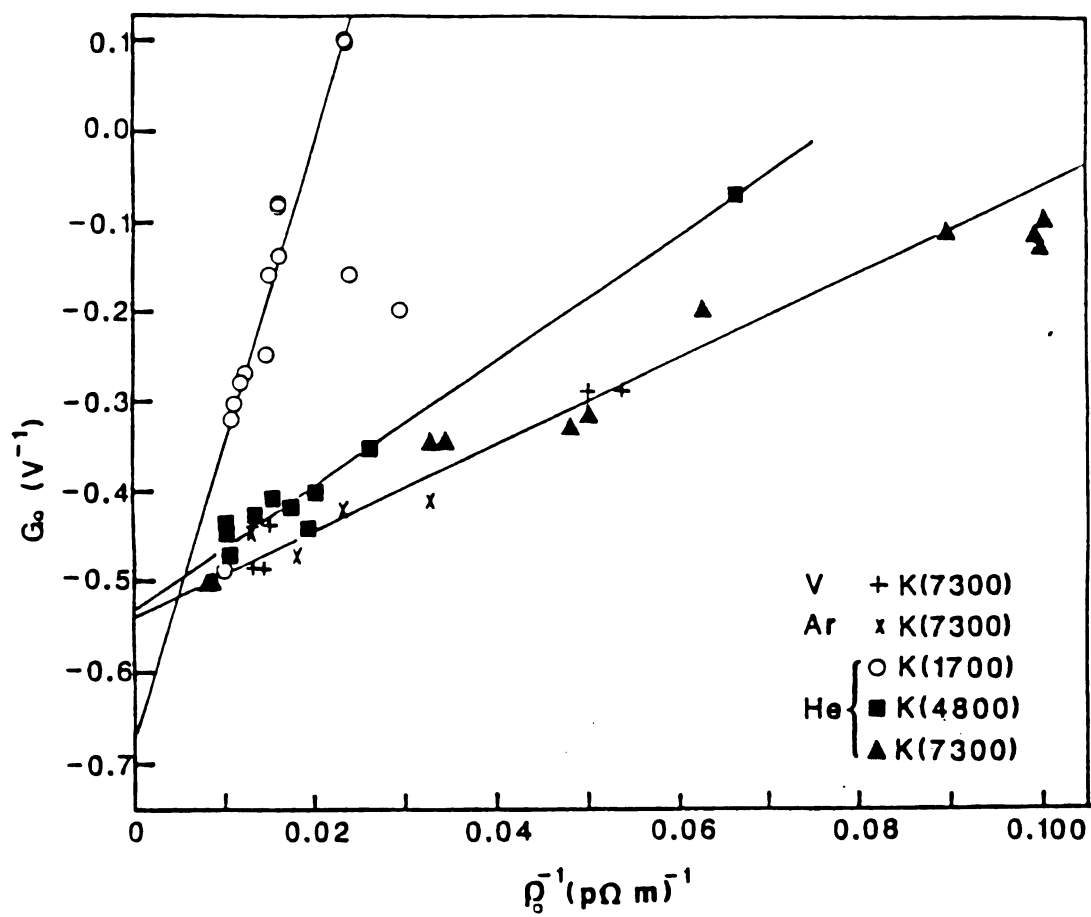


Figure 5:  $G_0$  versus  $1/\rho_0$  for the data of Figs. 1-4.

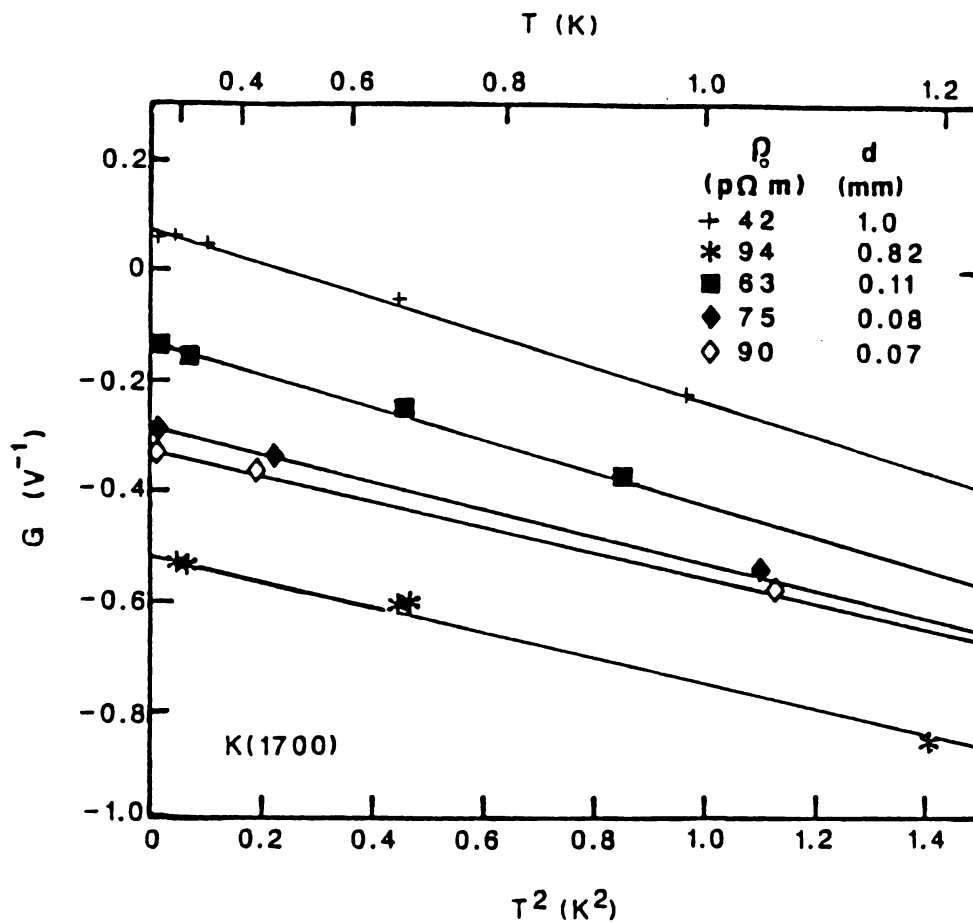


Figure 6: Test of  $G(T) = G_0 + DT^2$  below 1K for selected data from Fig. 4.

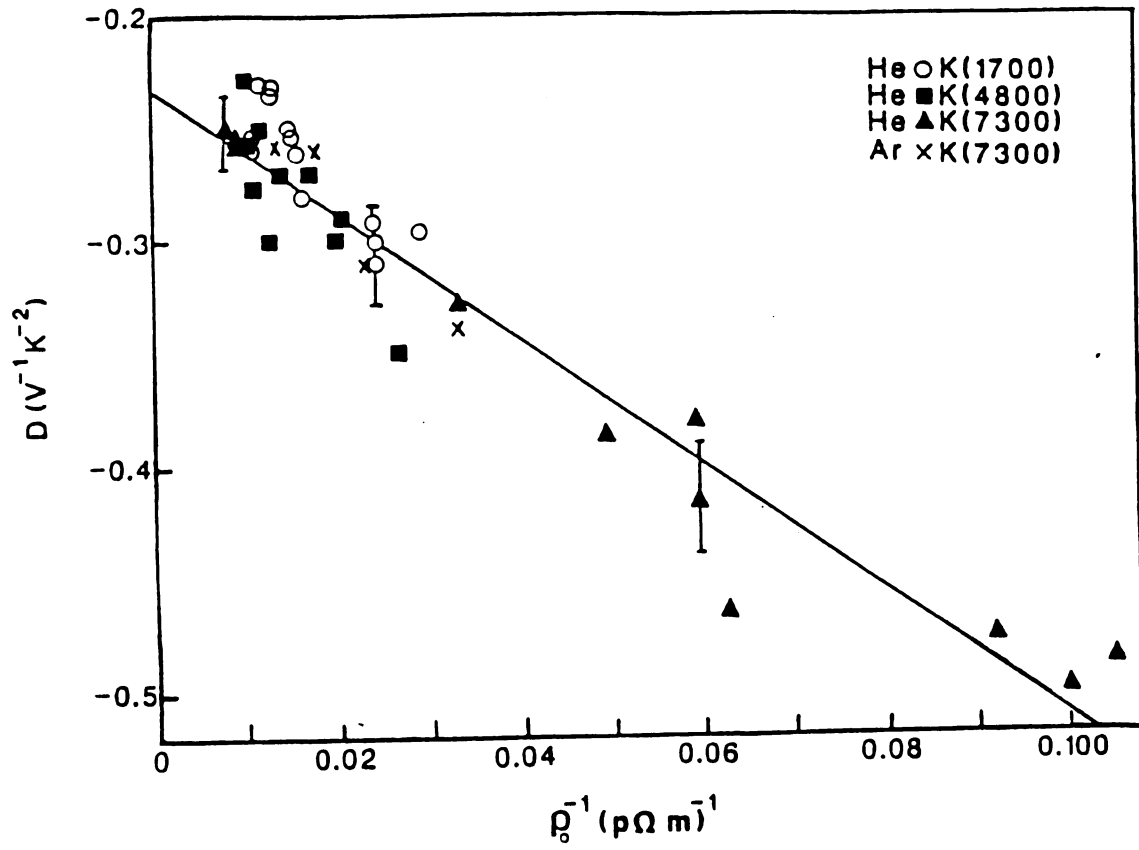


Figure 7: The  $T^2$  coefficient  $D$  from Fig. 6, versus  $\rho_0^{-1}$ , for the data of Figs.

1-4.



## APPENDIX 1

Because it is important to the vertex correction for elastic scattering proposed by Hu and Overhauser, here we discuss the magnitude of  $B$  in Eq.2.3 in more detail. The magnitude of  $B$  depends on two parameters: Debye temperature  $\Theta_D$ , (This is come from an approximation made for the density of phonon states at low temperatures), and the average momentum transfer per collision.

$\Theta_D$  generally varies with temperature and the experimental measuring methods. Since  $B$  is proportional to  $\Theta_D^{-3}$ , this could give an error in evaluating  $B$  as high as 30%. From the experimental data we know  $\Theta_D$  of K and Li have a smaller value at low temperatures than at high temperatures. The low temperature  $\Theta_D$  for K and Li obtained from the specific heat measurement are 90K and 350K respectively.

The average momentum transfer per collision  $K$  is defined as<sup>2</sup>

$$K_{av}^2 = \frac{\int_0^\pi P_{k',k} K^2 (1 - \cos\theta) d\Omega}{\int_0^\pi P_{k',k} (1 - \cos\theta) d\Omega}, \quad (A.1)$$

where  $P_{k',k}$  is the probability of electron with wave vector  $k$  scattering to state  $k'$ , ( from Fermi's golden rule  $P_{k',k} \propto V^2(K)$ ),  $V(K)$  is the Fourier transform of the scattering potential,  $\theta$  is the angle between  $k'$  and  $k$ , and  $K = |\vec{k} - \vec{k}'| = 2k_F \sin(\theta/2)$ . Eq.A.1 can be written as

$$K_{av}^2 = \frac{\int_0^{2k_f} K^5 V^2(K) dK}{\int_0^{2k_f} K^3 V^2(K) dK}, \quad (A.2)$$

Since no reliable pseudopotentials of Rb impurity in K and Mg impurity in Li seem to be available, approximation has to be made about  $V(K)$  in order to evaluate B.

For a  $\delta(r)$  potential,  $V(K)=\text{constant}$ , corresponds to isotropic scattering, Eq.A.2 gives  $K_{av} \approx 0.8(2k_f) \approx 2k_f$ . This is a very rough approximation, since  $2k_f$  is the maximum momentum transfer, however, several auothor<sup>30,35</sup> used this value to compare with their experimental results.

An Gaussian potential  $V(r)=V_0 \exp(-r^2/a^2 r_s^2)$ , where  $r_s$  is the Wigner-Seitz radius was chose by S. Hu and Overhouser<sup>66</sup> in their estimation of B. There are two independent parameters  $V_0$  and  $\alpha$ .  $K_{av}(\alpha)$  changes significantly with  $\alpha$  as showed in Fig.A.1, for examples when  $\alpha=1$   $K_{av}=0.52(2k_f)$  and  $\alpha=0.5$   $K_{av}=0.8(2k_f)$ , (this will result in Bs differ by a factor of two), thus without the justification of parameter  $\alpha$  such a potential can not provide quantitatively calculation.

A reasonable approximation of the scattering potential for heterovalent impurities LiMg is the screened Coulomb potential

$$V(r) = - \left( \frac{Ze^2}{r} \right) e^{-ar} \quad (A.3)$$

In this potential the only parameter  $1/a$  is the screening radius, which can be calculated, at least approximately, by the Fermi-Thomas method. This

gives  $\alpha = 1.5k_f$  for Li, and with this value,  $K_{av} = 0.77(2k_f)$ . The value of  $\alpha$  can also be estimated independently from the experimental result of  $d\rho_0/dc$ . (the change of the residual resistivity per atomic percent impurity in the alloy) With the Born approximation and the relaxation time approximation,

$$\frac{d\rho_0}{dc} = \frac{mv_f}{e^2} \left(\frac{2m}{h^2}\right)^2 \int_0^\pi \frac{(1 - \cos\theta)}{(K^2 + \alpha^2)} d\Omega \quad (A.4)$$

Solving Eq.A.4 with the experimental result  $d\rho_0/dc = 1.3 \times 10^{-8} \Omega\text{m/at\%}$  for LiMg alloys gives  $\alpha = 6.25k_f$ , which gives  $K_{av} = 0.76(2k_f)$  from Eq.A.2. This value is essentially the same as obtained from the Fermi-Thomas's approximation. Eq.A.2 is not very sensitive to the values of  $\alpha$  in such a range, as shown in Fig.A.1, where  $Y = 2k_f/\alpha$ . Thus a more plausible estimation of  $K_{av}$  for LiMg is

$$K_{av} = 0.77(2k_f) \quad (A.5)$$

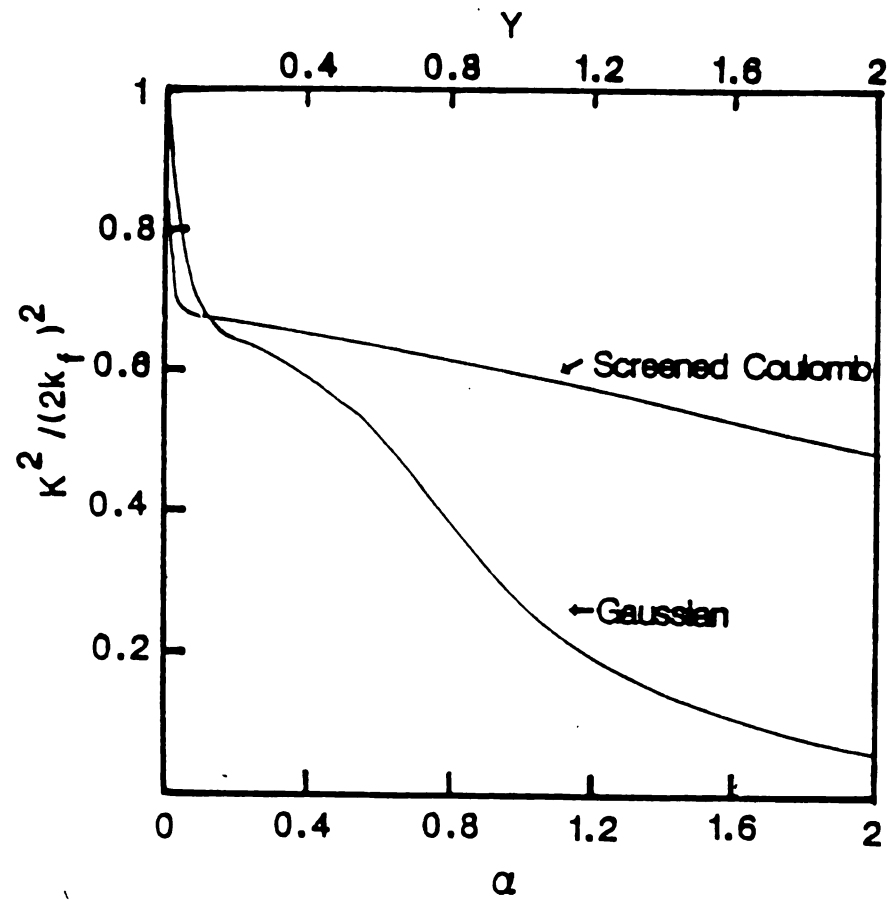


Figure A.1:  $K^2/(2k_f)^2$  versus  $\alpha$  and  $Y$ .

## APPENDIX 2

For LiMg alloy samples with concentrations up to 32%, we found that annealing begins to affect  $\rho(T)$ , and also that potential leads made by the soldering method can cause anomalous behavior in the  $\rho(T)$ . As discussed in Ch.3, the soldering method is no longer a proper way to make the potential leads for very high concentration LiMg alloys, instead, the later developed potassium cold welding technique is preferred. In Fig.A.2 we plot  $(1/T)d\rho/dT$  versus  $T^{-3/2}$  for all of 32% LiMg samples. In such a plot interaction effect would predict that the data fall on a straight line. There are two kinds of information contained in Fig. A.2. First, all samples which show peaks are those with potential leads prepared by soldering method. This suggests that the soldering method can cause anomalous peaks in such high concentration LiMg samples. Which might be due to the formation of compounds at the soldering spot, for example a very small spot on the sample surface during superconducting can cause such peak in  $d\rho/dT$ . Second, heat treatment of samples apparently affects  $\rho(T)$  as shown in Fig.A.2 Sample 1a and 1b were first made by put Mg turnings into molten Li and kept at temperature about  $500^\circ\text{C}$  inside the Ar filled glove box for about 40 minutes while stirring were applied. In order to make certain that the samples were well alloyed, we prepared the rest of 32%LiMg samples with about one and half hours heating and stirring. Thus, samples 1a and 1b may not be well alloyed, and they do show a different behavior at low temperatures. To see the annealing effect, we left sample 3a (filled circles) at room temperature for 22 days and remeasured it again as sample 3b (pen squares). We see that sample 3b behaves like sample 1a at high

temperatures and turn back to sample 3a at very low temperatures. Hence, it seems to suggest that microscopic differences within these alloys affect the data. The reasons are not yet clear. From Fig.A.2 we see the data of well annealed sample (2b) and quick measured sample (3a) all show a straight line behavior. Since, the soldering leads and sample heat treatment may influence the resistivity, in Ch.4 and we only consider one 32% LiMg samples 2b, for which we are sure the potential leads were good and the sample was well annealed. All 32% LiMg samples show similar thermoelectric ratio  $G$  behavior at low temperatures ( $T(1K)$ ), while the data show variations at high temperatures, which are apparently related to the bad potential leads, as shown in Fig.A.3.

Only one 49% LiMg sample were measured. The potential leads of the 49% LiMg sample were made together with the sample by melting the alloy inside a sample mold; thus the potential leads were reliable.

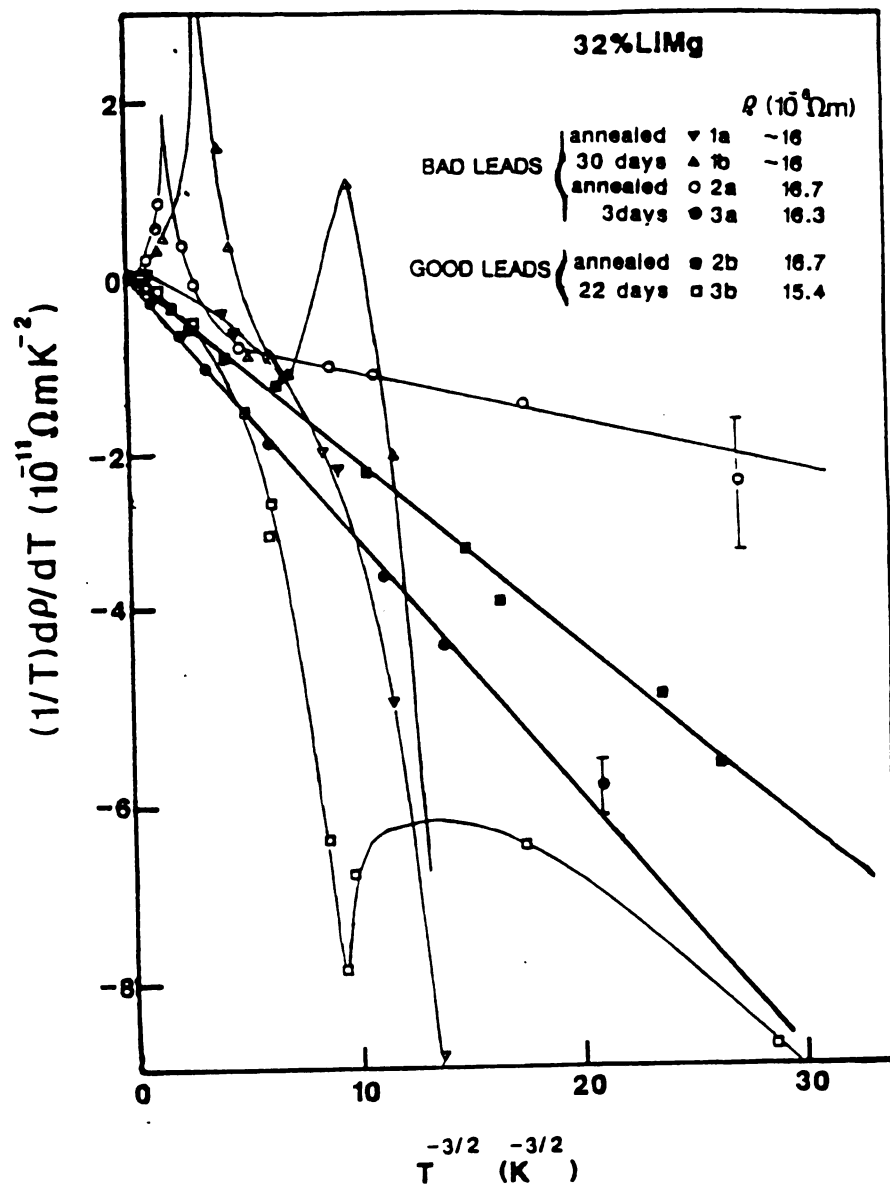


Figure A.2:  $(1/T)d\rho/dT$  versus  $T^{-3/2}$  for all 32% LiMg alloys.

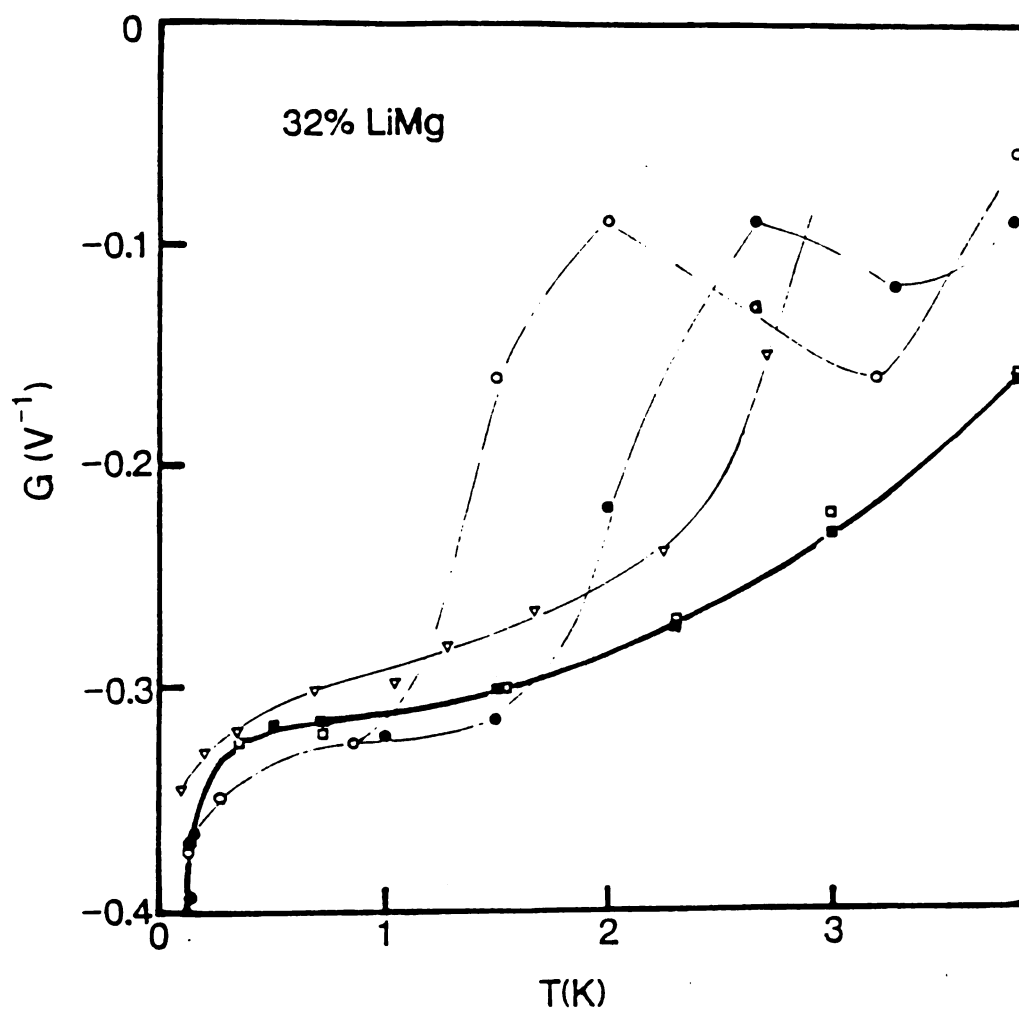


Figure A.3:  $G$  versus  $T$  for all 32% LiMg alloys.